

AD-A116 581

NEWCASTLE-UPON-TYNE UNIV (ENGLAND)

F/S 11/2

THE ROLE OF ADDITIVES IN THE DENSIFICATION OF NITROGEN CERAMICS--ETC(U)

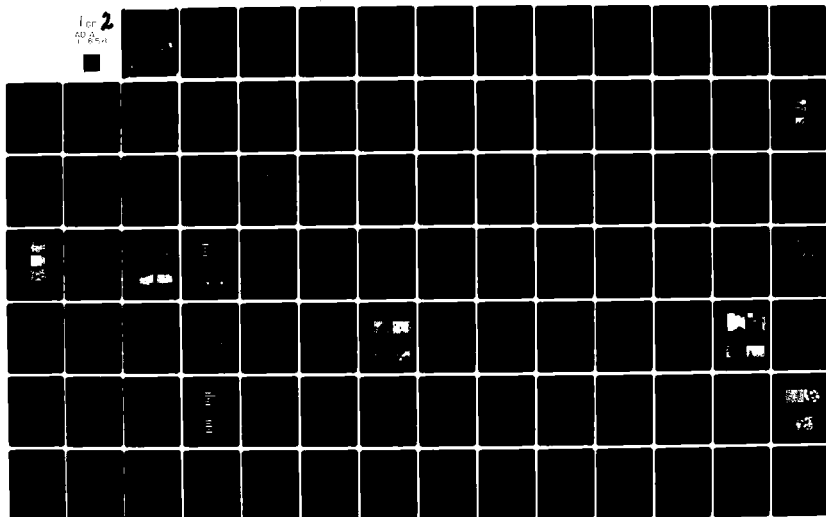
OCT 79 K H JACK

DA-ERO-78-6-012

NL

UNCLASSIFIED

for 2  
202  
1854



AD A116581

THE ROLE OF ADDITIVES IN THE DENSIFICATION  
OF NITROGEN CERAMICS

Second Annual and Final Technical Report

by

K.H. JACK

OCTOBER 1979

EUROPEAN RESEARCH OFFICE  
United States Army  
London W. I, England

Grant Number DAREO-78-G-012

University of Newcastle upon Tyne, United Kingdom

DTIC  
LECTER  
JUL 7 1982  
H

DTIC FILE COPY

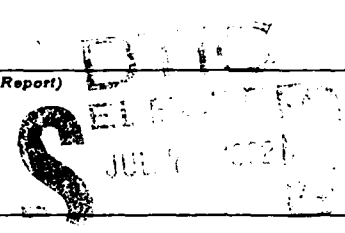
DISTRIBUTION STATEMENT A  
Approved for public release  
Distribution Unlimited

82 07 07 021

UNCLASSIFIED

R&amp;D 2352A-MS

SECURITY CLASSIFICATION OF THIS PAGE (When Data Entered)

REPORT DOCUMENTATION PAGE		READ INSTRUCTIONS BEFORE COMPLETING FORM
1. REPORT NUMBER	2. GOVT ACCESSION NO.	3. RECIPIENT'S CATALOG NUMBER
4. TITLE (and Subtitle) The Role of Additives in the Densification of Nitrogen Ceramics.		5. TYPE OF REPORT & PERIOD COVERED Second Annual and Final Technical Report Oct 79
		6. PERFORMING ORG. REPORT NUMBER
7. AUTHOR(s) K. H. Jack		8. CONTRACT OR GRANT NUMBER(s) DAER078-G-012
9. PERFORMING ORGANIZATION NAME AND ADDRESS Department of Metallurgy and Engineering The University of Newcastle upon Tyne Newcastle upon Tyne NE1 7RU		10. PROGRAM ELEMENT, PROJECT, TASK AREA & WORK UNIT NUMBERS IT161102BH57-04
11. CONTROLLING OFFICE NAME AND ADDRESS USARDSG-UK Box 65, FPO NY 09510		12. REPORT DATE October 79
		13. NUMBER OF PAGES 92
14. MONITORING AGENCY NAME & ADDRESS (if different from Controlling Office)		15. SECURITY CLASS. (of this report) Unclassified
		15a. DECLASSIFICATION/DOWNGRADING SCHEDULE
16. DISTRIBUTION STATEMENT (of this Report)  Approved for public release; Distribution unlimited		
17. DISTRIBUTION STATEMENT (of the abstract entered in Block 20, if different from Report)  		
18. SUPPLEMENTARY NOTES		
19. KEY WORDS (Continue on reverse side if necessary and identify by block number) Nitrogen Ceramics, Nitrogen Glasses, Silicon Nitride, Sialons, Sintering, Densifying Additives, Densification Kinetics, Hot-Pressing, Ceramic Processing, Sialon Polytypoids, Sialon X-phase, Sc-Si-Al-O-N System, $\alpha$ '- $\beta$ ' Relationships		
20. ABSTRACT (Continue on reverse side if necessary and identify by block number) Densification of silicon nitride by either hot-pressing or pressureless sintering requires an additive which reacts with the surface silica and some of the nitride to give an oxynitride liquid that promotes shrinkage and, at the same time, the phase transformation from $\alpha$ to $\beta$ . Silicon nitride is densified by hot-pressing with scandia additive but theoretical density is not achieved by pressureless sintering. The kinetics of densification are interpreted in terms of a Kingery model with a slope of		

DD FORM 1473  
1 JAN 73EDITION OF 1 NOV 65 IS OBSOLETE  
S/N 0102-LF-014-6601

UNCLASSIFIED

SECURITY CLASSIFICATION OF THIS PAGE (When Data Entered)

UNCLASSIFIED

SECURITY CLASSIFICATION OF THIS PAGE (When Data Entered)

20./...

one-third for the solution-precipitation stage indicating that solution of  $\alpha$  or precipitation of  $\beta$  is rate-controlling. Sintering with equal weights of scandia and alumina gives improved densities. An important advantage over  $\beta'$  yttrium sialon is that the quaternary scandium oxynitride and glassy grain boundary phases do not undergo catastrophic oxidation at 1000°C.

The preparation and properties of nitrogen-containing glasses in M-Si-O-N and M-Si-Al-O-N systems where M is Mg, Ca, Y and Nd are described. The glasses form the grain-boundary vitreous phases in silicon nitride and sialons and the characterisation of such glasses is therefore important as their presence often determines the high-temperature behaviour of the ceramic.

The structural characterisation of sialon polytypoids and sialon X-phase is discussed. The structures were determined by X-ray powder methods and direct visual confirmation obtained by comparison of high resolution electron micrographs with images computed on the basis of the X-ray structure.

The preparation and characterisation of sialons with structures based on  $\alpha$ -Si<sub>3</sub>N<sub>4</sub> extends the science and technology of "ceramic alloying" and also suggests possible relationships between the  $\alpha$  and  $\beta$  structures in both sialons and silicon nitrides. The relationships between  $\alpha'$  and  $\beta'$  support earlier proposals that  $\alpha$ -silicon nitride is a defect structure with a range of composition.



Accession	✓
NTIS	
ETIC	
Unannounced	
Justification	
By	
Distribution	
Availability	
Dist	
A	

THE ROLE OF ADDITIVES IN THE DENSIFICATION  
OF NITROGEN CERAMICS

Second Annual and Final Technical Report

by

K.H. JACK

OCTOBER 1979

EUROPEAN RESEARCH OFFICE  
United States Army  
London W. 1, England

Grant Number DAERO-78-G-012

University of Newcastle upon Tyne, United Kingdom

# TABLE OF CONTENTS

	Page No.
ABSTRACT	i
LIST OF FIGURES	ii
LIST OF TABLES	vii
I. INTRODUCTION	1
II. THE ROLE OF SCANDIA IN THE DENSIFICATION OF NITROGEN CERAMICS	4
II.1 Introduction and experimental methods	4
II.2 Phase relationships in the Sc-Si-Al-O-N system	5
II.3 Densification	7
II.4 Property measurements	7
II.5 Conclusions	15
III. NITROGEN GLASSES	16
III.1 Introduction	16
III.2 Experimental	17
III.3 Results & Discussion	19
IV. THE STRUCTURAL CHARACTERISATION OF SIALON POLYTYPIDS	35
IV.1 Introduction	35
IV.2 Characterisation	35
IV.3 Crystal structures	38
IV.4 Lattice imaging	46
IV.5 Summary	47
V. SIALON X-PHASE	50
V.1 Introduction	50
V.2 Unit cell	50
V.3 Structure determination and refinement	50
V.4 Discussion	50

	Page No.
VI. $\alpha'$ -SIALON CERAMICS	55
VI.1 Introduction	55
VI.2 Preparation and composition	55
VI.3 The $\alpha'$ structure	58
VI.4 Properties of $\alpha'$ -sialons	63
VII. THE CHARACTERISATION OF $\alpha$ - $\beta$ RELATIONSHIPS IN SIALONS AND SILICON NITRIDES	64
VII.1 $\alpha$ and $\beta$ Silicon nitrides	64
VII.2 Unit-cell dimensions	64
VII.3 Oxygen-containing $\alpha$ -" $\text{Si}_3\text{N}_4$ "	66
VII.4 The $\alpha/\beta$ silicon nitride question	66
VII.5 CVD silicon nitride	66
Appendix I	
X-ray diffraction data for sialon phases	70
Appendix II	
Attendance at scientific meetings	79
Appendix III	
Publications	80
REFERENCES	81

(1)

# ABSTRACT

Densification of silicon nitride by either hot-pressing or pressureless sintering requires an additive which reacts with the surface silica and some of the nitride to give an oxynitride liquid that promotes shrinkage and, at the same time, the phase transformation from  $\alpha$  to  $\beta$ . Silicon nitride is densified by hot-pressing with scandia additive but theoretical density is not achieved by pressureless sintering. The kinetics of densification are interpreted in terms of a Kingery model with a slope of one-third for the solution-precipitation stage indicating that solution of  $\alpha$  or precipitation of  $\beta$  is rate-controlling. Sintering with equal weights of scandia and alumina gives improved densities. An important advantage over  $\beta'$  yttrium sialon is that the quaternary scandium oxynitride and glassy grain boundary phases do not undergo catastrophic oxidation at 1000°C.

The preparation and properties of nitrogen-containing glasses in M-Si-O-N and M-Si-Al-O-N systems where M is Mg, Ca, Y and Nd are described. The glasses form the grain-boundary vitreous phases in silicon nitride and sialons and the characterisation of such glasses is therefore important as their presence often determines the high-temperature behaviour of the ceramic.

The structural characterisation of sialon polytypoids and sialon X-phase is discussed. The structures were determined by X-ray powder methods and direct visual confirmation obtained by comparison of high resolution electron micrographs with images computed on the basis of the X-ray structure.

The preparation and characterisation of sialons with structures based on  $\alpha$ -Si<sub>3</sub>N<sub>4</sub> extends the science and technology of "ceramic alloying" and also suggests possible relationships between the  $\alpha$  and  $\beta$  structures in both sialons and silicon nitrides. The relationships between  $\alpha'$  and  $\beta'$  support earlier proposals that  $\alpha$ -silicon nitride is a defect structure with a range of composition.



(ii)

# LIST OF FIGURES

- Figure 1. The behaviour diagram of the Sc-Si-O-N system at 1700°C.
- Figure 2. Shrinkage v. temperature for 5w/o additives in hot-pressed  $\text{Si}_3\text{N}_4$ .
- Figure 3. Pressureless sintering  $\text{Si}_3\text{N}_4$  with 2w/o  $\text{Sc}_2\text{O}_3$  at 1650 and 1700°C.
- Figure 4. Effect of replacing  $\text{Sc}_2\text{O}_3$  by  $\text{Al}_2\text{O}_3$  in pressureless sintering of  $\text{Si}_3\text{N}_4$  at 1700°C.
- Figure 5(a) Log shrinkage v. log time for  $\text{Si}_3\text{N}_4$  hot-pressed with 2 and 5w/o  $\text{Sc}_2\text{O}_3$  at 1700°C.
- 5(b) Log shrinkage v. log time for  $\text{Si}_3\text{N}_4$  hot-pressed with  $\text{Sc}_2\text{O}_3 + \text{Al}_2\text{O}_3$ .
- Figure 6(a) Log transformation rate v. time for  $\text{Si}_3\text{N}_4$  hot-pressed with 2w/o  $\text{Sc}_2\text{O}_3$ .
- 6(b) Arrhenius plot based on the data of Figure 6(a).
- Figure 7. Scanning electron micrographs of the surfaces of  $\text{Si}_3\text{N}_4$  hot-pressed with increasing amounts of  $\text{Sc}_2\text{O}_3 + \text{Al}_2\text{O}_3$  and oxidised for 100h at 1400°C.
- Figure 8. Creep resistance (1225°C, 77 MPa) of  $\text{Si}_3\text{N}_4$  hot-pressed with increasing amounts of scandia at 1700°C. The runs were repeated on material devitrified for 5 days.
- Figure 9. Creep resistance (1225°C, 77 MPa) of  $z = 0.75$   $\beta'$ -sialon hot-pressed at 1700°C from:
- (a)  $\text{Si}_3\text{N}_4$ , AlN,  $\text{Al}_2\text{O}_3 + 3\text{w/o } \text{Y}_2\text{O}_3$
- (b)  $\text{Si}_3\text{N}_4$ , 15R + 3w/o  $\text{Y}_2\text{O}_3$
- (x)  $\text{Si}_3\text{N}_4$ , AlN,  $\text{Al}_2\text{O}_3 + 3\text{w/o } \text{Sc}_2\text{O}_3$
- (y)  $\text{Si}_3\text{N}_4$ , 15R + 3w/o  $\text{Sc}_2\text{O}_3$
- Figure 10. X-ray photographs showing Mg-Si-O-N glass formation and devitrification.
- Figure 11. Representation of a five-component system (e.g. Mg-Si-Al-O-N) showing a plane of constant N:O ratio.

(iii)

- Figure 12. Glass formation in the Mg-Si-O-N system: cooled from 1700°C at 200°C min<sup>-1</sup>.
- Figure 13. Glass forming regions in M-Si-Al-O-N systems (M = Mg, Y, Ca) at different equivalent compositions of nitrogen.
- Figure 14. Glass forming region of the Mg-Si-Al-O-N system on cooling from 1700°C.
- Figure 15. Glass forming region of the Y-Si-Al-O-N system on cooling from 1700°C.
- Figure 16. Glass formation on quenching from 1700 - 1850°C in the Si-Al-O-N system.
- Figure 17. Variation of viscosity with temperature for Y-Si-Al-O-N glasses of different nitrogen concentrations.
- Figure 18. Viscosities of Y, Nd, Ca and Mg sialon glasses with 18e/o N and the same M:Si:Al cation ratios.
- Figure 19. Variation of glass transition temperature (T<sub>g</sub>) with nitrogen concentration for Y, Nd, Ca and Mg sialon glasses.
- Figure 20. DTA curves for Y-Si-Al-O-N glasses containing 5e/o N and 18e/o N.
- Figure 21. Variation of T<sub>g</sub> and T<sub>c</sub> with nitrogen concentration for Mg and Y sialon glasses.
- Figure 22. Variation of T<sub>g</sub> and T<sub>c</sub> with nitrogen concentration for Nd and Ca sialon glasses.
- Figure 23. Scanning electron micrographs of devitrification products of Y-Si-Al-O-N glasses with different nitrogen concentrations.
- Figure 24. Phase relationships during densification and post-preparative heat-treatment of β'-sialon.
- Figure 25. Formation of β''-Mg-sialon by devitrification  
(a) glass + β-Si<sub>3</sub>N<sub>4</sub> nuclei by cooling liquid from 1700°C  
(b) β'' grown epitaxially on β by heat-treatment at 930°C
- Figure 26. X-ray powder photographs of isostructural β-Si<sub>3</sub>N<sub>4</sub>, β' and β'' sialons.

(iv)

- Figure 27. Transparency of 1mm thick discs and 4mm thick blocks of (i) Ca-sialon and (ii) Mg-sialon glasses, both with 18e/o N.
- Figure 28. IR and UV transmission spectra for glasses in the Ca-Si-Al-O-N system.
- Figure 29. Refractive indices of Mg, Ca, Y and Nd sialon glasses.
- Figure 30. Dependence of a.c. electrical conductivity on frequency and composition for Ca and Mg sialon glasses.
- Figure 31. Phase relationships in the Si-Al-O-N system at 1700°C.
- Figure 32. Graph showing the variation of  $\alpha$  and  $c/n$  with the proportion of  $MX_2$  layers in sialon polytypoid phases.
- Figure 33. Planes of constant M:X ratio in the Mg sialon system.
- Figure 34. Phase relationships in the 6M:7X plane of the Mg sialon system.
- Figure 35. Phase relationships in the 7M:8X plane of the Mg sialon system.
- Figure 36. Phase relationships in the 8M:9X plane of the Mg sialon system.
- Figure 37. Phase relationships in the Be-Si-O-N system at 1780°C.
- Figure 38. Phase relationships in the  $MgO$ - $MgSiN_2$ - $Mg_3N_2$  part of the Mg-Si-O-N system.
- Figure 39. The atomic arrangement in 8H and 15R sialons. The structures are projected on (110) with metal atoms shown as circles. Shaded atoms are at height  $\frac{1}{2}$  above the plane of the paper.
- Figure 40. The atomic arrangement in 6H magnesium oxynitride and 12R magnesium silicon nitride. Symbols as for Figure 39.
- Figure 41. The atomic arrangement in 6H and 12H Mg sialons. Symbols as for Figure 39.
- Figure 42. (a) One-dimensional and (b) two-dimensional lattice images of 6H Mg sialon taken with the electron beam parallel to 010. Calculated images are outlined in white.

(v)

- Figure 43. (a) One-dimensional and (b) two-dimensional lattice images of 12H Mg sialon taken with the electron beam parallel to 010. Calculated images are outlined in white.
- Figure 44. Summary of the range of sialon polytypoid structures.
- Figure 45. The idealised atomic arrangement in low-X projected down the  $b$  axis. The c-face centred cell has been used.
- Figure 46. High-resolution lattice images of X-phase showing (a) twinning and (b) stacking faults. The separation of adjacent vertical (100) planes in both micrographs is  $7.8\text{\AA}$ .
- Figure 47. Optical micrographs of (a) low-X, and (b) high-X.
- Figure 48. Idealised Si-N layers in  $\alpha$  and  $\beta$  silicon nitrides: (a) AB layers, (b) CD layers.  $\alpha$  structure ABCE;  $\beta$  structure ABAB.
- Figure 49. Actual Si-N layers in  $\alpha$  and  $\beta$  silicon nitrides: (a) in  $\beta$ , (b) in  $\alpha$ .
- Figure 50. X-ray powder patterns showing transformations  $\alpha' - \beta'$ .  $\text{CuK}\alpha$  radiation.
- Figure 51. Typical X-ray powder patterns of Ca, Li and Y  $\alpha'$  sialons.  $\text{CuK}\alpha$  radiation.
- Figure 52. Observed, o, and calculated, c, unit-cell dimensions for  $\alpha'$  sialons.
- Figure 53. Observed and calculated diffracted intensities ( $F_p^2$  values) for  $\alpha\text{-Si}_3\text{N}_4$  and  $\alpha'$ -sialons. Thick ordinates are half-scale.
- Figure 54. Intensities of X-ray reflections ( $\text{CuK}\alpha_1$ ) for  $\alpha'$ -Ca-sialons with varying Ca content.
- Figure 55. Tentative phase relationships in part of the Ca-Si-Al-O-N system.
- Figure 56. Comparison of  $\alpha$  and  $\alpha'$  phases.
- Figure 57. Unit cell dimensions of different  $\alpha$ -silicon nitrides.
- Figure 58. The precipitation of  $\alpha$ - and  $\beta$ -silicon nitrides from Fe-Si alloys.

(vi)

- Figure 59. Thermochemical diagram for the Si-O-N system.
- Figure 60. White CVD  $\alpha$ -silicon nitride (x 50,000).
- Figure 61. Black CVD  $\alpha$ -silicon nitride showing disc-shaped precipitates on (00.1) (x 400,000).
- Figure 62. Black CVD  $\alpha$ -silicon nitride showing needle-bubbles on (hk.0) (x 400,000).

LIST OF TABLES

Table 1.	Analysis of starting materials.
Table 2.	Observed X-ray data for $\text{Sc}_2\text{SiO}_5$ and Q-phase.
Table 3.	Oxidation of hot-pressed $\text{Si}_3\text{N}_4$ in air.
Table 4.	Unit cell dimensions for the sialon polytypoids.
Table 5.	Unit cell dimensions for 6H, 14H and 8H Mg sialons.
Table 6.	Unit cell dimensions of Al-C-N and Al-Si-C phases.
Table 7.	Unit cell dimensions for X-phase.
Table 8.	Unit cell dimensions and densities of $\alpha'$ sialons and $\alpha$ and $\beta$ silicon nitrides.
Table 9.	$\alpha'$ Sialon compositions (atoms per unit cell).

## I. INTRODUCTION

In fabricating nitrogen ceramics the objective is to produce easily and economically a shaped component with high strength and oxidation resistance, negligible creep and good thermal shock properties, all at temperatures above 1400°C. In previous reports (K.H. Jack, Final Technical Report, Grant No. DAERO-76-G-067, and K.H. Jack, First Technical Report, Grant No. DAERO-78-G-012) it was shown that densification of silicon nitride and sialons by hot-pressing or by pressureless sintering required an additive, the function of which is to provide conditions for liquid phase sintering by a three stage Kingery mechanism. With  $Y_2O_3$  additive, diffusion through the liquid is slow and solution of  $\alpha-Si_3N_4$  and precipitation of  $\beta$  occurs without major transport of material and hence without densification. With MgO however, the relatively rapid transport of material through the low viscosity liquid ensures that any  $\alpha$ - $\beta$  transformation is accompanied by densification. Silicon nitride is shown in the present report to be densified by hot-pressing with less than 2w/o  $Sc_2O_3$  additive but full density cannot be achieved by pressureless sintering however much additive is used. Densification occurs via a scandium silicon oxynitride liquid and the kinetics are interpreted in terms of a Kingery model with a slope of one-third for the solution-precipitation stage of the log-shrinkage versus log-time plot indicating that either solution of  $\alpha$  or precipitation of  $\beta$  is rate controlling. Sintering with equal weights of scandia and alumina gives improved densities and a  $z = 0.75$   $\beta'$ -sialon composition can be sintered to greater than 90% theoretical density with 3w/o  $Sc_2O_3$ . Property measurements on scandia-densified dilute  $\beta'$ -sialons show good creep and oxidation resistance. An important advantage over  $\beta'$  yttrium sialon is that only one quaternary oxynitride phase,  $Sc_3SiO_5N$ , is formed and neither this phase nor the glassy grain boundary phases undergo catastrophic oxidation at 1000°C.

Grain boundary vitreous phases in silicon nitride and sialons densified with  $Y_2O_3$  and MgO have compositions within the nitrogen glass region of the appropriate system. The characterisation of such glasses is therefore important in describing the densification behaviour of nitrogen ceramics and because their presence often determines the high temperature behaviour of the material. The preparation and properties of nitrogen-containing glasses in M-Si-O-N and M-Si-Al-O-N where M is Mg, Ca, Y or Nd are described in the present report and comparisons of oxide and oxynitride glasses with the same cation composition but with varying N:O ratios show that the glass transition temperature, viscosity and refractive index all increase with increasing nitrogen content. As expected, replacement of oxygen by nitrogen results in a more strongly bonded glass network and changes in electrical properties with nitrogen content are discussed.

In the course of the present investigations into the role of additives on densification of nitrogen ceramics a large number of new crystalline phases have been prepared and characterised. In the previous report (K.H. Jack, First Technical Report, Grant No. DAERO-78-G-012) X-ray data for fifty compounds were listed and further data are appended to the present report. Several of the more important phases have been investigated however in greater detail and of these, the six polytypoid phases (8H, 15R, 12H, 21R, 27R and 2H<sup>6</sup>) and X-phase in the Si-Al-O-N system are reported. The structures of the polytypoids are determined by their metal: non-metal atom ratio M:X which is of the type  $m M:(m+1)X$  where  $m$  has the values 4, 5, 6, 7, 9 and 11 for 8H, 15R, 12H, 21R, 27R and 2H<sup>6</sup> respectively. Beryllium, magnesium, scandium and possibly other metal cations can be incorporated in these structures provided that charge balance is preserved and that the overall M:X ratio is retained. Sialon X-phase has a triclinic unit cell and a point composition close to  $Si_3Al_6O_{12}N_2$ . Its crystal structure is similar to mullite and consists of alternate chains of octahedra and tetrahedra linked to form sheets in the (100) plane. These sheets are joined together by a complex network of tetrahedra, some units of which resemble the  $Si_6N_8$  units in  $\beta$ - $Si_3N_4$ . The structures have been determined by X-ray powder methods but direct observation of the structures by high resolution lattice imaging electron microscopy gives results in excellent agreement with those obtained by calculation from the X-ray structures emphasising the value of such a combination of techniques in the investigation of structure.

The unresolved " $\alpha/\beta$  silicon nitride question" is extremely important in the study of nitrogen ceramics but the preparation and characterisation of sialons with structures based on  $\alpha$ - $Si_3N_4$  ( $\alpha'$ -sialons) extends the science and technology of ceramic alloying and suggests possible relationships between the  $\alpha$  and  $\beta$  structures in both sialons and silicon nitride. The  $\alpha'$  structure occurs in M-Si-Al-O-N systems and is derived from the  $Si_{12}N_{16}$  unit cell by partial replacement of  $Si^{4+}$  by  $Al^{3+}$  while vacancy compensation is by modifier cations (Li, Ca, Y and all of the rare earth elements except La and Ce) occupying the interstices of the (Si,Al)-N network. Where a modifier oxide is used, some O may also replace N, and because there are only two available interstitial sites per unit cell, the  $\alpha'$ -phases have the general composition  $M_x(Si,Al)_{12}(O,N)_{16}$  where  $x$  is not greater than 2. The transformations  $\alpha \rightleftharpoons \beta$  occur by chemical reactions and, by analogy, the relationships between  $\alpha'$  and  $\beta'$  support earlier proposals that  $\alpha$ -silicon nitride is a defect structure with a range of composition that can accommodate small amounts of oxygen. This accounts for the observed variation in density of  $\alpha$ , the relatively wide variation in unit-cell dimensions, the marked difference in properties between



3.

$\alpha$  produced by CVD and by  $\text{SiO}-\text{N}_2$  interaction, and also for the thermodynamics of the Si-O-N system. The discussion presented in the present report therefore provides some answers to the  $\alpha/\beta$  question which are relevant to the densification and properties of nitrogen ceramics.

## II. THE ROLE OF SCANDIA IN THE DENSIFICATION OF NITROGEN CERAMICS

### II.1 Introduction and experimental methods

In the last twenty five years, attempts have been made to develop silicon nitride as a high-temperature engineering material because of its excellent combination of thermal, chemical and mechanical properties. However, all the methods currently used to fabricate complex shapes degrade the properties of the final product. Thus, reaction bonding produces a material which contains up to 20% residual porosity, hot-pressing requires an oxide additive for densification which remains in the material as a grain-boundary glass and impairs high-temperature properties, and pressureless sintering until recently could not produce fully-dense material because large weight losses occurred at the temperatures needed for sintering. In sialon systems pressureless sintering can be carried out successfully because liquid phases form at lower temperatures and these allow material transport by particle rearrangement and solution-precipitation before significant weight losses occur. The residual liquid phase forms a grain-boundary glass on cooling which can be heat-treated to give a more refractory crystalline phase if improved high-temperature properties are required. Thus, dilute  $\beta'$  yttrium sialons sintered to maximum density have high strengths at room and elevated temperatures and are oxidation resistant to  $\sim 1350^\circ\text{C}$ .

Of the many additives used for densifying nitrogen ceramics, yttria is certainly the best and will benefit from further development. Among the additives which have not been explored, scandia is outstanding because Sc occurs in the same Periodic Group as Y and forms high-melting silicates and aluminates. In the present study, phase relationships in the more important areas of the Sc-Si-Al-O-N system have been determined and these have been used as a basis for interpreting the hot-pressing and sintering behaviour of silicon nitride and sialons densified with scandia.

Details of the major starting materials are given in Table 1.

Powders were dry mixed in a Glen Creston mixer-mill and were reacted either by hot-pressing in graphite dies at 27.6 MPa (4,000 psi) for 1h, or by pressureless sintering in flowing nitrogen in a tungsten element resistance furnace or in a graphite resistance furnace or, when large specimens were required, in a graphite crucible placed inside an inductively heated graphite die. Bulk densities were measured by mercury and water displacement and microstructures were examined using a Cambridge Stereoscan

Table 1.

Analysis of starting materials

Powder	Supplier	Grade	Particle size (um)
$\text{Si}_3\text{N}_4$	H.C. Starck-Berlin	High $\alpha$	1.5 - 2.5
$\text{AlN}$	H.C. Starck-Berlin	99%	3 - 8
$\text{SiO}_2$	B.D.H.	Precipitated	
$\text{Al}_2\text{O}_3$	Alcoa	Al6	3.5
$\text{Sc}_2\text{O}_3$	Rare Earth Products	99.99	

S600 scanning electron microscope. Chemical analyses were obtained by electron probe microanalysis using a Camebax instrument at A.E.R.E. Harwell, and phase identification was carried out by X-ray diffraction using a Hagg-Guinier XDC 700 camera and  $\text{CuK}\alpha_1$  radiation. Creep resistance was measured on a compressive creep rig operating at 1225°C and 77MPa (5tsi) and oxidation resistance of loose powder (for phase identification) and solid blocks (for weight gain measurement) was determined in air in a muffle furnace at 1000°C or 1400°C.

## II.2 Phase relationships in the Sc-Si-Al-O-N system

### The $\text{Sc}_2\text{O}_3$ - $\text{SiO}_2$ system

Mixtures of  $\text{Sc}_2\text{O}_3$  and  $\text{SiO}_2$ , hot-pressed for 1h at 1700°C show the existence of two ternary silicates,  $\text{Sc}_2\text{SiO}_5$  and  $\text{Sc}_2\text{Si}_2\text{O}_7$ . The latter is well known as the mineral thortveitite but the orthosilicate has not been fully characterized and its X-ray pattern is given in Table 2. The d spacings are not in good agreement with those of Toropov and Vasil'eva (1) but otherwise the present results support their phase diagram for the  $\text{Sc}_2\text{O}_3$ - $\text{SiO}_2$  system.

Table 2.

Observed X-ray data for  $\text{Sc}_2\text{SiO}_5$  and Q-phase

$\text{Sc}_2\text{SiO}_5$		Q-phase	
d	I	d	I
5.848	w	7.631	w
5.634	m	5.182	w
3.709	ms	3.376	w
3.471	ms	2.920	s
3.210	w	2.872	s
3.005	s	2.822	s
2.879	ms	2.860	s
2.820	vs	2.497	vvw
2.722	mw	2.442	m
2.673	mw	2.344	vw
2.564	m	2.333	vw
2.493	mw	2.275	vw

### The $\text{Sc}_2\text{O}_3$ - $\text{Al}_2\text{O}_3$ system

Mixtures of  $\text{Sc}_2\text{O}_3$  and  $\text{Al}_2\text{O}_3$ , hot-pressed or pressureless sintered at 1600-1850°C for 3h show only one ternary phase with a range of homogeneity extending from 37-57m/o  $\text{Sc}_2\text{O}_3$  at 1700°C. The diffraction pattern is similar to the high temperature metastable form of  $\text{InAlO}_3$  reported by Keith and Roy (2) and indexes on a hexagonal unit cell with  $a$ , 3.23-3.30Å and  $c$ , 8.29-8.62Å. This is in satisfactory agreement with the data of Schneider et al. (3) (who indexed this phase on a rhombohedral cell for which the equivalent hexagonal cell is four times the  $a$  and twice the  $c$  of the present cell) but is completely different from the results of Toropov & Vasil'eva (1) who reported a solid solution extending from 18-34.5m/o  $\text{Sc}_2\text{O}_3$  at 1650°C and a separate phase at the  $\text{ScAlO}_3$  composition. The agreement between observed and calculated  $\sin^2\theta$  values for the present data is extremely good, but in some of the patterns there are additional weak reflections possibly due to a super-lattice.

### The Sc-Si-O-N system

Mixtures of  $\text{Sc}_2\text{O}_3$ ,  $\text{SiO}_2$  and  $\text{Si}_3\text{N}_4$  hot-pressed at 1700°C for 1h gave the products illustrated on the behaviour diagram of Figure 1. Only one quaternary phase, "Q", occurs and its d-spacings are listed in Table 2. The composition, determined by electron probe microanalysis is  $\text{Sc}_{3.0}\text{Si}_{1.1}\text{O}_{4.8}\text{N}_{1.2}$  which, within experimental error, corresponds to  $\text{Sc}_3\text{SiO}_5\text{N}$ . The lowest solidus temperature in the system is just below 1600°C and at 1700°C a large area of the silica corner is completely molten. Compositions in this region form glasses on cooling similar to the Mg-Si-O-N and Y-Si-O-N systems (4): see also Chapter III of the present report.

### The Sc-Si-Al-O-N system

A complete study of the five-component system is beyond the scope of the present work, and investigations were restricted to compositions in the 3M:4X plane ( $M = \text{Sc}, \text{Si}, \text{Al}$ ;  $X = \text{O}, \text{N}$ ) in order to determine the solubility of scandium in  $\beta'$ -sialon. Mixtures of  $\text{Si}_3\text{N}_4$ ,  $\text{AlN}$ ,  $\text{Al}_2\text{O}_3$  and  $\text{Sc}_2\text{O}_3$  of overall composition  $\text{Si}_3(\text{Sc}, \text{Al})_3\text{O}_3\text{N}_5$ , hot-pressed at 1700°C for 1h gave a  $z = 1$   $\beta'$ -sialon plus a distorted 15R-sialon plus small amounts of other unknown phases. The intensities of the  $\beta'$  X-ray reflections were identical to those of normal  $\beta'$ -sialon and electron probe microanalysis confirmed that no scandium was present in the structure. This was true for all samples analysed. The 15R phase indexed on a hexagonal cell with  $a$ , 3.073Å and  $c$ , 40.93Å compared with the normal values  $a$ , 3.010Å and  $c$ , 41.81Å and electron probe results gave the

composition as  $\text{Sc}_{0.55}\text{Si}_{1.22}\text{Al}_{3.13}\text{O}_{2.41}\text{N}_{3.69}$ , i.e. 4.9M:6.1X which, within experimental error, corresponds to the 5M:6X composition expected for a 15R polytype and shows that approximately half the octahedrally coordinated aluminium has been replaced by scandium.

### II.3 Densification

Silicon nitride can be hot-pressed to maximum density using 2w/o  $\text{Sc}_2\text{O}_3$  at 1700°C. Densification starts at 1600°C and compared with other additives (Figure 2) proceeds very rapidly as the temperature increases. With an additional 1w/o  $\text{Al}_2\text{O}_3$ , densification is possible using only 1w/o  $\text{Sc}_2\text{O}_3$  because a liquid phase is formed at much lower temperatures ( $\sim 1400^\circ\text{C}$ ). Without applied pressure silicon nitride cannot be densified significantly using scandia alone (see Figure 3) because at the temperature required, appreciable volatilisation of silicon monoxide and nitrogen occurs. When alumina is present, densification starts at a lower temperature and for example 2.5w/o  $\text{Sc}_2\text{O}_3$  + 2.5w/o  $\text{Al}_2\text{O}_3$  gives > 90% theoretical density after 15 minutes at 1700°C (Figure 4). Increasing the total amount of additive and varying the  $\text{Sc}_2\text{O}_3$ : $\text{Al}_2\text{O}_3$  ratio failed to improve significantly this value.

The kinetics of densification are interpreted using the Kingery model (5) modified by the correction of Prill et al. (6) to allow for the large amounts of liquid present at hot-pressing temperatures. For prismatic particles a plot of  $\log(\Delta l/l_r)$  against  $\log(t-t_r)$  (where  $\Delta l$  is the shrinkage, measured from the end of rearrangement,  $t_r$ , at which time the specimen length is  $l_r$ ), should give a straight line of slope 1/3 if the rate-limiting step is solution or precipitation, and of slope 1/5 if the rate-limiting step is diffusion through the liquid. In all cases, slopes of 1/3 were observed (Figure 5); this corresponds to the presence of a large volume of low-viscosity liquid and is the most common regime in all sialon systems (7). As the solution-precipitation stage proceeds  $\alpha\text{-Si}_3\text{N}_4$  transforms to  $\beta$  ( $\beta'$ ) and Figure 6(a) shows the variation of  $\alpha:\beta$  ( $\beta'$ ) ratio with time for silicon nitride hot-pressed with 2w/o  $\text{Sc}_2\text{O}_3$ . The transformation shows first order kinetics and the activation energy for transformation, determined by the slope of the Arrhenius plot (Figure 6(b)) is in reasonable agreement with the dissociation energy for a silicon-nitrogen bond ( $435 \pm 38 \text{ kJmol}^{-1}$ ) which has been found for  $\alpha:\beta$  or  $\alpha:\beta'$  transformation in other sialon systems (7).

### II.4 Property measurements

#### Oxidation resistance

Table 3 shows the relative weight gains of samples oxidized for 120 hours at 1000°C. The  $\text{Sc}_2\text{O}_3$  +  $\text{Y}_2\text{O}_3$  materials show

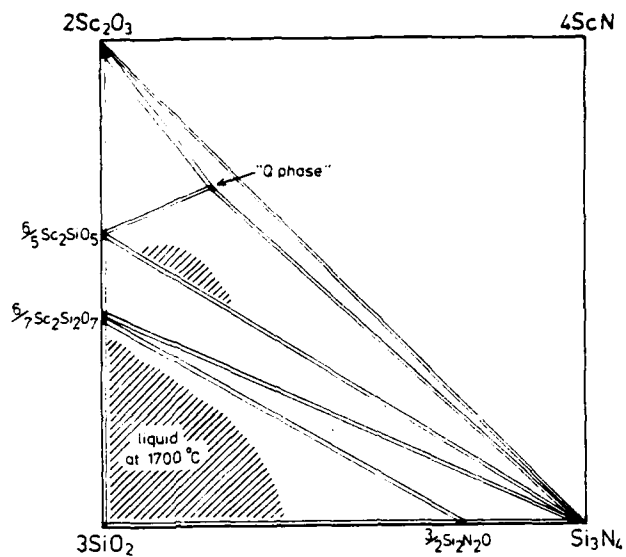


Figure 1. The behaviour diagram of the Sc-Si-O-N system at 1700°C

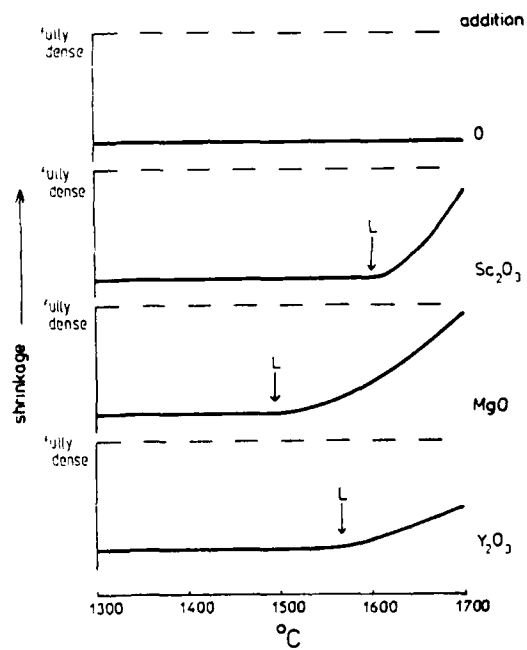


Figure 2. Shrinkage v. temperature for 5w/o additives in hot-pressed  $\text{Si}_3\text{N}_4$

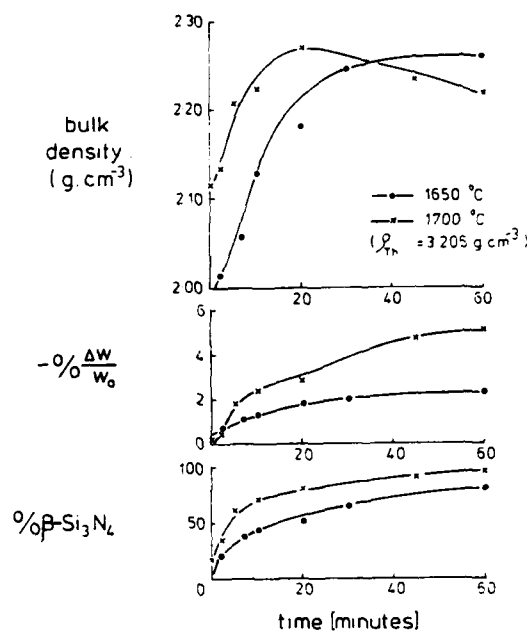


Figure 3. Pressureless sintering  $\text{Si}_3\text{N}_4$  with 2w/o  $\text{Sc}_2\text{O}_3$  at 1650 and 1700°C

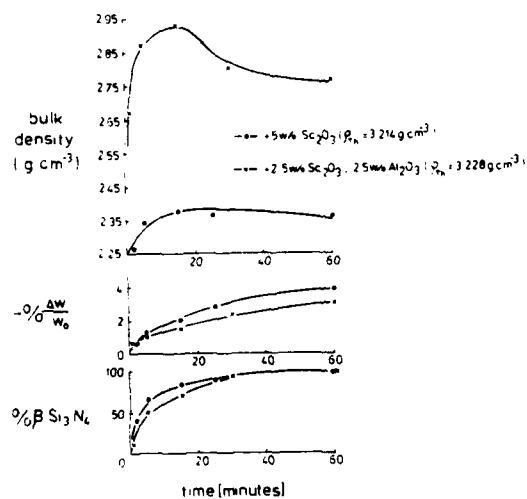


Figure 4. Effect of replacing  $\text{Sc}_2\text{C}_3$  by  $\text{Al}_2\text{C}_3$  in pressureless sintering of  $\text{Si}_3\text{N}_4$  at 1700°C

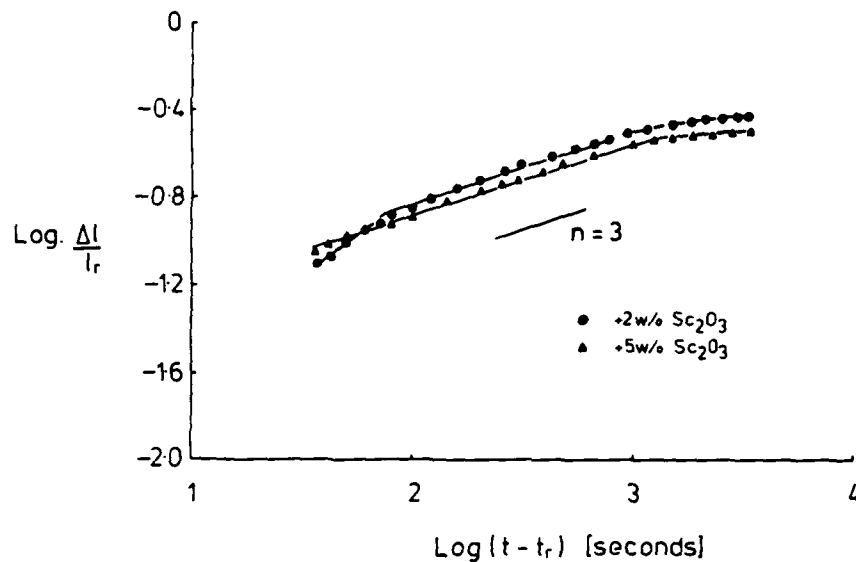


Figure 5(a) Log shrinkage v. log time for  $\text{Si}_3\text{N}_4$  hot-pressed with 2 and 5w/o  $\text{Sc}_2\text{O}_3$  at  $1700^\circ\text{C}$

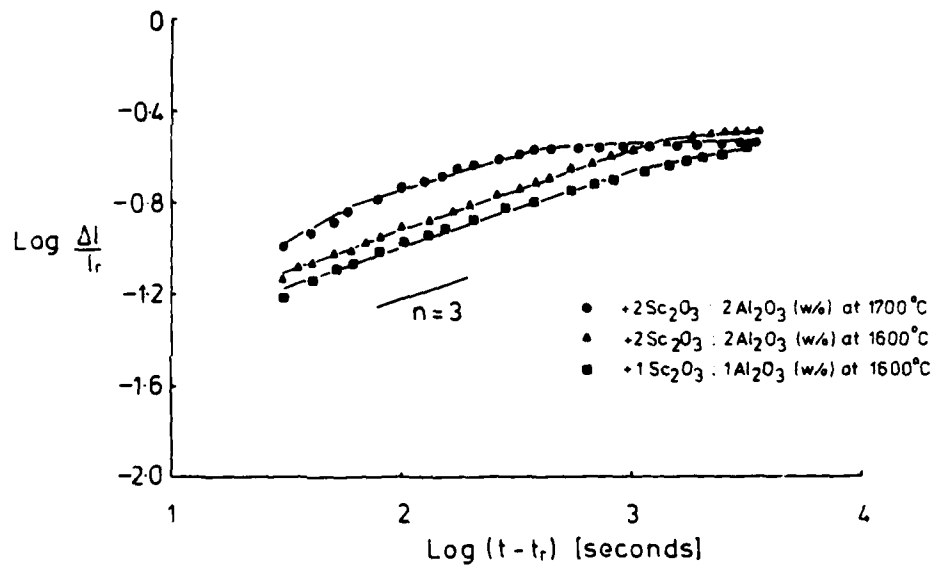


Figure 5(b) Log shrinkage v. log time for  $\text{Si}_3\text{N}_4$  hot-pressed with  $\text{Sc}_2\text{O}_3 + \text{Al}_2\text{O}_3$



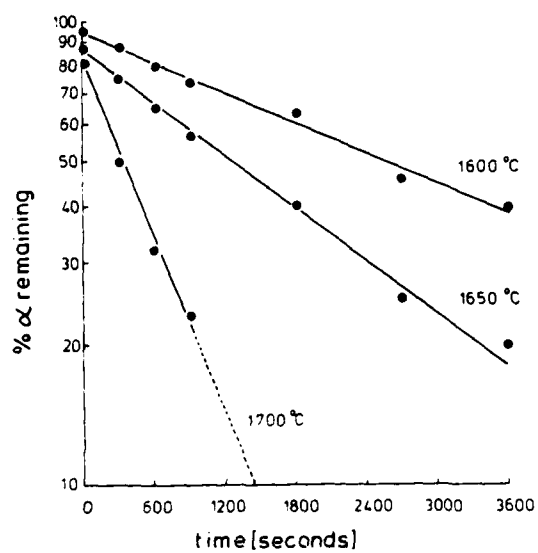


Figure 6(a) Log transformation rate v. time for  $\text{Si}_3\text{N}_4$  hot-pressed with 2w/o  $\text{Sc}_2\text{O}_3$

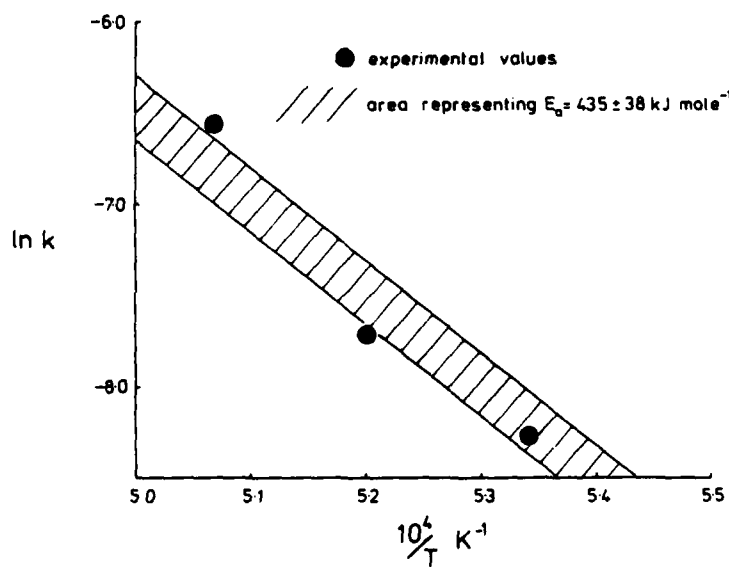


Figure 6(b) Arrhenius plot based on the data of Figure 6(a)

very poor oxidation resistance because they both contain small amounts of an unknown phase which undergoes catastrophic oxidation similar to the nitrogen melilite in the Y-Si-O-N system (8). In the remaining samples oxidation generally increases with increasing total amount of additive but the surfaces are not seriously corroded. At 1400°C (Table 3), weight gains are usually larger and compositions densified with  $\text{Sc}_2\text{O}_3$  alone give the best results.  $\text{Sc}_2\text{O}_3 + \text{Al}_2\text{O}_3$  materials show an unexpected improvement after passing through the 2w/o level probably because this composition is closest to the eutectic in the ternary oxide system. The surface oxide layer is much thicker in this sample (see Figure 7) and the large bubbles suggest that at 1400°C the surface was quite viscous. EDAX analysis shows enrichment of scandium and calcium (present as impurity) at the surface due to cation diffusion through the grain boundaries (9).

#### Creep resistance

The creep behaviour of  $\text{Si}_3\text{N}_4 + \text{Sc}_2\text{O}_3$  materials at 1225°C and 77MPa (5tsi) shown in Figure 8 indicates enhanced creep as the level of additive and hence the amount of glassy phase is increased. Figure 9 compares  $\beta'$ -sialons of similar composition prepared from  $\text{Si}_3\text{N}_4$  and 15R sialon (b,y) or  $\text{Si}_3\text{N}_4$ , AlN and

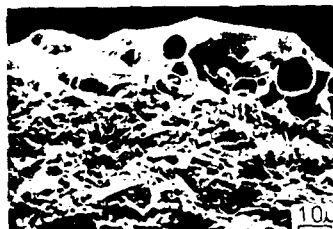
Table 3

Oxidation of hot-pressed  $\text{Si}_3\text{N}_4$  in air

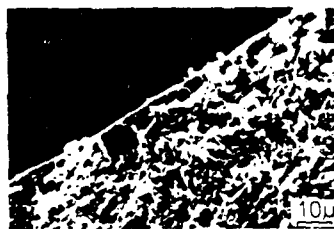
Additive	Weight gain after 120h at 1000°C ( $\text{mgcm}^{-2}$ )	Weight gain after 100h at 1400°C ( $\text{mgcm}^{-2}$ )
$2\text{Sc}_2\text{O}_3$	0.02	0.25
$5\text{Sc}_2\text{O}_3$	0.13	0.51
$10 \text{Sc}_2\text{O}_3$	0.50	0.30
$1\text{Sc}_2\text{O}_3:1\text{Al}_2\text{O}_3$	0.02	0.60
$2\text{Sc}_2\text{O}_3:2\text{Al}_2\text{O}_3$	0.46	1.00
$5\text{Sc}_2\text{O}_3:5\text{Al}_2\text{O}_3$	0.45	0.28
$2.5\text{Sc}_2\text{O}_3:2.5\text{Y}_2\text{O}_3$	2.43	0.87
$5\text{Sc}_2\text{O}_3:5\text{Y}_2\text{O}_3$	2.62	0.51
$5\text{Y}_2\text{O}_3:5\text{SiO}_2$	0.02	0.48
2MgO	0.02	1.29



+1Al<sub>2</sub>O<sub>3</sub> .  
1Sc<sub>2</sub>O<sub>3</sub> (w%)



+2Al<sub>2</sub>O<sub>3</sub> .  
2Sc<sub>2</sub>O<sub>3</sub> (w%)



+5Al<sub>2</sub>O<sub>3</sub> .  
5Sc<sub>2</sub>O<sub>3</sub> (w%)

Figure 7. Scanning electron micrographs of the surfaces of Si<sub>3</sub>N<sub>4</sub> hot-pressed with increasing amounts of Sc<sub>2</sub>O<sub>3</sub> + Al<sub>2</sub>O<sub>3</sub> and oxidised for 100h at 1400°C

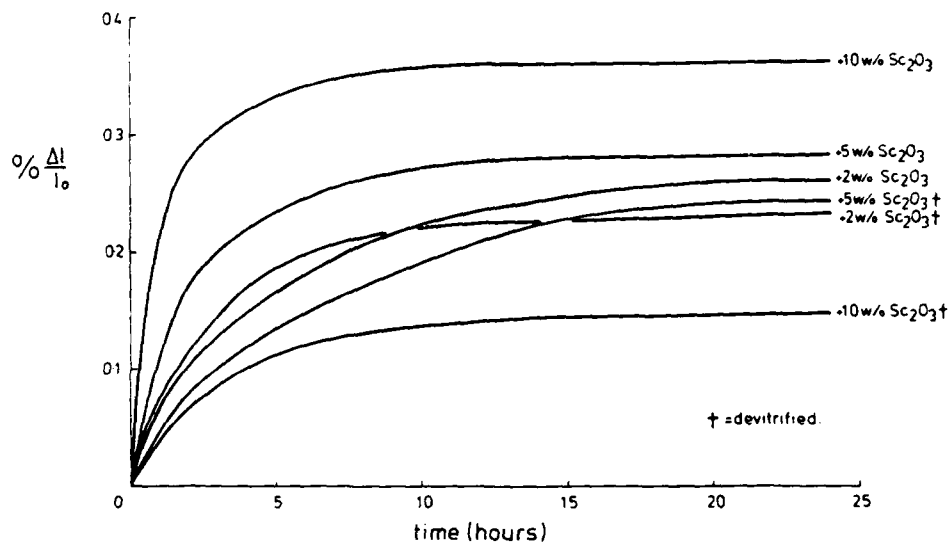


Figure 8. Creep resistance (1225°C, 77 MPa) of  $\text{Si}_3\text{N}_4$  hot-pressed with increasing amounts of scandia at 1700°C. The runs were repeated on material devitrified for 5 days

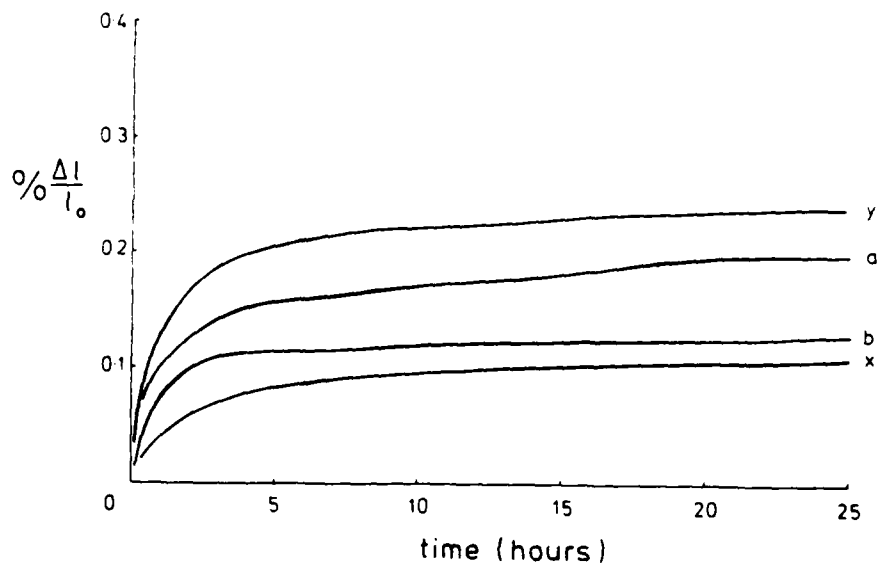


Figure 9. Creep resistance (1225°C, 77 MPa) of  $z = 0.75$   $\beta'$ -sialon hot-pressed at 1700°C from:

- (a)  $\text{Si}_3\text{N}_4$ , AlN,  $\text{Al}_2\text{O}_3$  + 3w/o  $\text{Y}_2\text{O}_3$
- (b)  $\text{Si}_3\text{N}_4$ , 15F + 3w/o  $\text{Y}_2\text{O}_3$
- (x)  $\text{Si}_3\text{N}_4$ , AlN,  $\text{Al}_2\text{O}_3$  + 3w/o  $\text{Sc}_2\text{O}_3$
- (y)  $\text{Si}_3\text{N}_4$ , 15F + 3w/o  $\text{Sc}_2\text{O}_3$

$\text{Al}_2\text{O}_3$  (a,x) hot-pressed with either 3w/o  $\text{Sc}_2\text{O}_3$  (x,y) or 3w/o  $\text{Y}_2\text{O}_3$  (a,b). The slopes of the secondary stages of the curves are very similar and the differences in total compaction can be correlated with slight differences in porosity rather than with starting composition or additive. Further work is needed, but the implication is that comparable scandium and yttrium sialon compositions have similar creep behaviour.

## II.5 Conclusions

Scandia is a promising additive for nitrogen ceramics in that it performs the basic role of an additive viz: reaction with silica and alumina to form a high temperature liquid which can dissolve silicon nitride and hence promote densification and  $\alpha$ - $\beta'$  conversion. As yet it is impossible to say whether scandia is better than yttria because the processing variables have not been optimised. However, scandia does have the following advantages over yttria:

- (i) Scandia forms only one quaternary phase ( $\text{Sc}_3\text{SiO}_5\text{N}$ ) in the Sc-Si-O-N system which, in contrast with the yttrium silicon oxynitrides, shows good oxidation resistance at 1000°C;
- (ii) Liquid phases occur in the Sc-Si-O-N and Sc-Si-Al-O-N systems at slightly higher temperature than in the corresponding yttrium systems. This should give some improvement in high-temperature properties - particularly oxidation resistance;
- (iii) Compositions which give  $\beta'$ -sialon plus yttrium aluminium garnet (YAG) in the yttrium sialon system give  $\beta'$  plus  $(\text{Sc,Al})_2\text{O}_3$  in the scandium sialon system. The variability in oxide composition might allow increased flexibility in the choice of starting composition;
- (iv) The existence of scandium-containing polytype phases allows  $\beta'$ -sialons to be prepared from only two starting powders. This should promote more uniform reaction and give a more homogeneous product provided that sufficient liquid is available for densification.

Most of these points require further exploration but there is good reason to expect that this will lead to improved materials with properties at least as good as current  $\beta'$  yttrium sialons.

### III. NITROGEN GLASSES

#### III.1 Introduction

The mechanical properties of silicon nitride and  $\beta'$ -sialons at elevated temperatures are often controlled by the presence of a grain boundary glass and in the first investigation (10) of the role of magnesia in hot-pressed silicon nitride, the glass formed by cooling the "magnesium silicate" liquid gave silicon oxynitride as one of its devitrification products and so must have contained nitrogen. Further evidence of this was provided by Nuttall and Thompson (11) who found well-formed hexagonal  $\beta$ - $\text{Si}_3\text{N}_4$  crystals nucleated and grown from the grain boundary liquid.

Small concentrations of nitrogen in oxide glasses were reported (12, 13) to increase their softening temperature, viscosity and resistance to devitrification. Studies of the reaction kinetics of  $\text{Si}_3\text{N}_4$  with oxide glass melts (14, 15) led to a proposed mechanism for incorporating nitrogen as nitride groups in the glass under reducing conditions. The solubility of up to 3a/o nitrogen in aluminosilicate slag melts (16) was confirmed as a chemical phenomenon and suggestions were made concerning the exchange of nitrogen for bridging oxygens in the glass structure.

Jack (17, 18) was the first to report the accommodation of much greater concentrations of nitrogen (up to 10a/o) in glasses, e.g. in the Mg-Si-Al-O-N and Y-Si-Al-O-N systems. The formation of Mg-Si-O-N glasses is remarkably easy as shown by the series of X-ray photographs of Figure 10. When mixtures of 20w/o MgO:80w/o  $\text{SiO}_2$  are heated at 1700°C without  $\text{Si}_3\text{N}_4$  the products, as expected, are crystalline protoenstatite and cristobalite. Addition of 10w/o  $\text{Si}_3\text{N}_4$  to this same mix gives, after the same treatment, a completely vitreous product that can be devitrified to give cristobalite, clinoenstatite and silicon oxynitride.

Additions of  $\text{Al}_2\text{O}_3$  to Mg-Si-O-N compositions extends the vitreous region and mixtures of  $\text{MgO}$ ,  $\text{SiO}_2$  and AlN give glasses with up to 10a/o N (18). Further work on this and the Y-Si-Al-O-N system (19) investigated glass forming regions in the sub-systems MgO- $\text{SiO}_2$ -AlN and  $\text{Y}_2\text{O}_3$ - $\text{SiO}_2$ -AlN but these do not necessarily include the regions of maximum nitrogen solubility in the complete five-component systems.

Following the work at Newcastle, Loehman (20) used  $\text{Y}_2\text{O}_3$ : $\text{SiO}_2$ :AlN mixtures to prepare glasses containing up to 7a/o N and reported that glass transition temperature, hardness and fracture toughness all increased with increasing nitrogen content.

The ease of shaping glasses and the possibility of producing glass-ceramics (21) in which the crystalline phases are refractory nitrides and oxynitrides suggest that nitrogen-containing glasses are well worth scientific and technological investigation.

### III.2 Experimental

#### Preparation of glasses

Investigation of glasses in the sub-system explored previously at Newcastle (19) and by Loehman (20) cannot satisfactorily determine the full extent of glass formation in the whole of a system. Using the triangular prism representation (22) illustrated in Figure 11, the glass-forming region on a plane of constant O:N ratio was determined in the present work at a particular temperature, varying only the cation ratios. Having established the glass region for one plane, planes of progressively increasing N:O ratio were then studied until the limit of nitrogen solubility was reached.

Powder mixtures of  $\text{SiO}_2$ ,  $\text{Al}_2\text{O}_3$ ,  $\text{AlN}$ ,  $\text{Si}_3\text{N}_4$  and the appropriate metal oxide were dry-mixed, cold-pressed into cylindrical pellets and fired in a boron nitride crucible in a tungsten element resistance furnace in purified nitrogen for one hour at the required temperature. The cooling rate was approximately  $200^\circ\text{Cmin}^{-1}$  but fast cooling rates were only important near the limits of the glass-forming region.

All samples were examined by X-ray diffraction to identify crystalline phases and by scanning electron microscopy to assess homogeneity. Selected samples were analysed by electron probe micro-analysis at A.E.R.E. Harwell, using "Camebax" equipment capable of analysing simultaneously for three or more heavy elements with an energy-dispersive analyser and two light elements (O and N) on wavelength-dispersive spectrometers. This allows a comparison of initial and final compositions.

#### Properties of glasses

The glass transition,  $T_g$ , was detected by DTA using a Stanton-Redcroft 873-4 differential thermal analyser. Since there is a change in specific heat at  $T_g$ , the value of  $dH/dT$  changes and causes an endothermic drift in the  $\Delta T$  trace, the minimum point of which corresponds to the end of the transition range. DTA also detects the glass crystallisation temperature  $T_c$ , usually as an exothermic peak.

Viscosities were measured using a high temperature deformation-under-load apparatus. The viscosities of "Spectrosil" vitreous silica, measured over a temperature range  $1000^\circ\text{--}1300^\circ\text{C}$  as a standard to check the validity of the method, were in good agreement with those reported by Hetherington et al. (23) on the same material using a fibre elongation method.

Devitrification was carried out in standard laboratory tube furnaces in a nitrogen atmosphere.

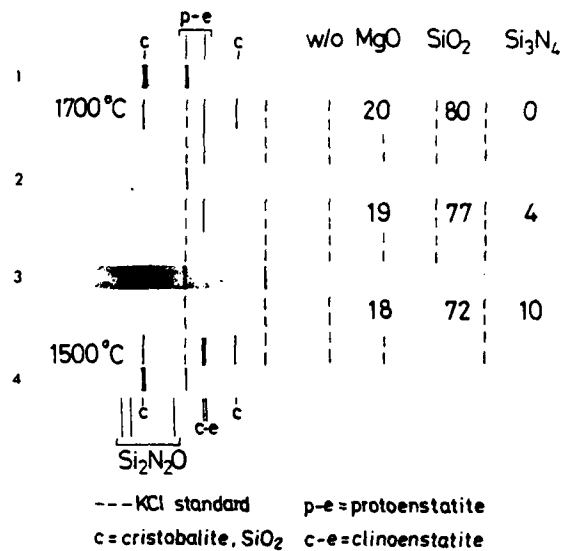


Figure 10. X-ray photographs showing Mg-Si-O-N glass formation and devitrification

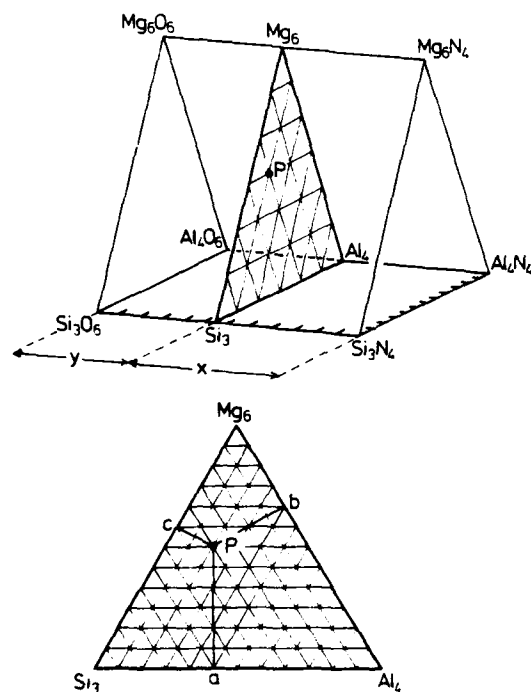


Figure 11. Representation of a five-component system (e.g. Mg-Si-Al-O-N) showing a plane of constant N:O ratio



The "immersion technique" was used for refractive index measurements and UV and IR transmission spectra were obtained with a Beckman DK2A recording spectrophotometer.

### III.3 Results and discussion

#### Glass formation

Hampshire and Jack (24) showed that nitrogen lowers the eutectic temperature in metal oxide-silica systems. Qualitative observations during and after firing suggest that nitrogen increases the viscosity of the liquid and this, combined with a lower solidus and hence a larger melting range, reduces the tendency to undergo a discontinuous change from liquid to solid and increases the tendency to form a glass. Thus, although glass formation does not occur in the  $\text{MgO-SiO}_2$  system (see previous section), it does in  $\text{Mg-Si-O-N}$  and Figure 12 shows the small, homogeneous glass region on cooling from  $1700^\circ\text{C}$  at about  $200^\circ\text{Cmin}^{-1}$ . By cooling from below  $1650^\circ\text{C}$  and also in the more  $\text{SiO}_2$ -rich compositions from higher temperatures, phase-separated glasses are obtained. Similar regions are found in the  $\text{Ca-Si-O-N}$ ,  $\text{Y-Si-O-N}$  and  $\text{Ce-Si-O-N}$  systems, though in the latter two cases glass preparation is difficult and is usually accompanied by bloating and high weight losses due to nitrogen evolution.

In  $\text{M-Si-Al-O-N}$  systems (where M is Mg, Y or Ca), the vitreous regions are much more extensive and the glasses are completely homogeneous. Typical glass forming regions at different equivalent concentrations of nitrogen in the different systems are shown in Figure 13; Figure 13(d) for  $\text{Ca-Si-Al-O-N}$  illustrates how nitrogen solubility increases with temperature.

A three dimensional representation of the complete glass region in the  $\text{Mg-Si-Al-O-N}$  system is shown in Figure 14. Starting from the oxide face and with increasing replacement of oxygen by nitrogen, the extent of the glass region at first expands and then contracts above about 10e/o N with a simultaneous shift towards slightly more Al-rich compositions.

Although magnesium is usually octahedrally co-ordinated by oxygen and is a "net-work modifier" in oxide glasses, the  $\text{Mg}^{2+}$  cation has a high field strength similar to that of "intermediate oxide" cations. In nitrides it is always tetrahedrally coordinated by nitrogen and so in oxynitride glasses it is undoubtedly a "net-work former". This explains why replacement of oxygen by nitrogen facilitates glass formation in some systems, e.g.  $\text{Mg-Si-O-N}$ ,  $\text{Mg-Si-Al-O-N}$  and  $\text{Ca-Si-Al-O-N}$ . At the same time, the more covalent and directional bonding of nitrogen compared with oxygen increases the tendency to crystallisation and results in a limit to glass formation when, depending upon

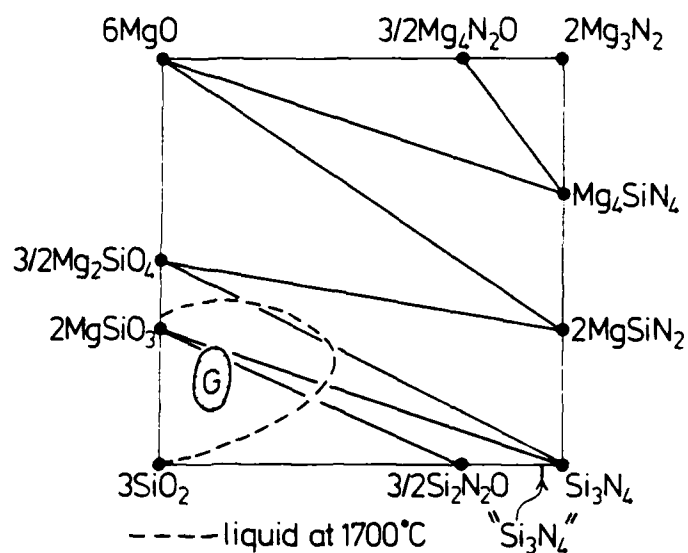


Figure 12. Glass formation in the Mg-Si-C-N system: cooled from 1700°C at 200°C min<sup>-1</sup>

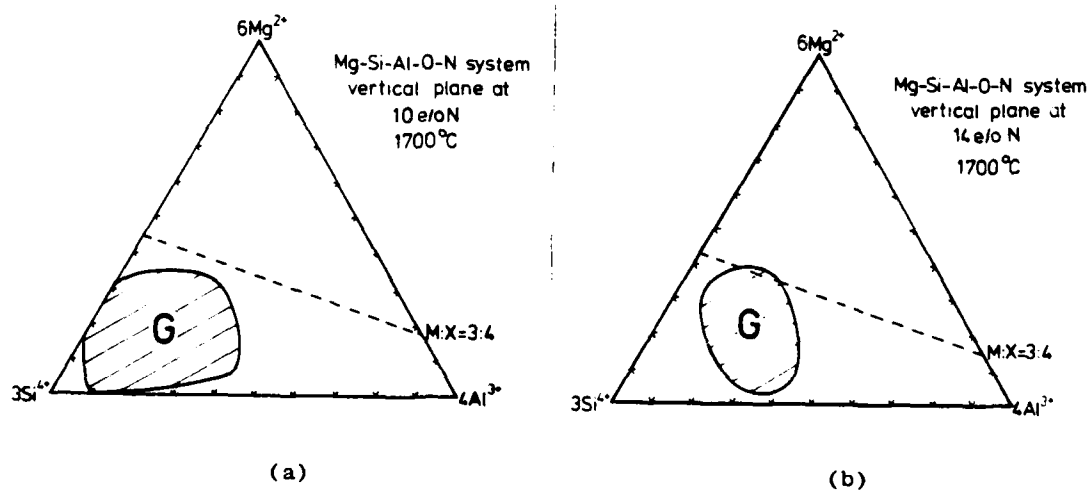


Figure 13. Glass forming regions in M-Si-Al-C-N systems (M = Mg, Y, Ca) at different equivalent compositions of nitrogen

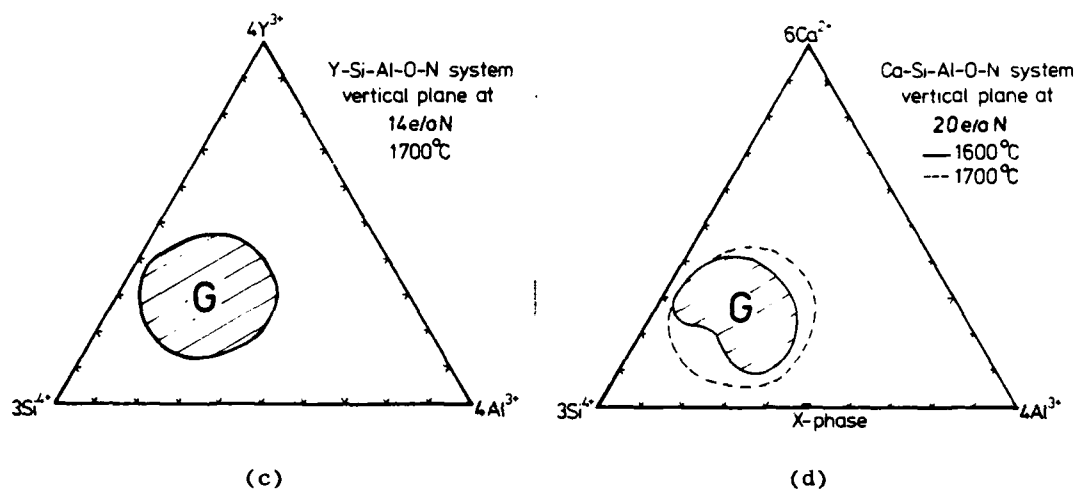


Figure 13. (continued)

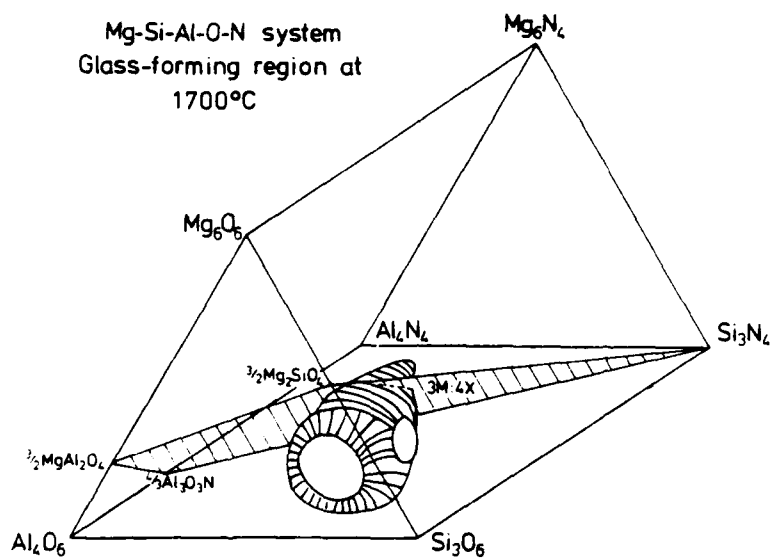


Figure 14. Glass forming region of the Mg-Si-Al-O-N system on cooling from 1700°C

the system, 25-35e/o of oxygen atoms are replaced by nitrogen.

At 22e/o N in Mg-Si-Al-O-N the glass region is fairly small and now passes through the 3M:4X plane. The limit of glass formation is at about 25e/o N (10.3a/o) and corresponds to a composition  $\text{Mg}_{22.9}\text{Si}_{16.7}\text{Al}_{3.7}\text{O}_{46.4}\text{N}_{10.3}$  in which 1 in 5.5 oxygen atoms have been replaced by nitrogen. The glass region in Ca-Si-Al-O-N is similar with a maximum nitrogen content of 26e/o N (11a/o) corresponding to  $\text{Ca}_{18}\text{Si}_{18}\text{Al}_6\text{O}_{47}\text{N}_{11}$ .

The three dimensional representation of the glass region in the Y-Si-Al-O-N system is shown in Figure 15. The expansion away from the oxide face at 10e/o N is less than in Mg-Si-Al-O-N but the maximum nitrogen solubility is much greater. Recently, a glass  $\text{Y}_{15}\text{Si}_{15}\text{Al}_{10}\text{O}_{45}\text{N}_{15}$  has been produced, i.e. in which one of every four oxygens is replaced by nitrogen.

Lang et al. (25) obtained glassy phases at 1350°C in various Ln-Si-Al-O-N systems. In the present work, Nd-Si-Al-O-N glasses have been prepared with up to 25e/o N and glass formation is generally similar to that in the Y-Si-Al-O-N system.

In the Si-Al-O-N system without modifier additions, the liquid region at 1700°C is extensive (26, 27, 28) and Roebuck (27) has reported the formation of glass by rapid cooling. Present work shows that these glasses are unstable and require a liquid quench at greater than  $500^\circ\text{Cmin}^{-1}$  to obtain a completely vitreous product. Cooling at these rates from 1700°-1850°C gives glasses within the composition region shown by Figure 16. The liquid close to the sialon X-phase composition is very fluid but the viscosity increases rapidly for a given temperature as the composition approaches the silica ( $\text{Si}_3\text{O}_6$ ) corner. However, weight losses also increase due to volatilisation in the reducing environment of the graphite furnace i.e.  $\text{SiO}_2 + \text{C} \rightarrow \text{SiO} + \text{CO}$ .

#### Properties of nitrogen glasses

##### (a) Viscosity, glass transition and crystallization

Glasses with a fixed cation composition of 28e/o M:56e/o Si:16e/o Al and with varying N:O ratios were prepared to allow direct comparison between different M-Si-Al-O-N systems (M = Mg, Ca, Y and Nd) and the effect of replacing oxygen by nitrogen within each system.

Figure 17 shows the variation of viscosity with temperature for Y-Si-Al-O-N glasses of the standard composition containing 0, 5, 10 and 18e/o N. Clearly, nitrogen increases the glass viscosity

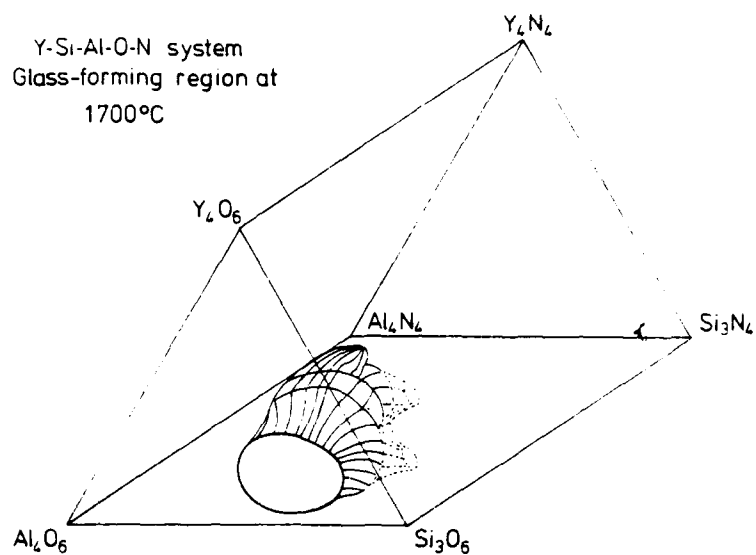


Figure 15. Glass forming region of the Y-Si-Al-O-N system on cooling from 1700°C

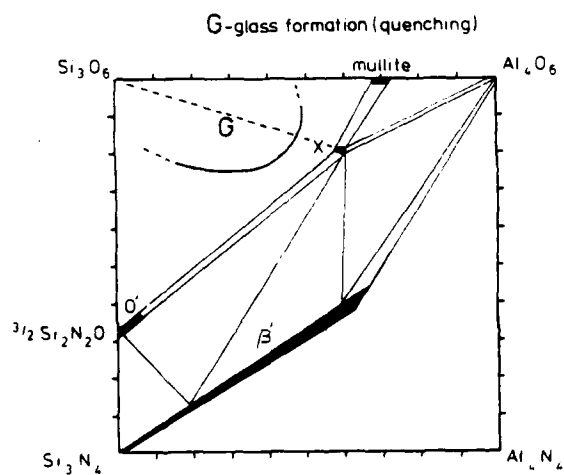
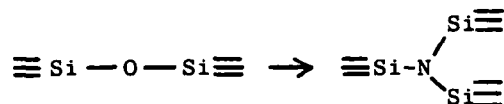


Figure 16. Glass formation on quenching from 1700-1850°C in the Si-Al-O-N system

at any temperature; similar observations are made in the other systems. Figure 18 compares the viscosities of different M-Si-Al-O-N glasses with the same cation ratios containing 18e/o N. The Y-Si-Al-O-N glasses have the highest viscosities and the Mg-Si-Al-O-N glasses the lowest with Nd and Ca intermediate. There are similar trends in the glass transition temperature with nitrogen content (see Figure 19);  $T_g$  increases by substituting nitrogen for oxygen and also by changing the modifying cation,  $Y > Nd > Ca > Mg$ . Mulfinger (14) pointed out that substitution of oxygen by nitrogen

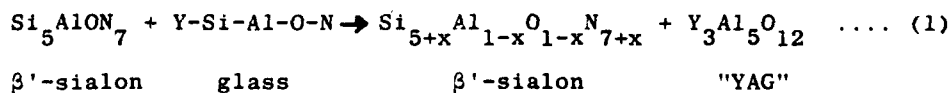


must lead to a higher average coordination of the non-metal atoms and the increased crosslinking should produce a more rigid glass network. The suggestion is strongly supported by the present observations that glass transition temperature and viscosity increase with increasing nitrogen concentration in all systems.

Figure 20 shows the shift in the  $T_g$  DTA peak to higher temperature with increasing nitrogen content for Y-Si-Al-O-N glasses; the corresponding increase in the crystallization temperature  $T_c$  is also significant. Similar changes occur in Mg-Si-Al-O-N glasses as shown in Figure 21. By contrast, Ca and Nd glasses show no such increase in  $T_c$ ; see Figure 22. For the yttrium-sialon glasses the scanning electron micrographs of Figure 23 show that the devitrification products change with changing nitrogen concentration and so  $T_c$  might be expected to change also. In the calcium glasses, gehlenite is observed as a devitrification product at all nitrogen concentrations; it has a wide range of homogeneity, probably from  $\text{Ca}_2\text{SiAl}_2\text{O}_7$  to  $\text{Ca}_2\text{Si}_3\text{O}_5\text{N}_2$ , and so its crystallization temperature might not be expected to vary too widely.

#### (b) Devitrification of vitreous phases

The liquid that is necessary for the high-temperature densification of nitrogen ceramics generally cools to give some intergranular oxynitride glass and suitable post-preparative heat-treatment to obtain refractory crystalline phases offers a method of improving properties. With  $\beta'$ -sialon pressureless sintered with yttria, the glass reacts with the matrix to give a slightly changed  $\beta'$  composition and yttrium-aluminium garnet:



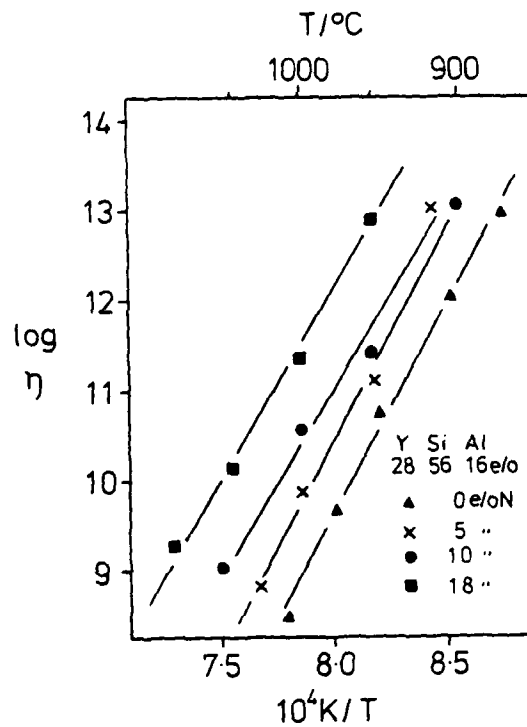


Figure 17. Variation of viscosity with temperature for Y-Si-Al-O-N glasses of different nitrogen concentrations

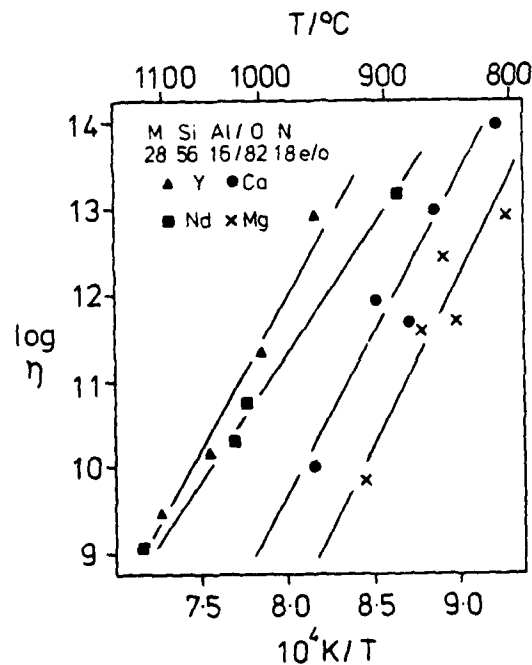


Figure 18. Viscosities of Y, Nd, Ca and Mg sialon glasses with 18e/o N and the same M-Si:Al cation ratios

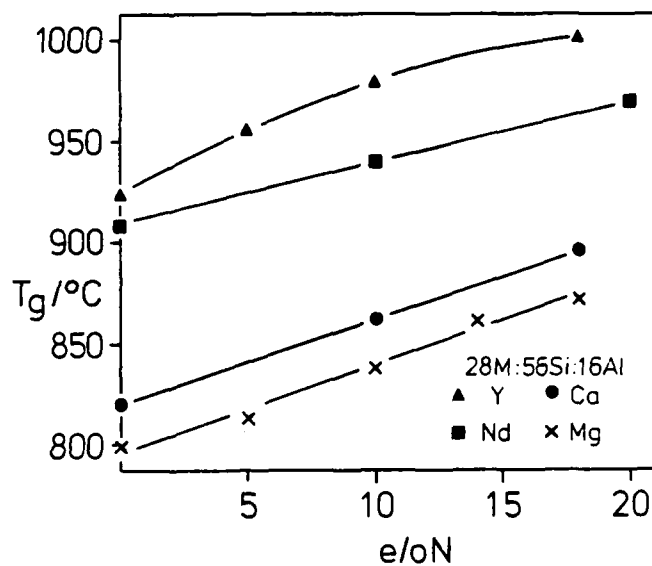


Figure 19. Variation of glass transition temperature ( $T_g$ ) with nitrogen concentration for Y, Nd, Ca and Mg sialon glasses

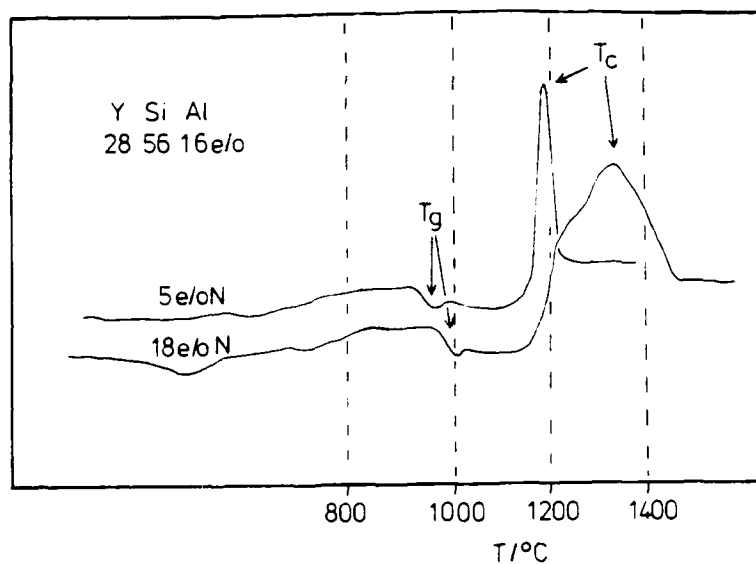


Figure 20. DTA curves for Y-Si-Al-O-N glasses containing 5e/o N and 18e/o N



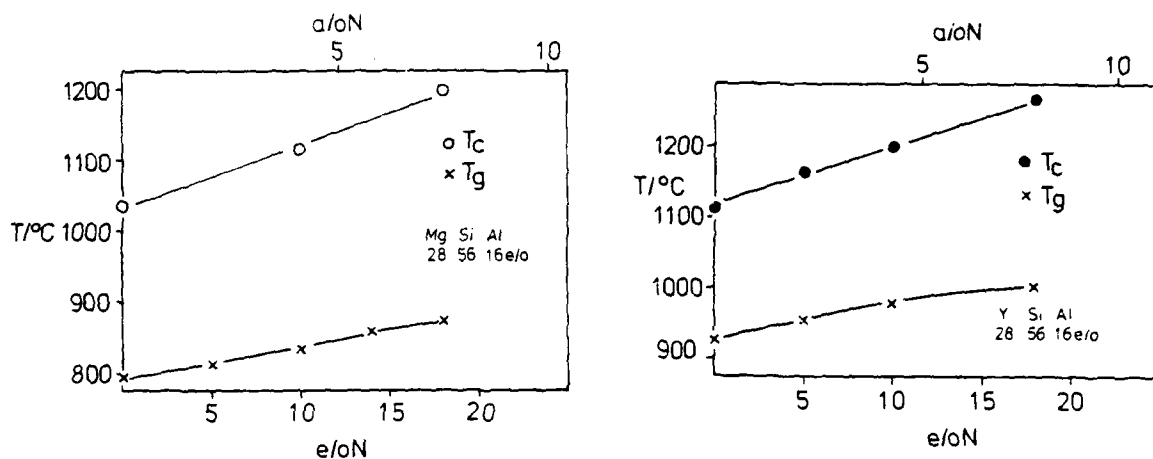


Figure 21. Variation of  $T_g$  and  $T_c$  with nitrogen concentration for Mg and Y sialon glasses

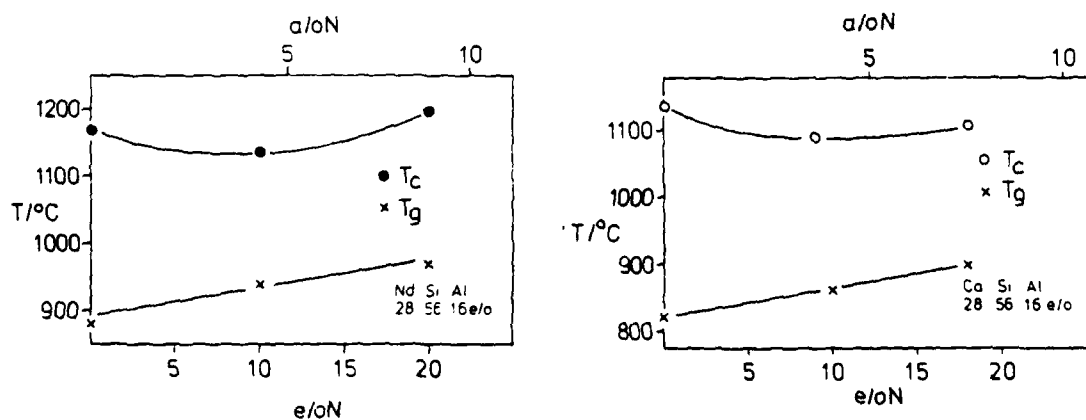


Figure 22. Variation of  $T_g$  and  $T_c$  with nitrogen concentration for Nd and Ca sialon glasses

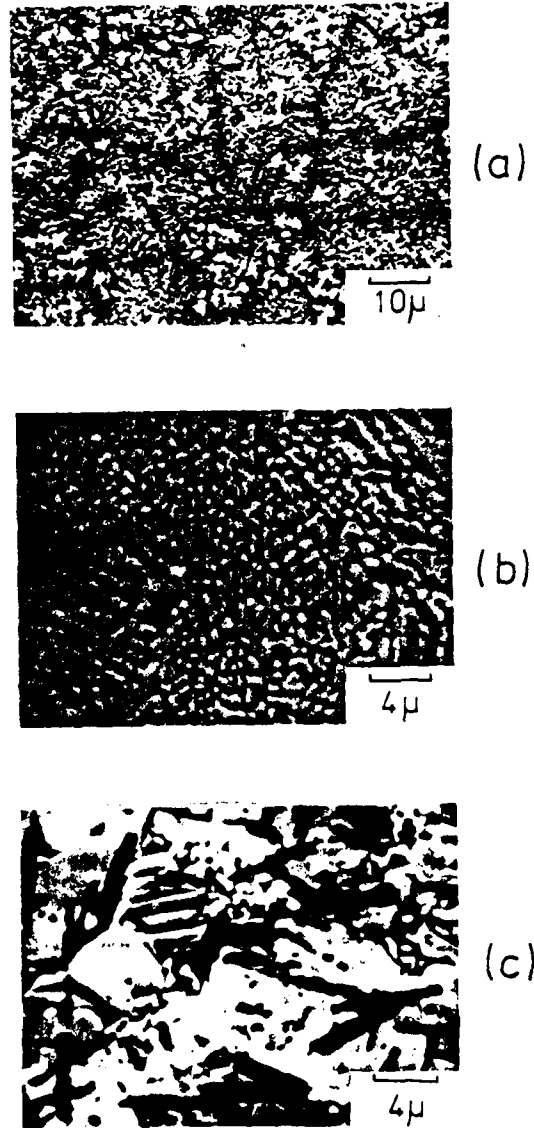
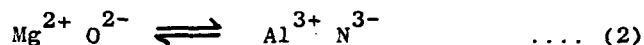


Figure 23. Scanning electron micrographs of devitrification products of Y-Si-Al-C-N glasses with different nitrogen concentrations

The phase relationships are shown schematically by Figure 24 and can be applied generally to other systems.

As with oxide glasses, devitrification can give phases, sometimes metastable, that are unobtainable by direct methods. The glass forming region of the Mg-Si-Al-O-N system protrudes through the 3M:4X plane (Figure 14) and if liquid of composition just outside this region is cooled from above 1600°C the product is glass with a small amount of dispersed  $\beta$ -Si<sub>3</sub>N<sub>4</sub>. Heating at 800-950°C devitrifies the glass to give a  $\beta''$ -phase which grows epitaxially on the  $\beta$  nuclei; see Figure 25.  $\beta''$  has a range of unit-cell dimensions larger than those of the highest-z  $\beta'$ -sialon (Figure 26). Although it has a phenacite structure, its range of composition approaches forsterite (Mg<sub>2</sub>SiO<sub>4</sub>) in which only a small proportion of O is replaced by N with simultaneous replacement of Mg by Al:



The closeness in the lattice energies of the two  $\text{M}_3\text{X}_4$  structures, forsterite and phenacite, is clearly demonstrated.

Also in the Mg-sialon system, a glass composition  $2\text{MgO} \cdot 5\text{SiO}_2 \cdot 3\text{AlN}$  partially devitrifies on cooling from 1750°C to give a phase  $\text{Mg}_2\text{SiAlO}_4\text{N}$  that is isostructural with lithium disilicate ( $\text{Li}_2\text{Si}_2\text{O}_5$ ) and with petalite ( $\text{LiAlSi}_4\text{O}_{10}$ ).

In the Y-sialon system the solid solution intermediate between N- $\alpha$ -wollastonite ( $\text{YSiO}_2\text{N}$ ) and  $\text{YAlO}_3$  is  $\text{Y}_2\text{SiAlO}_5\text{N}$ ; it is obtained by heat-treatment at 1100°C of a glass composition  $3\text{YN} \cdot 3\text{SiO}_2 \cdot \text{Al}_2\text{O}_3$  prepared by quenching from 1700°C.

#### (c) Optical and electrical properties

All glasses prepared were grey or bluish-grey, the colouration increasing with the amount of nitride in the initial mix and varying slightly with the source of silicon nitride. Thus, impurities or micro-heterogeneities are thought to be responsible for the opacity. However, Figure 27 shows that 1mm thick discs are quite transparent although the small 4mm thick blocks have greatly reduced transparencies.

Figure 28 shows typical IR and UV transmission spectra for glasses in the Ca-Si-Al-O-N system. The upper curves show that the near infra-red transmission is increased by incorporation of nitrogen; this probably lowers the concentration of structural "water" in the glass because the absorption band at 2.7 $\mu\text{m}$ , characteristic of the Si-OH stretching frequency, is no longer observed.

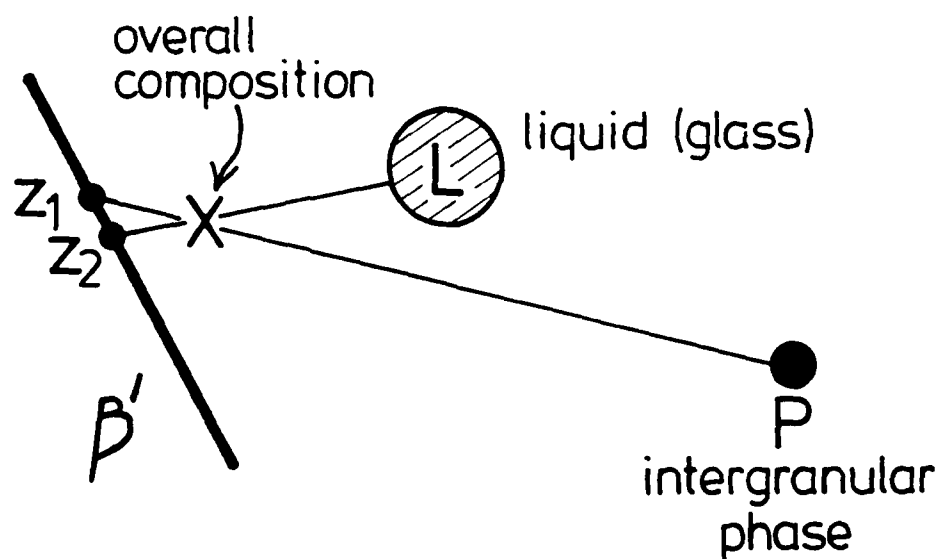


Figure 24. Phase relationships during densification and post-preparative heat-treatment of  $\beta'$ -sialon

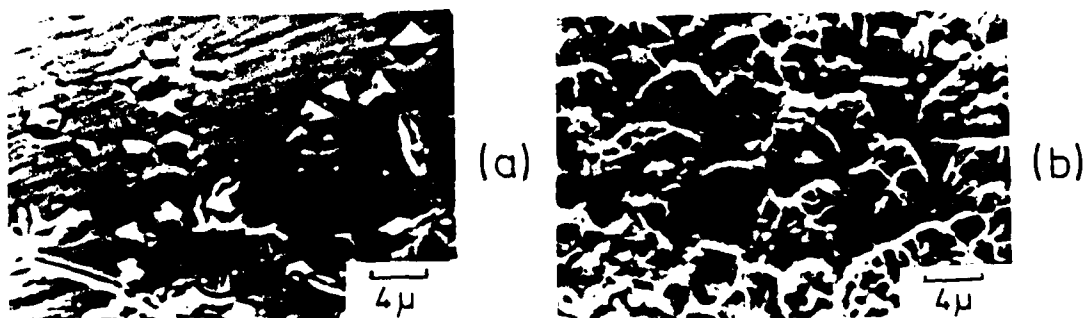


Figure 25. Formation of  $\beta''$ -Mg-sialon by devitrification

(a) glass +  $\beta$ - $\text{Si}_3\text{N}_4$  nuclei by cooling liquid from 1700°C

(b)  $\beta''$  grown epitaxially on  $\beta$  by heat-treatment at 930°C

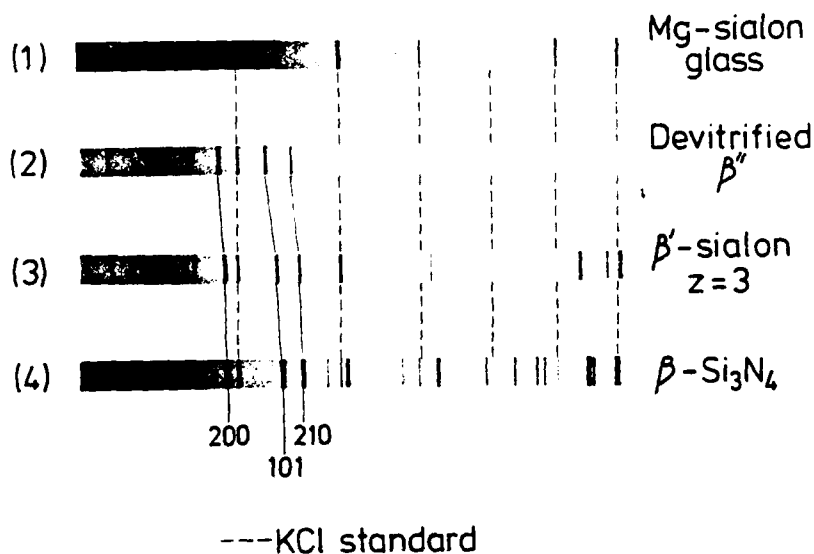


Figure 26. X-ray powder photographs of isostructural  $\beta$ - $\text{Si}_3\text{N}_4$ ,  $\beta'$  and  $\beta''$  sialons

stare.—*v.i.* to emit a hard, fierce, dazzling light: to be obtrusively noticeable: to stare fiercely.—*adj.* glar'ing, bright and dazzling: flagrant.—*adv.* glar'ingly.—*n.* glar'ingness. [*N.E.* glären, to shine; akin to glass, *O.E.* glær, amber, *L. Ger.* glaren, to glow.]

glass, gläs, *n.* a hard, brittle substance, usually transparent, generally made by fusing together a silica (as sand) with an alkali (q.v.) and another base (q.v.): an article made of or with glass, esp. a drinking-vessel, a mirror, a weather glass, a telescope, &c.: the quantity of liquid a glass holds: (*pl.*) spectacles.—*adj.* made of glass.—*v.t.* to case in glass: to furnish with glass: to polish highly.—*ns.* gl'ass-blow'ing, one process of making glass: gl'ass-blow'er; gl'ass-cl'oth a cloth for drying glasses: a material woven from

Figure 27. Transparency of 1mm thick discs and 4mm thick blocks of (i) Ca-sialon and (ii) Mg-sialon glasses, both with 18e/o N

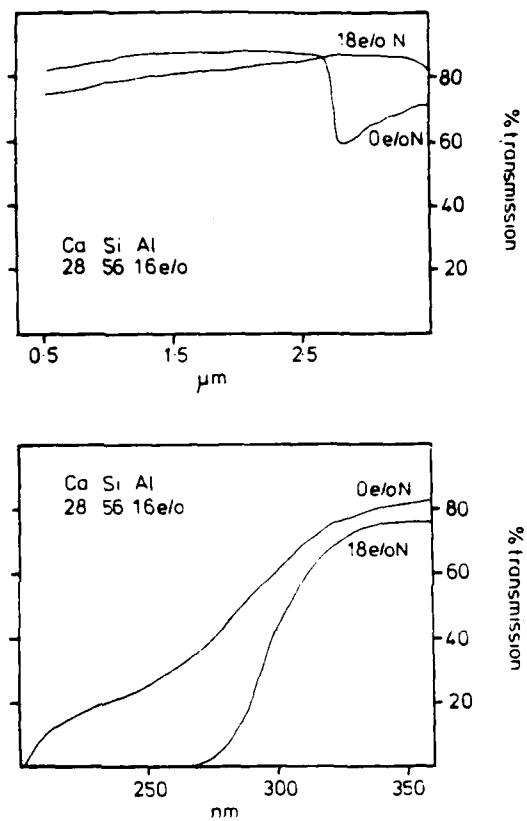


Figure 28. IR and UV transmission spectra for glasses in the Ca-Si-Al-O-N system

The UV spectra of the same glasses shown in the lower curves suggest that nitrogen impairs the UV transmission by moving the cut-off at 250nm to longer wavelengths. This effect could also be attributed to impurities introduced from the silicon nitride!

With the replacement of oxygen by nitrogen there is a significant increase in the refractive index ( $n$ ) of all glasses; see Figure 29. Because the cation ratios remain constant the increase must be due to particular features of the nitrogen bonding in the glass structure. The values now reported for Y-Si-Al-O-N glasses are much higher than those of their oxide equivalents (29) and show that nitrogen glasses might have applications based on their optical properties; the refractive indices of the Nd-sialon glasses are even higher.

The electric properties reported by Thorp and Kenmuir (30) on calcium and magnesium sialon glasses prepared at Newcastle show that  $\epsilon'$ , the real part of the dielectric constant, fits well with the Universal dielectric response law

$$(\epsilon' - \epsilon_{\infty}) \propto \omega^{(n-1)} \quad \dots (3)$$

with  $n = 0.99 \pm 0.02$ . With increasing nitrogen,  $\epsilon'$  increases. The conductivities (see Figure 30) vary as expected for a hopping conductivity mechanism in that  $\sigma_{ac} \propto \omega^n$ , with  $n$  agreeing with the value found from the  $\epsilon'$  data. The conductivities and the increases in  $\epsilon'$  due to nitrogen are similar to those found for yttrium sialon glasses by Leedecke and Loehman (31).

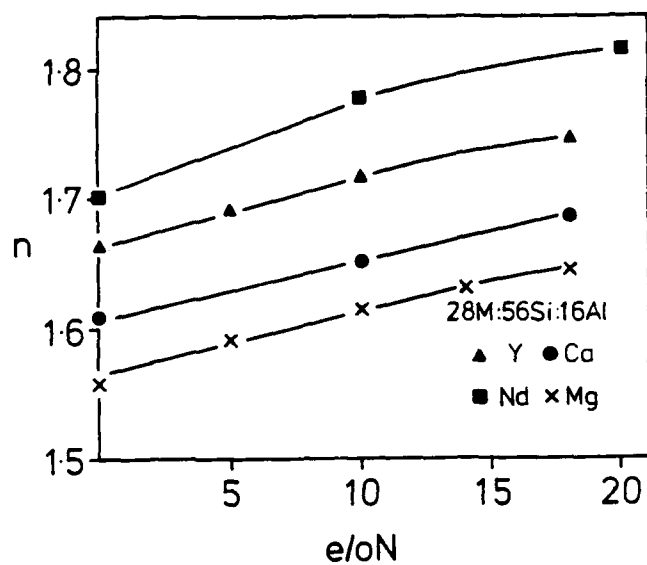


Figure 29. Refractive indices of Mg, Ca, Y and Nd sialon glasses

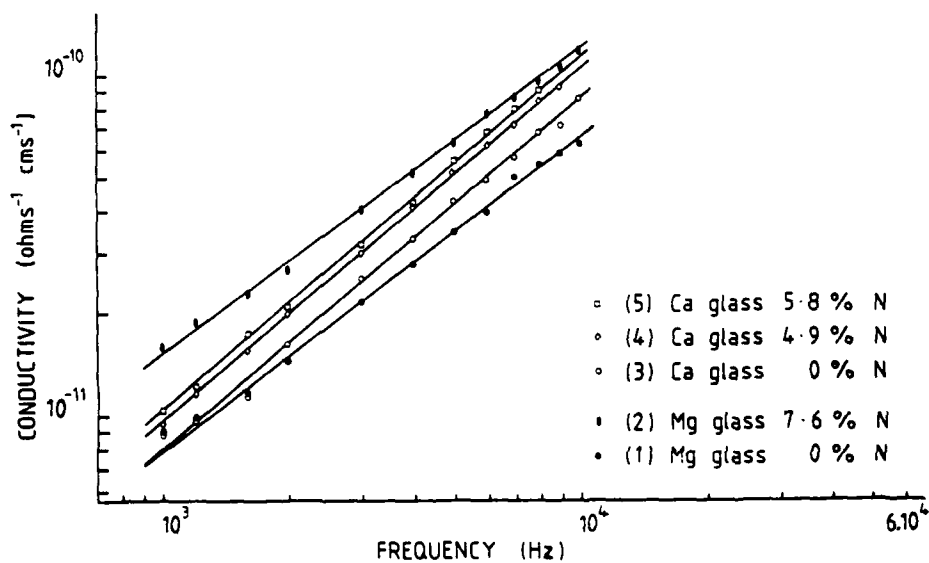


Figure 30. Dependence of a.c. electrical conductivity on frequency and composition for Ca and Mg sialon glasses



#### IV. THE STRUCTURAL CHARACTERISATION OF SIALON POLYTYPIDS

##### IV.1 Introduction

The six structurally similar phases which occur near the aluminium nitride corner of the  $\text{Si}_3\text{N}_4$ - $\text{SiO}_2$ - $\text{Al}_2\text{O}_3$ -AlN system and extend into other metal sialon systems have been variously described in the literature. Early work at Newcastle assigned the letters P, Y, M, Q, T, R to these phases (Jack (32)) whilst Gauckler et al. (33) called them  $X_4$ ,  $X_2$ ,  $X_5$ ,  $X_6$ ,  $X_7$  ( $X_7 = \text{T}$  and  $\text{R}$ ); after structural characterisation (see Jack (34)) they were described as "polytypes" with Ramsdell symbols 8H, 15R, 12H, 21R, 27R, 2H. In the strictest sense, polytypes are layer structures which, within very narrow limits, preserve a constant chemical composition and differ only in the way the layers are stacked together. The repeat distances within each layer are identical for every member of the series but perpendicular to the layer the structure repeats after different multiples of the interlayer separation. Common examples of polytypic materials are silicon carbide, zinc sulphide and cadmium iodide (see, for example, Verma and Krishna (35)). In the sialon "polytypes", both the composition and the unit cell dimensions show a systematic variation with structure type and the International Union of Crystallography has assigned the name "polytypoids" to such series (36).

##### IV.2 Characterisation

The first sialon layer structures to be characterised were those in the  $\text{Si}_3\text{N}_4$ - $\text{SiO}_2$ - $\text{Al}_2\text{O}_3$ -AlN system (Figure 31). The unit cells are hexagonal or rhombohedral with  $a$ ,  $\sim 3\text{\AA}$  and  $c$ , large and widely varying (see Table 4). In polytype structures, the number of layers per

Table 4.

Unit cell dimensions for the sialon polytypoids

Type	M:X	No. of layers per block	$a$	$c$	$c/n$
8H	4:5	4	2.988	23.02	2.88
15R	5:6	5	3.010	41.81	2.79
12H	6:7	6	3.029	32.91	2.74
21R	7:8	7	3.048	57.19	2.72
27R	9:10	9	3.059	71.98	2.67
2H	11:12	11	3.079	5.30	2.65
2H	1:1	1	3.114	4.986	2.49

$c$  repeat distance (and hence the Ramsdell symbol) is obtained from the  $l$  value of the first strong 001 reflection, the  $d$  spacing of which gives the interlayer spacing,  $c/n$ . Table 4 shows that this decreases systematically with increasing AlN content. Absent

reflections in the X-ray patterns of the hexagonal phases are due to a  $c$  glide plane of symmetry which relates the upper and lower halves of the unit cell; in a similar way the rhombohedral phases have absent reflections corresponding to the unit cell being split up into three symmetry-related blocks of structure. The number of layers per block in each phase can therefore be evaluated from the Ramsdell symbol and Table 4 shows that this increases by one from one member of the series to the next. Note that a 16H sialon which should occur between 21R and 27R has not been observed.

From their positions in the phase diagram, the sialon polytypoid phases must either accommodate additional non-metal atoms or be deficient in metal atoms relative to an MX wurtzite composition. Thus the five layers in each block of 15R must consist either of four MX plus one  $\text{MX}_2$  layers (five metal atom layers) or three MX plus one  $\text{MX}_2$  layers (five non-metal atom layers). Density measurements show conclusively that the first alternative is correct. The fundamental block of structure in each member of the series has the composition  $\text{M}_m\text{X}_{m+1}$ , where  $m$  takes the values, 4, 5, 6, 7, 9 and 11 as shown in Table 4. Note that preparative evidence alone is not sufficient to determine the composition. At the high temperatures needed for the preparation of these compounds, weight losses due to silicon monoxide and nitrogen are sufficient to move the overall composition from one phase to the next.

The additional non-metal atom in the  $\text{MX}_2$  layer increases the thickness of this layer so that the average interlayer spacing  $c/n$  increases with frequency of  $\text{MX}_2$  layers as shown in Figure 32. The spacing corresponding to zero  $\text{MX}_2$  layers, 2.49Å, agrees exactly with the interlayer separation in aluminium nitride. From the slope of the graph, the  $\text{MX}_2$  layer is 1.5Å thicker than an MX layer, or alternatively 1.0Å thinner than two MX layers. This latter way of expressing the result is more useful because, as discussed in later sections, the structures are more satisfactorily described in terms of layers of non-metal atoms with occasional metal atoms omitted.

The X-ray pattern of the  $2\text{H}^6$  phase has only the lines of aluminium nitride ( $2\text{H}$ ), with 001 and hko reflections sharp and hkl reflections broadened. Electron micrographs show extensive faulting on the basal plane. The  $c/n$  value corresponds to a 33R structure but the absence of additional reflections and the broadening of the lines show that  $\text{MX}_2$  layers are incorporated randomly with an average separation of eleven layers. Compositions richer in AlN than  $2\text{H}^6$  occur as two-phase mixtures of AlN and  $2\text{H}^6$  rather than as longer-period polytypes.

At higher temperatures the range of homogeneity of the polytypoids increases and extends to the  $\text{Al}_2\text{O}_3$ -AlN join. Collongues et al. (37) reported an "X" phase which indexes primarily as 21R and Gauckler (38) gave a phase diagram for the  $\text{Al}_2\text{O}_3$ -AlN system which

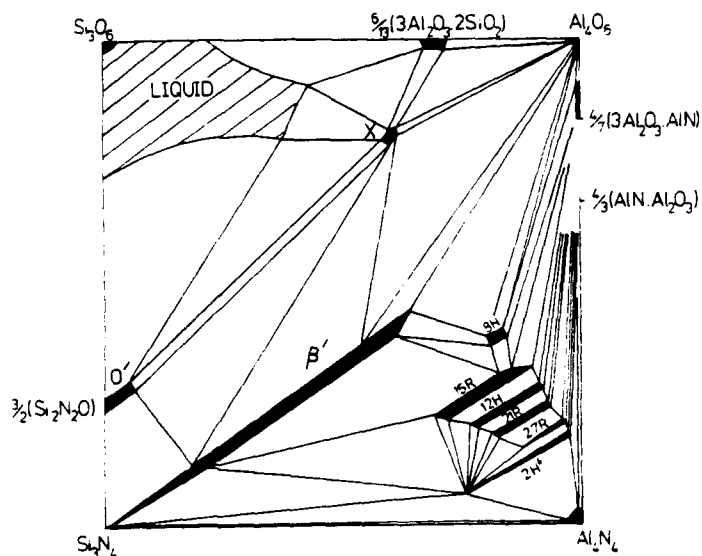


Figure 31. Phase relationships in the Si-Al-O-N system at 1700°C

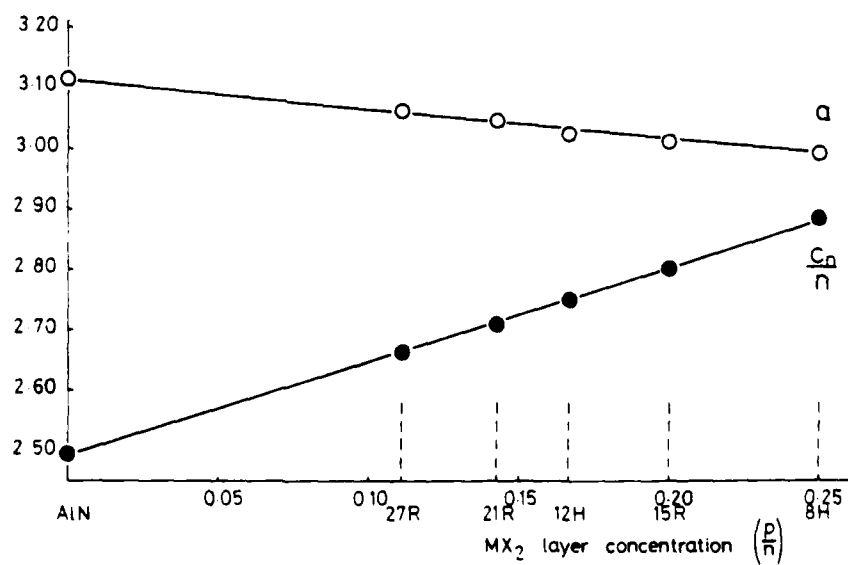


Figure 32. Graph showing the variation of  $a$  and  $c/n$  with the proportion of  $MX_2$  layers in sialon polytypoid phases

included both 21R and 27R compounds. Sakai (39) prepared a 16H aluminium oxynitride, the first known occurrence of this structure and Bartram and Slack (40) reported 27R and 20H compounds.

Other cations can be incorporated into polytypoid phases provided the overall metal:non-metal ratio is retained and electrical neutrality is preserved. The additional cation extends the range of homogeneity from a line to a plane of constant M:X ratio (see Figure 33). Figures 34 and 35 show the extent of 12H and 21R formation in the magnesium sialon system; the other polytypoid phases accommodate less magnesium (see Buang (41)). Beryllium, lithium and scandium can also be incorporated into these structures. Figures 34, 35 and 36 show a different series of polytypoid phases occurring at more magnesium- and oxygen-rich compositions in the magnesium sialon system. They are described by the Ramsdell symbols 6H (6M:7X), 14H (7M:8X) and 8H (8M:9X); unit cell dimensions are given in Table 5.

Table 5.

Unit cell dimensions for 6H, 14H and 8H magnesium sialons

Type	M:X	<u>a</u>	<u>c</u>
6H	6:7	3.061	16.33
14H	7:8	3.070	37.52
8H	8:9	3.083	21.15

Aluminium carbonitrides  $\text{Al}_5\text{C}_3\text{N}_2$ ,  $\text{Al}_6\text{C}_3\text{N}_2$ ,  $\text{Al}_7\text{C}_3\text{N}_3$  and  $\text{Al}_8\text{C}_3\text{N}_4$  have structures similar to 8H, 15R and 12H sialons but with metal and non-metal atoms reversed. The two aluminium silicon carbides  $\text{Al}_4\text{SiC}_4$  and  $\text{Al}_4\text{Si}_2\text{C}_5$  are also similar (see Table 6). Phase relationships in the  $\text{Be}_3\text{N}_2$ - $\text{Si}_3\text{N}_4$ - $\text{SiO}_2$ -BeO system (Figure 37) were studied by Huseby et al. (42), Thompson (43) and Thompson and Gauckler (44) who showed that all the sialon polytypoid structures plus a 9R of composition  $\text{M}_4\text{X}_3$  and 4H  $\beta$ -beryllium nitride ( $\text{M}_3\text{X}_2$ ) occurred with very extensive ranges of homogeneity along lines of M:X ratio greater than unity. The Mg-Si-O-N system is completely different (Figure 38) and only two polytypoid phases occur;  $\text{Mg}_4\text{N}_2\text{O}$  has a 6H structure and  $\text{Mg}_4\text{SiN}_4$  a 12R structure.

#### IV.3 Crystal structures

Structure determinations have been carried out on several phases using X-ray powder methods and the results compared with direct observation of the structures by high resolution electron microscopy.

The structures of 8H and 15R sialons were reported by Thompson (45) (see Figure 39) and consist of layers of  $(\text{Si},\text{Al})(\text{O},\text{N})_4$  tetrahedra

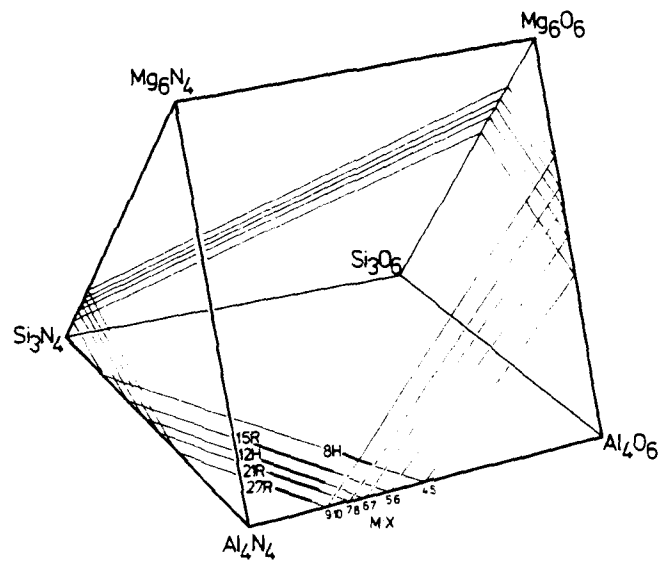


Figure 33. Planes of constant M:X ratio in the Mg sialon system

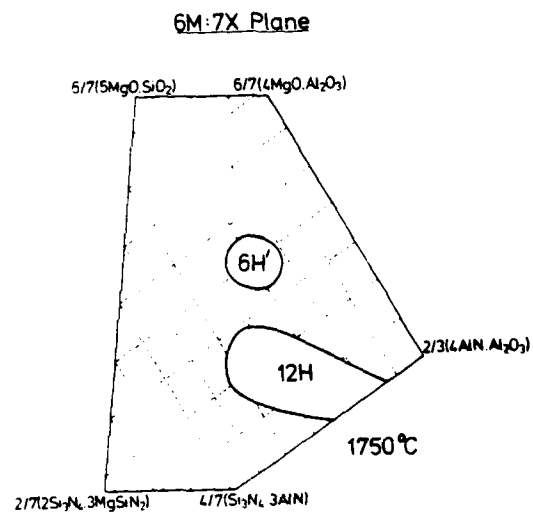


Figure 34. Phase relationships in the 6M:7X plane of the Mg sialon system

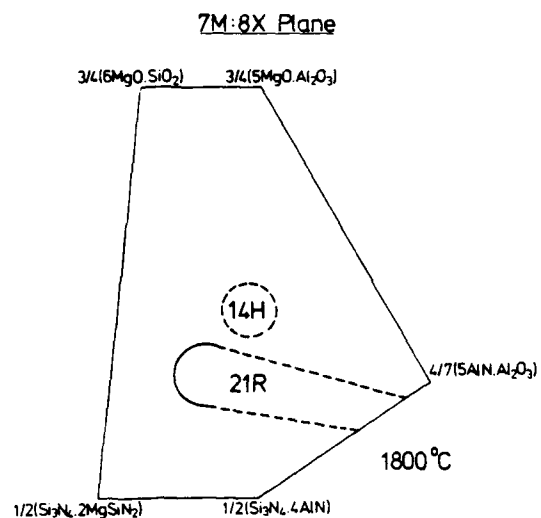


Figure 35. Phase relationships in the 7M:8X plane of the Mg sialon system

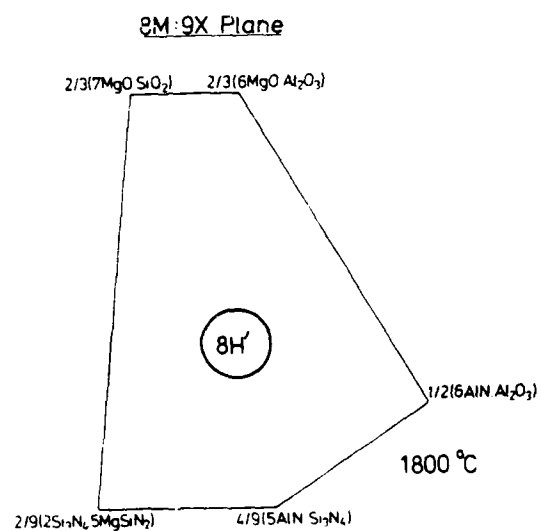


Figure 36. Phase relationships in the 8M:9X plane of the Mg sialon system

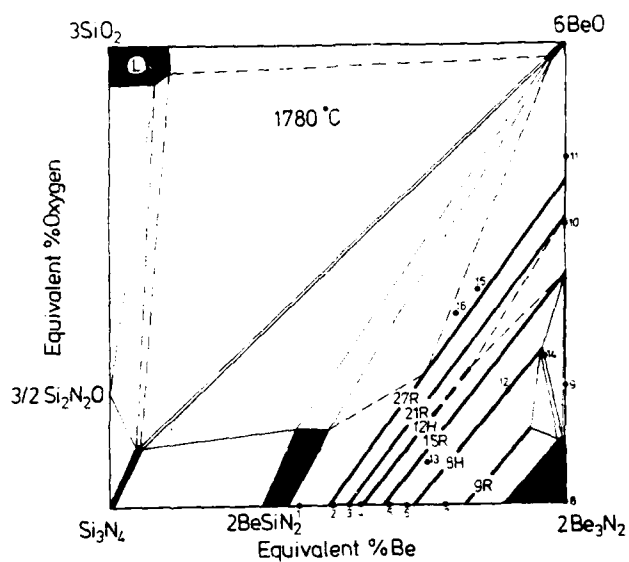


Figure 37. Phase relationship in the Be-Si-O-N system at 1780°C

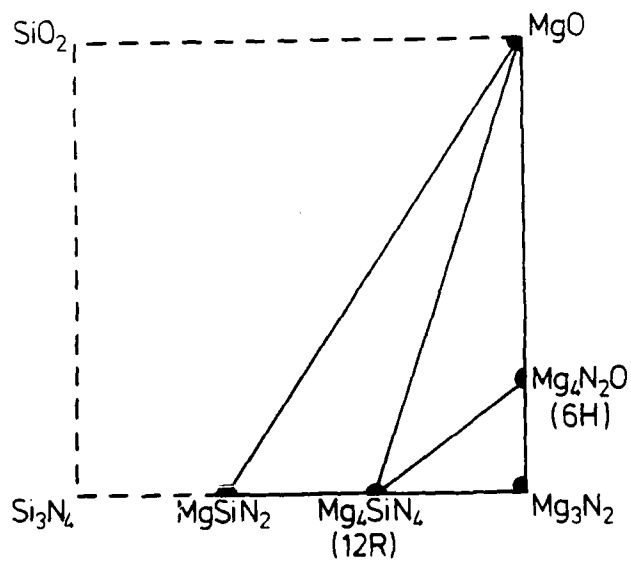


Figure 38. Phase relationships in the MgO-MgSiN<sub>2</sub>-Mg<sub>3</sub>N<sub>2</sub> part of the Mg-Si-O-N system

Table 6.

Unit cell dimensions of Al-C-N and Al-Si-C phases

Compound	Type	M:X	<u>a</u>	<u>c</u>
$\text{Al}_5\text{C}_3\text{N}$	8H	5:4	3.281	21.67
$\text{Al}_6\text{C}_3\text{N}_2$	15R	6:5	3.248	40.03
$\text{Al}_7\text{C}_3\text{N}_3$	12H	7:6	3.226	31.70
$\text{Al}_8\text{C}_3\text{N}_4$	21R	8:7	3.211	55.08
$\text{Al}_4\text{SiC}_4$	8H	5:4	3.277	21.68
$\text{Al}_4\text{Si}_2\text{C}_5$	15R	6:5	3.251	40.11

modified by two additional structural features. In each block of structure one layer of aluminium atoms occupies 6-fold coordinated sites and half way between these layers metal atoms are shared between two adjacent tetrahedral sites. In 8H only one layer of metal atoms is shared but in 15R the symmetry requires to layers to be shared. This arrangement provides the  $\text{MX}_2$  layer which reduces the overall M:X ratio below unity and also inverts the sequence of tetrahedra so that it is back in register at the next layer of octahedra. Both structural features are necessary for the structure to occur, but the fundamental reason for the deviation from aluminium nitride stacking is the increased oxygen content which allows 6-fold coordination of aluminium by oxygen.

The structures of other members of the series follow the same principles but incorporate additional  $(\text{Si},\text{Al})(\text{O},\text{N})_4$  tetrahedra in each block of structure. Buang (41) determined the structure of 12H magnesium sialon (Figure 41) and showed that it was consistent with the scheme observed in 8H and 15R; the magnesium atoms occupy both 4-fold and 6-fold coordinated sites.

No X-ray structure determinations have been carried out on antitypic Be-Si-O-N compounds. Clarke, Shaw and Thompson (46) interpreted lattice images of 15R and 12H beryllium silicon nitrides in terms of three blocks of five and two blocks of six layers respectively and Shaw and Thomas (47) proposed that the structures of all the compounds in the series were made up of different numbers of  $\text{BeSiN}_2$  and  $\text{Be}_3\text{N}_2$  units joined together. Further work is needed to confirm this. In  $6\text{H Mg}_4\text{N}_2\text{O}$  (Figure 40) the non-metals are stacked in a predominantly cubic close-packed sequence with all the magnesium atoms in 4-fold coordination and a well-defined  $\text{M}_2\text{X}$  layer. Note that the non-metal atoms associated with this layer are in distorted 5-fold and 7-fold coordination and therefore antitypes based on this structure are not observed. A diagram of the expected structure of  $12\text{R Mg}_4\text{SiN}_4$  is shown in Figure 40 assuming that it incorporates additional layers of  $\text{SiN}_4$  tetrahedra into each block of



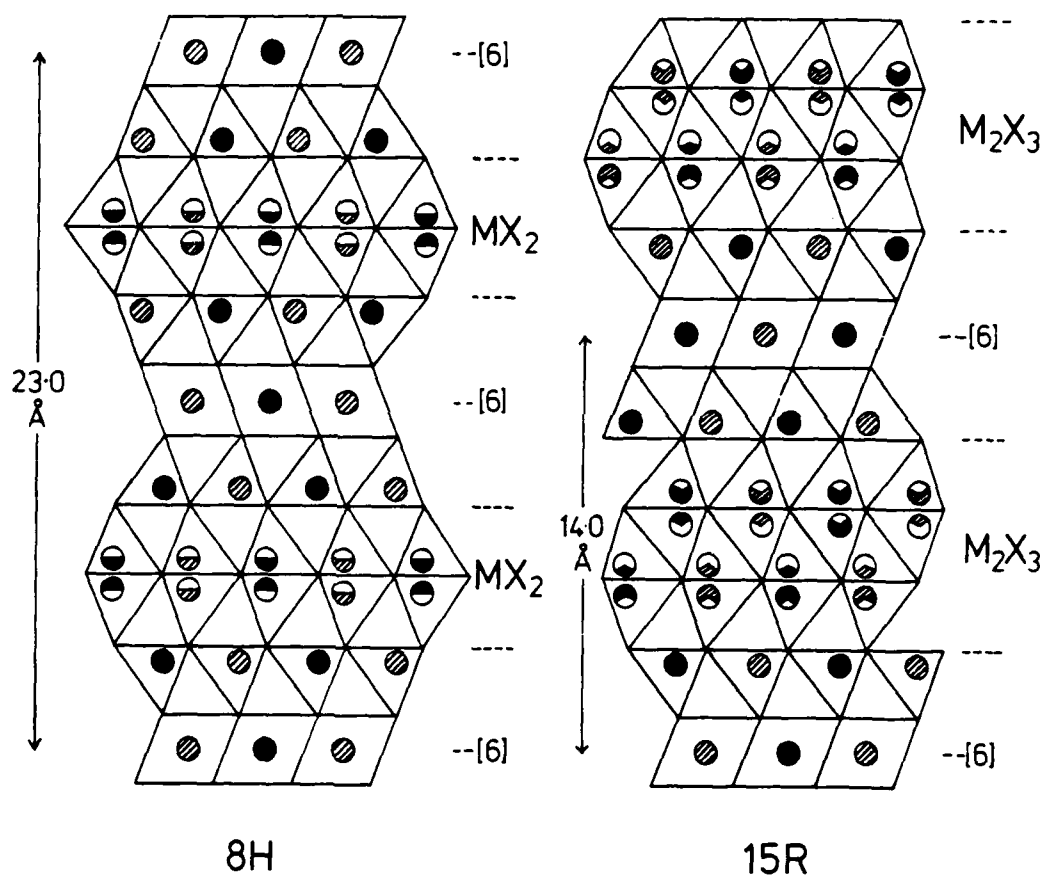


Figure 39. The atomic arrangement in 8H and 15R sialons. The structures are projected on (110) with metal atoms shown as circles. Shaded atoms are at height  $\frac{1}{2}$  above the plane of the paper

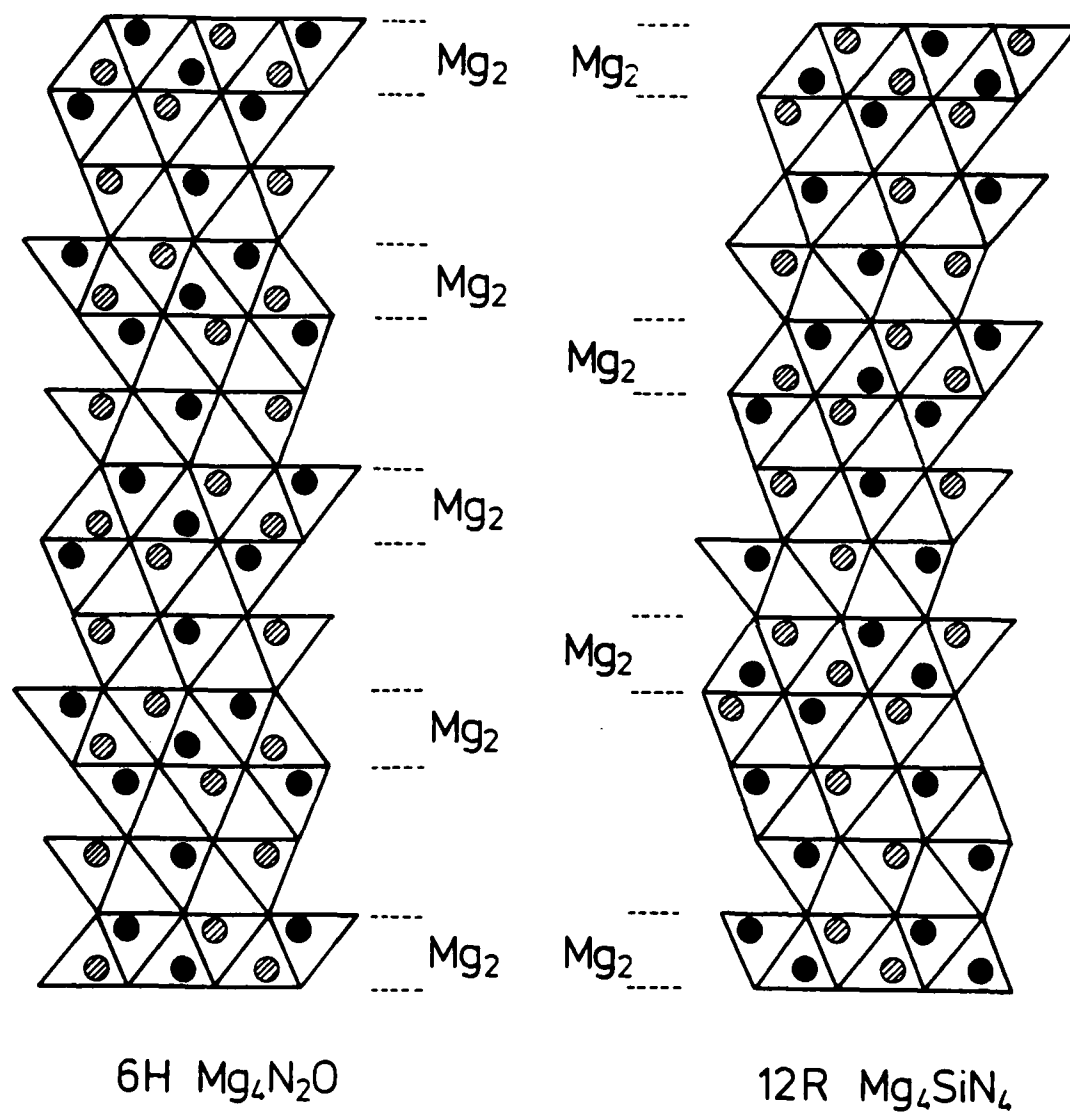


Figure 40. The atomic arrangement in 6H magnesium oxynitride and 12R magnesium silicon nitride. Symbols as for Figure 39

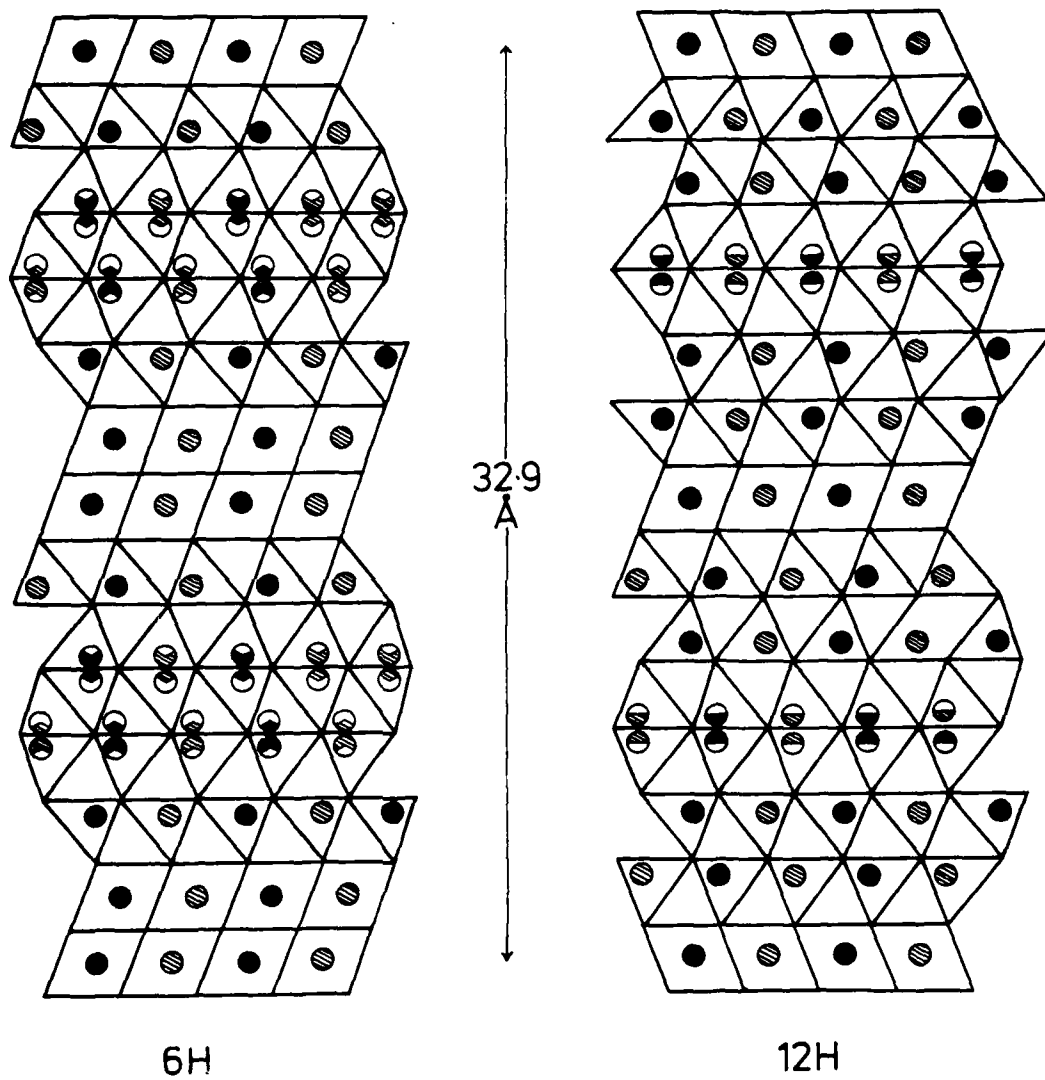


Figure 41. The atomic arrangement in 6H and 12H Mg sialons.  
Symbols as for Figure 39

the 6H structure; this still requires confirmation by X-ray diffraction.

The stacking sequence in 6H magnesium sialon is similar to that in the sialon polytypoid series but two adjacent layers of octahedra are incorporated into each block of structure. In Figure 41 two unit cells of 6H are compared with one cell of 12H magnesium sialon (Buang (41)) which contains only one layer of octahedra per block. Again, metal atoms are shared between adjacent tetrahedra half way between layers of octahedra. The double layers of octahedra arise because the composition of 6H is richer in magnesium and oxygen than 12H and magnesium prefers to be 6-fold coordinated by oxygen. The structures of 14H and 8H, which occur in the same series as 6H, have not been determined but by analogy with other series will be similar to 6H but with one and two additional layers of tetrahedra per block respectively.

#### IV.4 Lattice imaging

The structures discussed in the previous section were all determined by X-ray powder methods because single crystals were not available. The R indices after refinement were never lower than 6% and were sometimes higher than 10%. In such circumstances it is desirable to obtain independent confirmation of the structures and lattice (or structure) imaging is a useful technique for this purpose. Lattice imaging can be used to observe fine-scale structural defects and Clarke, Shaw and Thompson (46), Clarke and Shaw (48) and Hendry and Johnson (49) have used this method to show that intergrowths frequently occur between adjacent polytypoid structures. Even "single-phase" material has a certain number of such defect regions and this is probably the most important reason why the X-ray structure determinations give high R values.

In order to compare lattice images with the actual atomic arrangement, it is necessary to calculate the image contrast for a particular specimen thickness and orientation from a knowledge of the crystallographic parameters and the operating conditions of the microscope. Figure 42 shows one- and two-dimensional observed and calculated images for 6H magnesium sialon taken with the beam parallel to  $[010]$ . In both cases the agreement is excellent. Figure 43 shows similar comparisons for 12H magnesium sialon and again the agreement between observed and calculated images supports the correctness of the X-ray structure. The technique is not sufficiently sensitive to determine metal ordering or local variations in the occupation scheme in the  $MX_2$  layer since the scattering factors of magnesium, aluminium and silicon for electrons are all similar and furthermore the specimen thickness corresponds to several unit cells superimposed on top of one another and this averages out variations from cell to cell.

#### IV.5 Summary

Figure 44 summarises the polytypoid series so far observed in sialon systems. A combination of X-ray methods and high resolution electron microscopy has been used to characterise these materials and their structures are now established. No detailed evaluation of the ceramic properties of any of the polytypoid phases has yet been attempted. Further work is needed in this area before their usefulness as engineering ceramics can be determined.

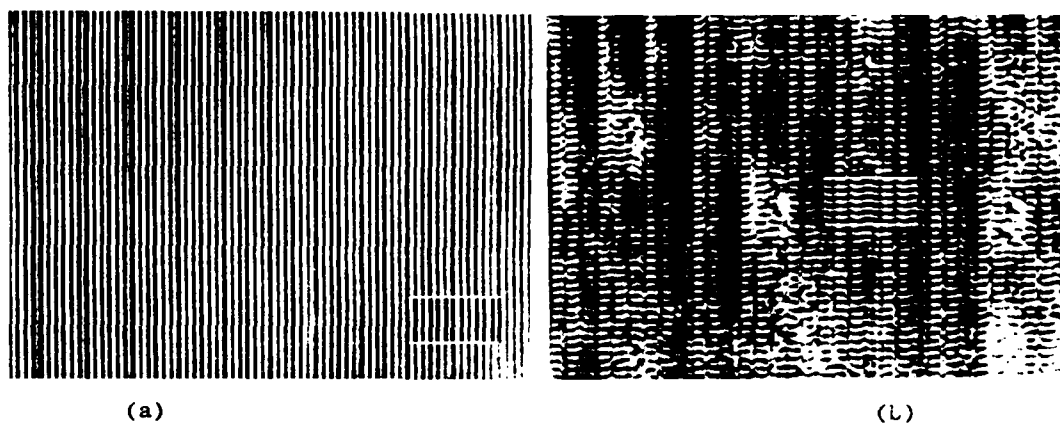


Figure 42. (a) One-dimensional and (b) two-dimensional lattice images of 6H Mg sialon taken with the electron beam parallel to 010 . Calculated images are outlined in white

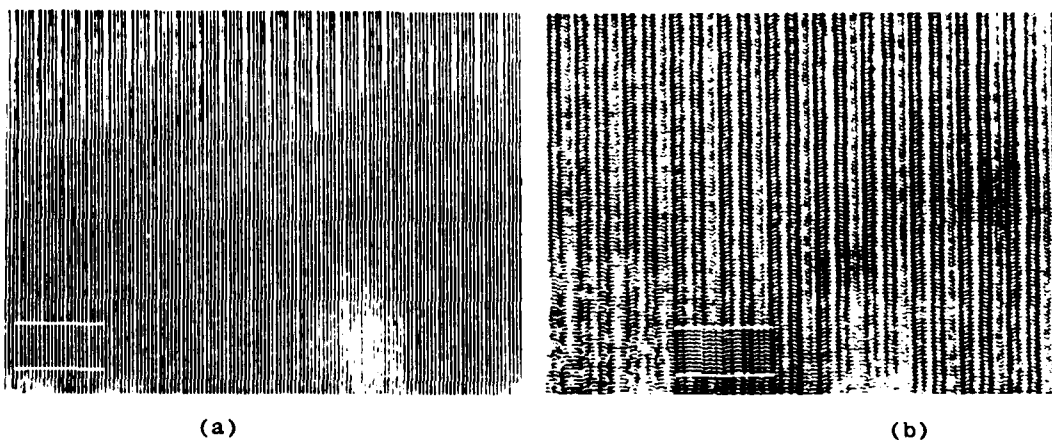


Figure 43. (a) One-dimensional and (b) two-dimensional lattice images of 12H Mg sialons taken with the electron beam parallel to 010 . Calculated images are outlined in white.

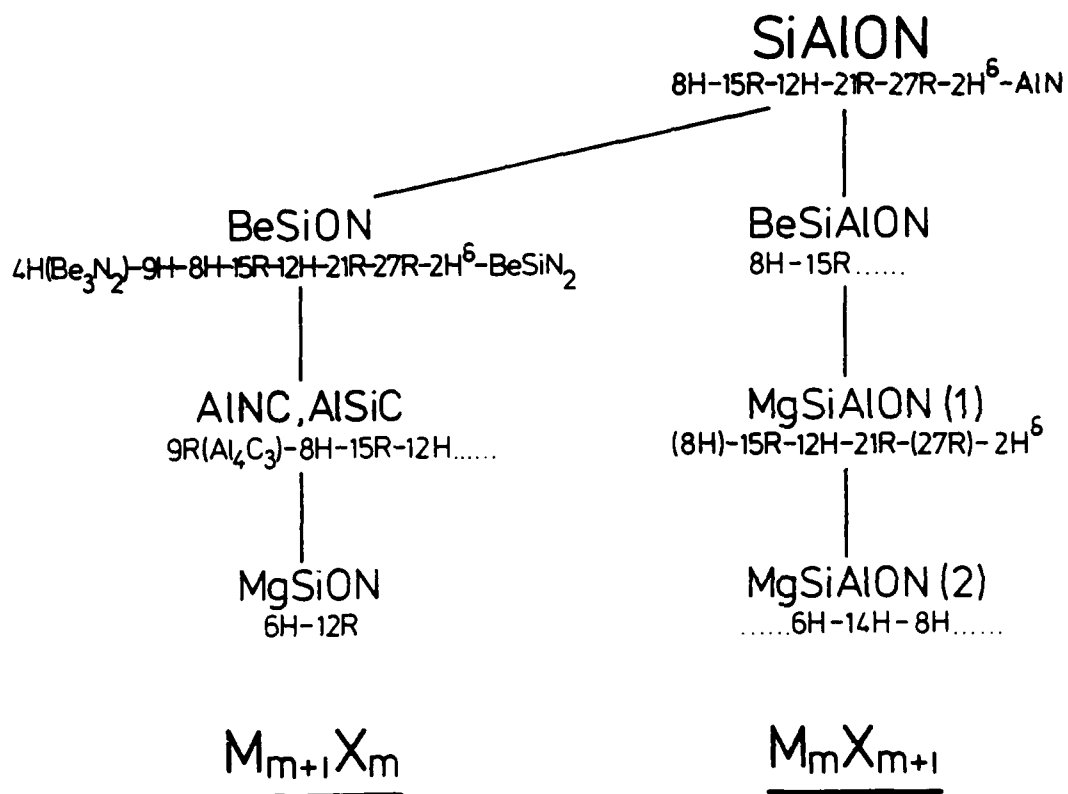


Figure 44. Summary of the range of sialon polytypoid structures

## V. SIALON X-PHASE

### V.1 Introduction

Sialon X-phase was discovered independently by Oyama and Kamigaito (50) and by Jack and Wilson (51) as a second phase when silicon nitride and alumina were hot-pressed together at 1700°C. Its composition is close to  $\text{Si}_3\text{Al}_6\text{O}_{12}\text{N}_2$  with a very small range of homogeneity. The crystal structure is complex and for this reason many of the early attempts to characterise X-phase (see, for example, Drew and Lewis (52); Wild (53); Gugel et al. (54); Jack (34) were unsuccessful. In the present work the crystal structure has been determined by single crystal X-ray methods and this has been used to interpret results obtained by optical and electron microscopy.

### V.2 Unit cell

Jack (34) reported that the X-ray pattern of X-phase was not always the same and two different forms, high-X and low-X, could be distinguished. Low-X occurs at the composition given above but high-X is formed at more silica-rich compositions. Electron probe microanalysis shows that high-X is a mixture of low-X plus glass but structurally low-X is a superlattice of high-X with the *b* edge-length of high-X one third of that of low-X. The unit cells of both forms are triclinic with the dimensions given in Table 7. The different ways of describing the low-X cell arise because the present authors and Zangvil et al. (57) have used the Delauney cell (shortest edge-lengths with all angles  $\approx 90^\circ$ ) whereas Zangvil (55) used the cell with shortest edge-lengths and Okamura and Inoue (56) used a C face-centred cell with the angles nearest  $90^\circ$ .

### V.3 Structure determination and refinement

A crystal of low-X, prepared by slow cooling from the melt, was set up on a Syntex P2<sub>1</sub> 4-circle diffractometer and 6897 X-ray intensities were collected using  $\text{MoK}\alpha$  radiation. An *L*<sub>p</sub> correction was applied but absorption effects were neglected. A model for the structure proposed by Okamura and Inoue (56) was used to initiate refinement. The final R-index of 9% was obtained after very little refinement of atomic parameters but the occupation scheme for tetrahedral sites required considerable adjustment. This was due to twinning and stacking faults in the crystal which resulted in occupation of certain empty sites. For the purpose of discussion it is convenient to first consider the idealised structure and then show how this is modified by defects.

### V.4 Discussion

Figure 45 shows the idealised structure projected down the *b* axis.



Table 7

## Unit cell dimensions for X-phase

Form	a	b	c				
Low	9.69	8.56	9.85	81	70	81	Zangvil (55)
Low	15.93	8.54	11.17	90.0	91.0	100.3	Okamure & Inoue (56)
Low	9.68	8.54	11.19	90.0	124.3	99.2	Zangvil et al. (57)
Low	9.68	8.56	11.21	90.0	124.4	98.5	} Present work
High	9.66	2.84	11.17	90.0	124.4	98.5	

All the atoms occur in layers perpendicular to  $b$  at intervals of one-sixth. Numbers in the diagram express the heights of atoms in numbers of sixths above the plane of the paper. In this orientation octahedra project as parallelograms and tetrahedra as isosceles triangles. Because of the similarity in atomic number between silicon and aluminium and between oxygen and nitrogen, metal and non-metal ordering schemes cannot be determined from X-ray data alone. Aluminium is probably coordinated by oxygen in octahedral sites.

The structure consists of chains of octahedra parallel to  $b$  linked together in the  $c$  direction by chains of tetrahedra and in the  $a^*$  direction by two distinct types of tetrahedral network. Type I networks, illustrated in the bottom left and top right quadrants of Figure 45, consist of two groups of three tetrahedra joined together with the non-metal atoms in the centre of each group in three-planar coordination. This arrangement is similar to that of the six tetrahedra in the unit cell of  $\beta$ - $\text{Si}_3\text{N}_4$  but in X-phase is only repeated once in every three layers. Type II networks are shown in the top left and bottom right quadrants of Figure 45 and consist of tetrahedra pointing inwards towards a central region which is occupied by two tetrahedra separated by intervals of  $b/2$ . Whereas the structure is similar to mullite in the linking of chains of octahedra and tetrahedra in the  $c$  direction, the increased proportion of tetrahedra in X-phase result in a larger repeat distance in the  $a^*$  direction and hence a more complex cell of lower symmetry. The unit cell contents of  $\text{M}_{52}\text{X}_{84}$  correspond quite well to six  $\text{Si}_3\text{Al}_2\text{O}_{12}\text{N}_2$  formula units, giving a calculated density of  $3010\text{kg.m}^{-3}$  in good agreement with measured values ( $2850$ – $3000\text{ kg.m}^{-3}$ , present work;  $300\text{ kg.m}^{-3}$ , Zangvil et al. (57)).

The actual structure differs from that described above in the occupation of additional tetrahedral sites. Thus, for example, in the Type I unit in the bottom left-hand quadrant of Figure 45, there are vacant sites at height 3 immediately below the left-hand tetrahedron and at height 2 immediately above the right-hand tetrahedron.

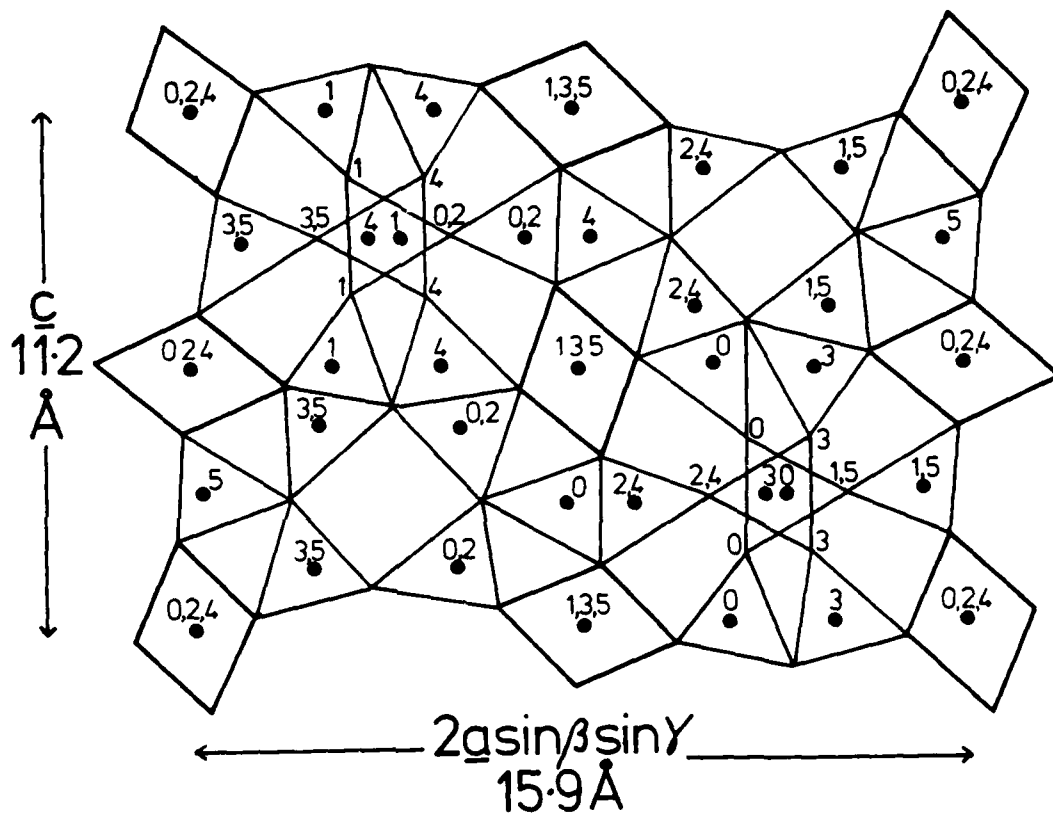


Figure 45. The idealised atomic arrangement in low-X projected down the  $\underline{b}$  axis. The c-face centred cell has been used.

Occupation of these sites instead of the normal sites results in the adjacent Type II units being displaced up or down by intervals of  $b/3$ . Whether the result is a twin or a fault depends on the continued occupation scheme for these vacant sites in adjacent unit cells. Both types of defect are observed on high resolution lattice images (see Figure 46) but whereas twinning occurs in almost every specimen and is difficult to eliminate, stacking faults can be removed by careful annealing. Thus low-X, prepared by slow-cooling of the  $\text{Si}_3\text{Al}_6\text{O}_{12}\text{N}_2$  composition from the melt, has a large grained microstructure (Figure 47(a)) which is submicroscopically twinned but is almost unfaulted. High-X prepared at more silica-rich compositions, crystallizes rapidly at lower temperatures from a highly viscous supercooled sialon liquid and is therefore fine-grained (Figure 47(b)) and heavily faulted. This smears out the metal atoms in tetrahedral sites to give an apparent  $b$  repeat distance of one-third of that of low-X. The difference between the two forms is therefore very satisfactorily explained in terms of the frequency of stacking faults in the structure.

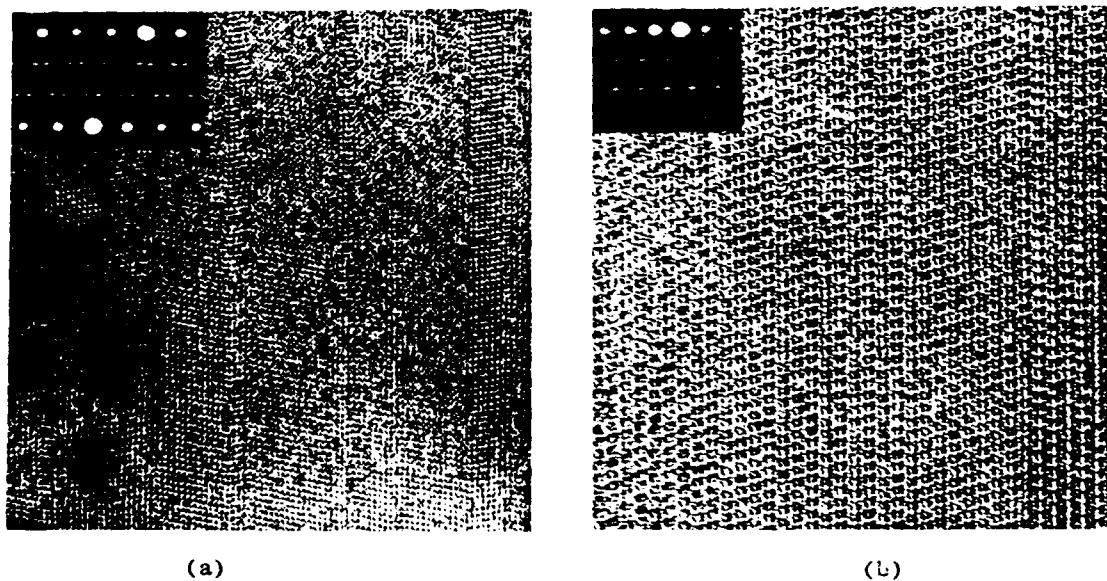


Figure 46. High-resolution lattice images of X-phase showing (a) twinning and (b) stacking faults. The separation of adjacent vertical (100) planes in both micrographs is  $7.8\text{\AA}$

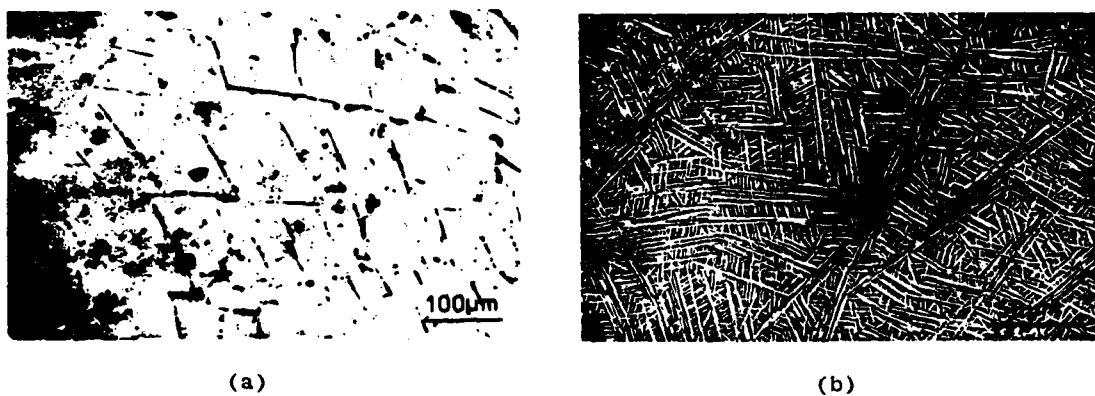


Figure 47. Optical micrographs of (a) low-X, and (b) high-X

VI.  $\alpha'$ -SIALON CERAMICS

## VI.1 Introduction

In the earliest work at Newcastle on sialons (51), expanded  $\alpha$ -silicon 'nitride' structures were obtained by reaction of lithium-silicon nitride,  $\text{LiSi}_2\text{N}_3$ , with alumina. The unit-cell dimensions of one example ( $a$ , 7.822;  $c$ , 5.677Å) gave a cell volume about 3% greater than that of  $\alpha$ -silicon nitride. Jama et al. (58) showed a variation in dimensions for the  $\alpha'$ -lithium sialon when lithium aluminate,  $\text{LiAlO}_2$ , was reacted in different proportions with  $\text{Si}_3\text{N}_4$ . However, other phases, such as  $\beta'$ -sialon and nitrogen-eucryptite, were always present and the product never contained more than 30% of the  $\alpha'$  material.  $\alpha'$ -Sialons were also found in the Mg-Si-Al-O-N system (34) but again never pure, and were observed by Masaki et al. (59) during the nitriding of silicon with AlN and  $\text{Al}_2\text{O}_3$  additions. A claim has also been made by Mitomo (60) of  $\alpha'$  solid solutions of  $\text{Si}_3\text{N}_4$ - $\text{Al}_2\text{O}_3$  and/or  $\text{Si}_3\text{N}_4$ - $\text{Y}_2\text{O}_3$  occurring during the sintering of  $\text{Si}_3\text{N}_4$  at 1700-1800°C with  $\text{Al}_2\text{O}_3$ - $\text{Y}_2\text{O}_3$  mixtures. The present investigation reports the preparation and characterisation of pure  $\alpha'$ -phases in M-Si-Al-O-N systems where M is Li, Ca or Y and such phases also occur where M is each of the rare earth elements except La and Ce.

The 'idealised' silicon nitride structure can be described as a stacking of Si-N layers in either an ABAB ... ( $\beta$ ) or an ABCD ... ( $\alpha$ ) sequence as shown in Figure 48. This gives long continuous channels in  $\beta$ , parallel to the hexagonal  $c$ -direction and centred at  $2/3$ ,  $1/3$  in the outlined cell of Figure 48(a). In  $\alpha$ , the  $c$ -glide plane relating the layers CD with AB replaces the continuous channels of the  $\beta$  structure by large closed interstices at  $1/3$ ,  $2/3$ ,  $3/8$  and  $2/3$ ,  $1/3$ ,  $7/8$ . In the  $\alpha$  unit cell containing, ideally,  $\text{Si}_{12}\text{N}_{16}$  there are therefore two sites large enough to accommodate other atoms or ions. Although the Si-N layers in the actual  $\beta$  structure are almost identical with the 'ideal' configurations (see Figure 49), those of  $\alpha$  are considerably distorted and nitrogen atoms at heights approximately  $3/8$  and  $7/8$  are shifted towards the centres of the two respective interstices.

## VI.2 Preparation and composition

All the  $\alpha'$ -sialons have compositions represented by  $\text{M}_x(\text{Si},\text{Al})_{12}(\text{O},\text{N})_{16}$  where  $x \leq 2$ . Cell dimensions of examples where  $x \leq 1$ , are compared with those of  $\alpha$  and  $\beta$  silicon nitrides in Table 8.

The  $\alpha'$ -structure is derived from  $\alpha$ - $\text{Si}_{12}\text{N}_{16}$  by partial replacement of Si with Al. Valency compensation is effected by the 'modifying' cations (Li, Ca, Y) occupying the interstices of the (Si,Al)-N 'network' but where a modifier oxide is used, oxygen may also replace nitrogen. When  $\alpha'$  is synthesised entirely from nitrides, for example, a mixture of  $\text{Si}_3\text{N}_4$ , AlN and  $\text{Ca}_3\text{N}_2$ , the product contains no oxygen, and valency compensation is due solely to the introduction of modifying cations. Because there are only two sites per unit cell for these,

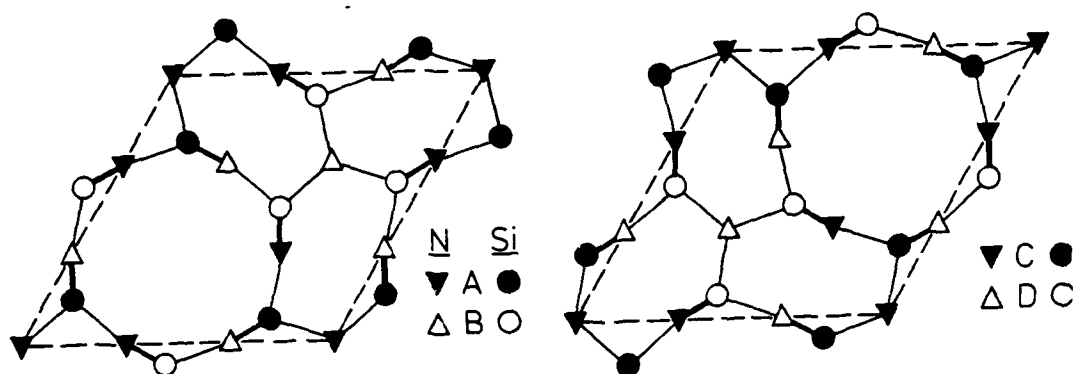


Figure 48. Idealised Si-N layers in  $\alpha$  and  $\beta$  silicon nitrides:  
 (a) AB layers, (b) CD layers.  $\alpha$  structure ABCD;  
 $\beta$  structure ABAB.

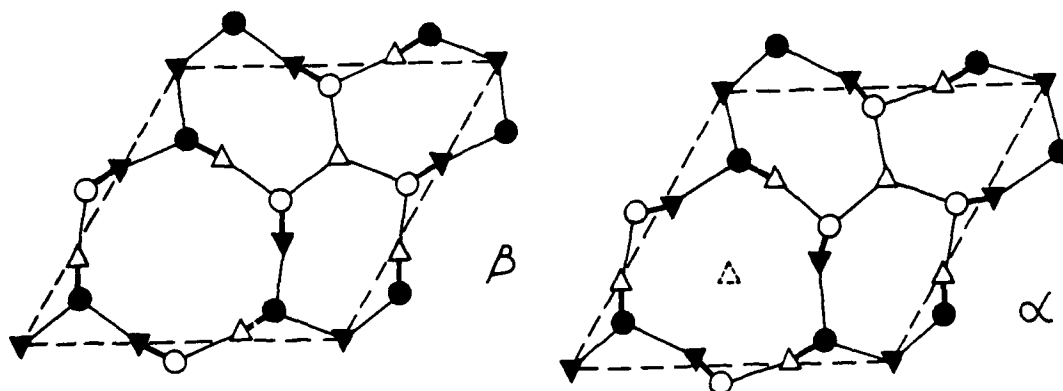


Figure 49. Actual Si-N layers in  $\alpha$  and  $\beta$  silicon nitrides:  
 (a) in  $\beta$ , (b) in  $\alpha$

Table 8

Unit-cell dimensions and densities of  $\alpha'$ -sialons and  
 $\alpha$  and  $\beta$  silicon nitrides

	a	c	c/a	d <sub>o</sub>	d <sub>c</sub>
$\beta$ -Si <sub>3</sub> N <sub>4</sub>	7.61	2.91	0.765/2	3.192	3.192
$\alpha$ -Si <sub>3</sub> N <sub>4</sub>	7.76	5.62	0.724	3.16 <sup>x</sup>	3.183
LiSi <sub>10</sub> Al <sub>2</sub> ON <sub>15</sub>	7.83	5.67	0.724	3.12	3.14
Ca <sub>0.5</sub> Si <sub>10.5</sub> Al <sub>1.5</sub> O <sub>0.5</sub> N <sub>15.5</sub>	7.82	5.68	0.727	3.16	3.20
Ca <sub>0.8</sub> Si <sub>9.2</sub> Al <sub>2.8</sub> O <sub>1.2</sub> N <sub>14.8</sub>	7.86	5.71	0.727	3.19	3.26
Y <sub>0.4</sub> Si <sub>10</sub> Al <sub>2</sub> O <sub>18</sub> N <sub>15.2</sub>	7.81	5.69	0.729	3.23	3.25
Y <sub>0.6</sub> Si <sub>9.2</sub> Al <sub>2.8</sub> O <sub>1.1</sub> N <sub>14.9</sub>	7.83	5.71	0.729	3.28	3.36

d<sub>o</sub>, observed density; d<sub>c</sub>, calculated density;

<sup>x</sup> Range of values 3.167<sup>c</sup>-3.171 g ml<sup>-1</sup> obtained by Wild et al.  
(61) for  $\alpha$ -needles produced by SiO-N<sub>2</sub> reaction.

the limiting composition for Ca- $\alpha'$ -nitride is Ca<sub>2</sub>Si<sub>8</sub>Al<sub>4</sub>N<sub>16</sub>. The limit for the corresponding oxynitride is also two calciums per unit cell.

The  $\alpha'$ -sialons are prepared by heating appropriate mixtures of nitrides or nitrides plus oxides at 1,750°C in one atmosphere of molecular nitrogen or argon for 15 min. Weight losses are negligible and the composition of the initial mix, calculated from the proportions of powder constituents with allowance for surface oxide on the nitrides, is virtually identical with direct microanalysis of the product using a Camebax electron probe at AERE, Harwell.

Table 9

$\alpha'$ -Sialon compositions (atoms per unit cell)

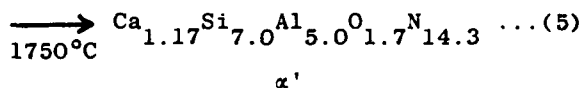
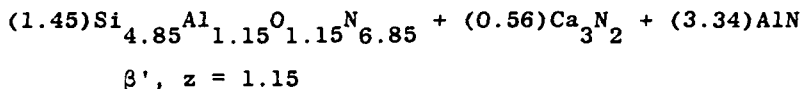
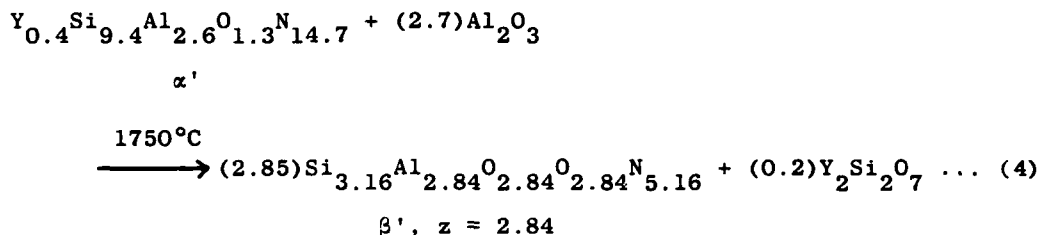
	Ca	Si	Al	O	N	Y	Si	Al	O	N
I-m	0.5	10.6	1.4	1.3	15.0	{0.3	10.0	2.0	1.3	14.8
a	{0.5	10.5	1.6	0.7	14.8	{0.5	10.0	2.0	0.8	15.3
I-m	1.1	9.1	2.9	1.8	14.5	{0.5	8.3	3.7	1.5	14.3
a	{0.9	9.2	2.8	1.4	14.6	{0.6	9.2	2.8	1.1	14.9

I-m: initial mix

a: Camebax electron probe analysis at AERE, Harwell

Moreover, densities calculated from compositions, cell dimensions and the proposed structures are, as shown in Table 8, in excellent agreement with the observed densities.

The X-ray photographs of Figure 50 show that  $\alpha'$  reacts with  $\text{Al}_2\text{O}_3$  to give  $\beta'$  and  $\beta'$  reacts with  $\text{AlN}$  plus the appropriate modifier nitride (such as  $\text{Ca}_3\text{N}_2$ ) to give  $\alpha'$ . Equations corresponding to these reactions are:



Just as  $\beta'$ -sialons can be produced by nitriding mixtures of oxides and carbon with molecular nitrogen, so also can these  $\alpha'$ -phases. Calcium compounds have been prepared in this way at temperatures as low as  $1400^\circ\text{C}$ .

La and Ce do not give  $\alpha'$ -phases but compositions  $0.25\text{RE}_2\text{O}_3 : 3\text{Si}_3\text{N}_4 : 4\text{AlN}$  all gave more than 90%  $\alpha'$  together with unreacted  $\text{AlN}$  after 15 minutes at  $1750^\circ\text{C}$  when rare earths (RE) of even atomic number elements 60-70 (i.e. Nd, Sm, Gd, Dy, Er and Yb) were used. It is reasonable to assume that the odd-numbered elements behave similarly and that La and Ce do not react because their atomic or ionic radii exceed a critical value.

### VI.3 The $\alpha'$ structure

Typical X-ray photographs of Ca, Li and Y  $\alpha'$ -sialons are shown in Figure 51 from which it is clear that exactly the same product is obtained starting with  $\beta$ - $\text{Si}_3\text{N}_4$  as with  $\alpha$ - $\text{Si}_3\text{N}_4$ . Unlike the  $\beta'$ -sialons,  $\text{Si}_{6-2z}\text{Al}_z\text{O}_z\text{N}_{8-2z}$ , where the replacement without structural change is  $(\text{Si}-\text{N})$  by  $z(\text{Al}-\text{O})$ , the replacement in  $\alpha'$ -phases is largely  $(\text{Si}-\text{N})$  by  $(\text{Al}-\text{N})$ . With bond lengths  $\text{Si}-\text{N} \sim 1.74$ ,  $\text{Al}-\text{O} \sim 1.75$  and  $\text{Al}-\text{N} \sim 1.87\text{\AA}$ , the relative increase in unit-cell dimensions for  $\alpha - \alpha'$  are much greater than for  $\beta - \beta'$ . For a general composition



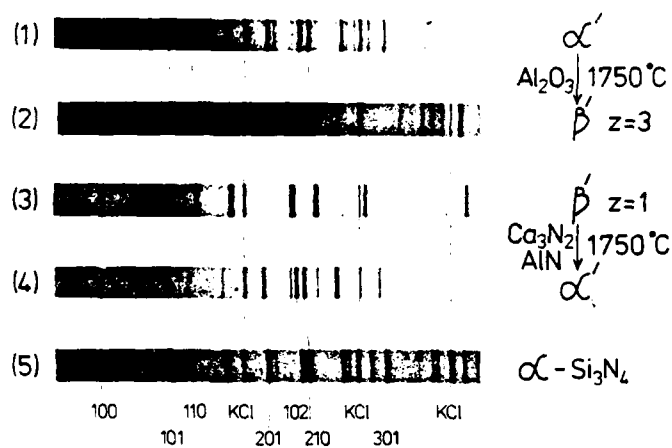


Figure 50. X-ray powder patterns showing transformations  $\alpha'$  -  $\beta'$ .  $\text{CuK}\alpha$  radiation

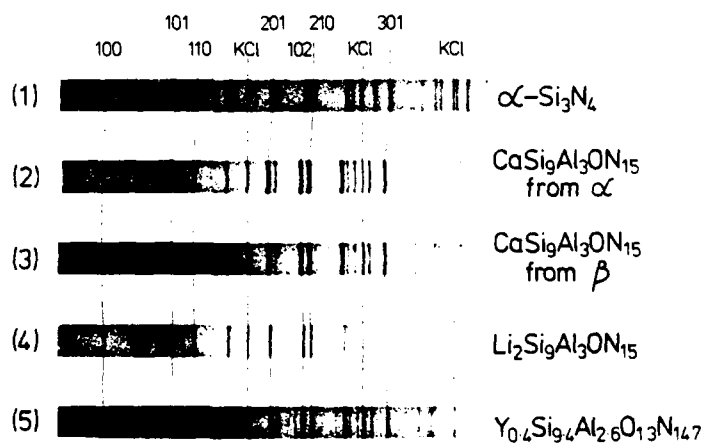
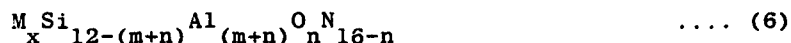


Figure 51. Typical X-ray powder patterns of Ca, Li and Y  $\alpha'$  sialons.  $\text{CuK}\alpha$  radiation



there are  $m(\text{Si-N})$  replaced by  $m(\text{Al-N})$  and  $n(\text{Si-N})$  replaced by  $n(\text{Al-O})$ . If the unit-cell dimensional changes corresponding to these respective replacements are in the ratio 5:1, Figure 52 shows that observed dimensions for a range of  $\alpha'$ -phases fit the relationships:

$$\Delta a (\text{\AA}) = 0.045m + 0.009n \quad \dots (7)$$

$$\Delta c (\text{\AA}) = 0.04m + 0.008n \quad \dots (8)$$

Table 8 compares the cell dimensions and densities of typical  $\alpha'$ -sialons with those of  $\alpha$  and  $\beta$  silicon nitrides. Although the diffraction patterns for  $\alpha$  and  $\alpha'$  are similar, there are small but distinct differences in intensities that are shown schematically in Figure 53 for a composition  $\text{CaSi}_9\text{Al}_3\text{ON}_{15}$ . Comparison of (i) and (ii) shows the expected good agreement between the observed intensities ( $\alpha$ ) for  $\alpha$ - $\text{Si}_3\text{N}_4$  and those calculated ( $\alpha$ ) from its known structure. In Figure 53(iii) the intensities observed for  $\alpha'$ -Ca-sialon ( $\alpha'$ ) are modified from those of  $\alpha$ ; e.g. reflexions 100, 101 and 110 are weakened while 102 and 210 are stronger and reversed relative to each other. A complete structure refinement (61) accounts for these changes and shows that each of the two interstitial sites in the unit cell contains, on average, one-half of a Ca atom; compare Figures 53(iii) and 53(iv). More recently, four  $\alpha'$ -Ca-sialons with 0.6, 0.9, 1.5 and 1.8 Ca atoms per unit cell have been compared. Their observed intensities are plotted against  $\theta$  in Figure 54 with those of  $\alpha$ - $\text{Si}_3\text{N}_4$ . There are systematic intensity changes due to the increasing contribution of Ca to the structure amplitude F. Thus, the 100 intensity decreases to zero at 1.5 Ca and then re-appears at 1.8 Ca as F passes through zero and changes sign.

The structure refinement of a composition  $\text{Ca}_{1.83}\text{Si}_{8.34}\text{Al}_{3.66}\text{N}_{16}$  was terminated at  $R = 0.06$ . Each Ca is coordinated by seven N atoms at an average distance of 2.53\AA whereas the corresponding Ca-N distance in  $\text{CaSi}_9\text{Al}_3\text{ON}_{15}$  is 2.59\AA; average (Si,Al)-N distances are respectively 1.79 and 1.76\AA compared with 1.74\AA for Si-N in  $\alpha$ - $\text{Si}_3\text{N}_4$ . With increasing Ca and Al there is, as might be expected, an overall expansion and an increase in the average (Si,Al)-N distance but, at the same time, the increased bond strength between Ca and its ligands shortens the average Ca-N distance.

The  $\alpha'$ -structure is derived from  $\alpha$ - $\text{Si}_3\text{N}_4$  by partial replacement of  $\text{Si}^{4+}$  with  $\text{Al}^{3+}$ , and valency compensation is effected by "modifying" cations such as  $\text{Li}^+$ ,  $\text{Ca}^{2+}$  and  $\text{Y}^{3+}$  occupying the interstices of the (Si,Al)-N network. The materials are similar to the "stuffed" derivatives of quartz in which  $\text{Al}^{3+}$  replaces  $\text{Si}^{4+}$  and positive valency deficiencies are compensated by "stuffing" cations like  $\text{Li}^+$  and  $\text{Mg}^{2+}$  into interstitial sites. When  $\alpha'$  is synthesised entirely from nitrides the product should contain no oxygen and valency compensation is due solely to the introduction of the modifier cations.

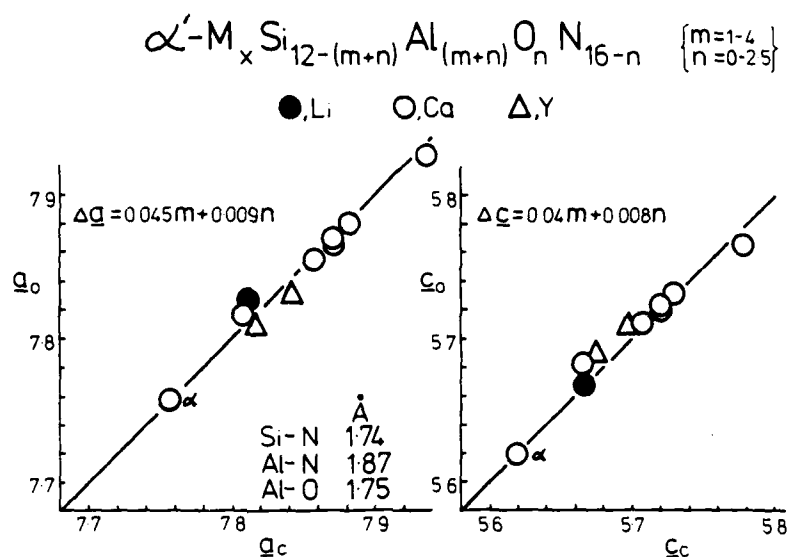


Figure 52. Observed, o, and calculated, c, unit-cell dimensions for  $\alpha'$  sialons

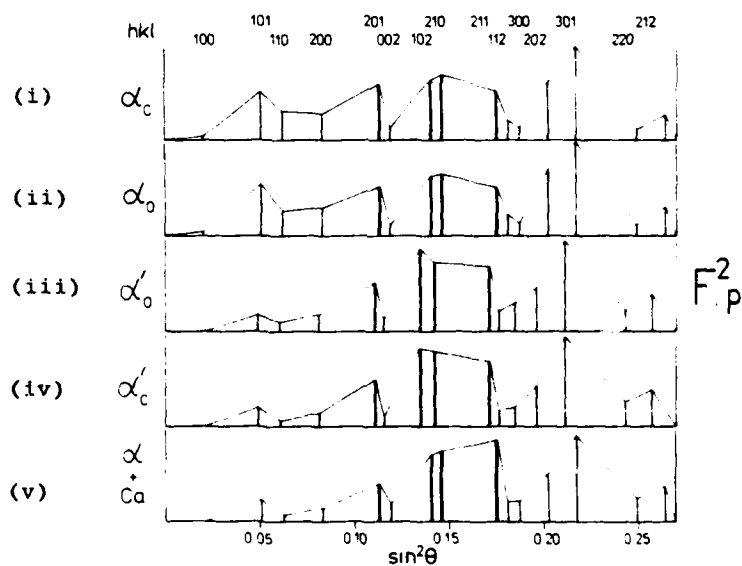
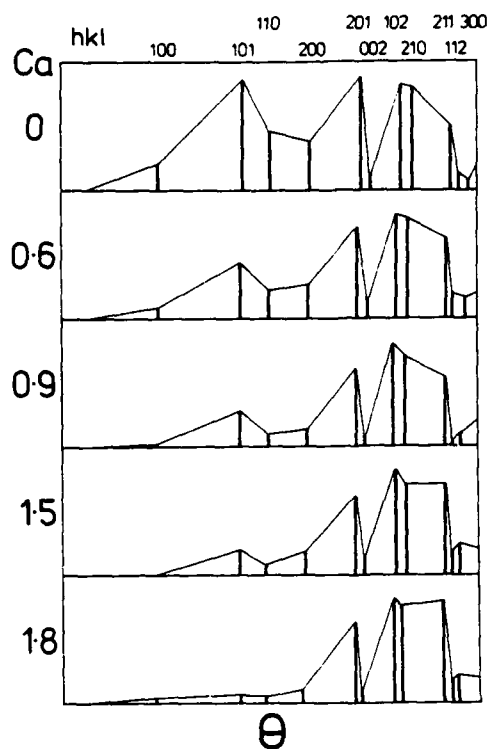


Figure 53. Observed and calculated diffracted intensities ( $F_p^2$  values) for  $\alpha$ - $Si_3N_4$  and  $\alpha'$ -sialons. Thick ordinates are half-scale



I. Figure 54. Intensities of X-ray reflections ( $\text{CuK}\alpha_1$ ) for  $\alpha'$ -Ca-sialons with varying Ca content

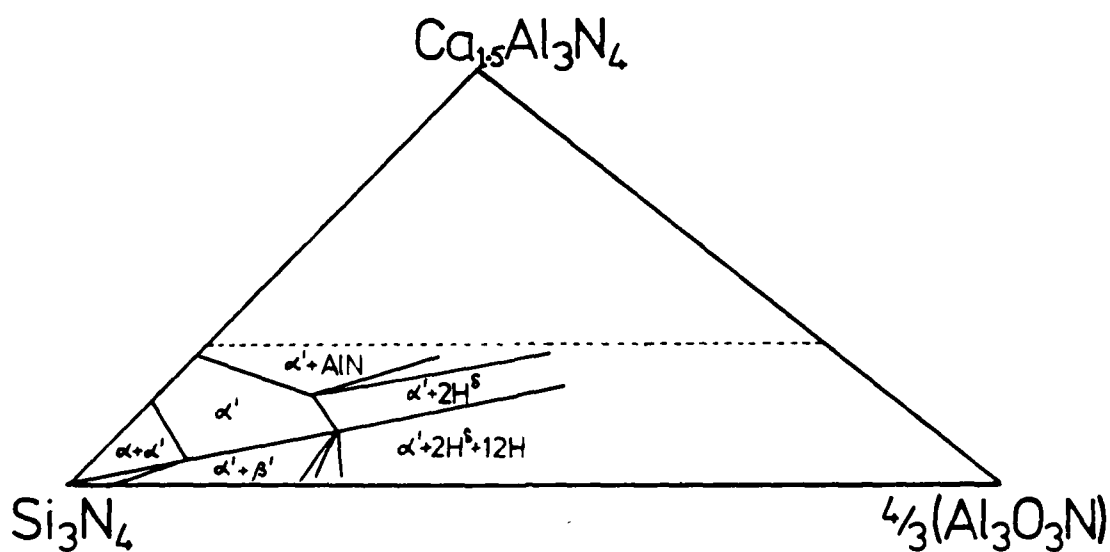


Figure 55. Tentative phase relationships in part of the Ca-Si-Al-O-N system

Because there are only two sites per unit cell for these, the limiting compositions for  $\alpha'$ -nitrides might be expected to be  $\text{Ca}_2\text{Si}_8\text{Al}_4\text{N}_{16}$  and  $\text{Y}_2\text{Si}_6\text{Al}_6\text{N}_{16}$ . These limits have not been achieved, possibly because it is difficult to avoid surface oxide on the nitrides. Where a modifier oxide is used, oxygen replaces nitrogen but the extent to which this can occur and still retain the  $\alpha'$ -structure is probably not more than one oxygen atom per unit cell; attempts to prepare  $\text{Ca}_2\text{Si}_6\text{Al}_6\text{O}_2\text{N}_{14}$  have not been successful.

#### VI.4 Properties of $\alpha'$ -sialons

In inert (argon), nitriding or carburizing atmospheres  $\alpha'$ -sialons remain unchanged up to 1750°C. As well as this thermal stability, the thermal expansion is linear over the range 0-1250°C and is almost isotropic with the following low values for the coefficients:

$$\alpha_a = 3.3 \times 10^{-6}/^\circ\text{C}; \quad \alpha_c = 3.5 \times 10^{-6}/^\circ\text{C}$$

The ease of preparation, the thermal and chemical stability and the low coefficient of thermal expansion suggest that  $\alpha'$  sialons might make useful engineering ceramics. Mitomo et al. (62) have recently prepared fully dense and 98% theoretical density  $\alpha'$ -Y-sialon of composition  $\text{Y}_{0.5}\text{Si}_{9.5}\text{Al}_{2.5}\text{O}_{1.0}\text{N}_{14.9}$  by respectively hot pressing and pressureless sintering powder mixtures of  $\text{Si}_3\text{N}_4$ , AlN and  $\text{Y}_2\text{O}_3$  at 1750°C. These had respective bend strengths of 650 and 450 MN/m<sup>2</sup> at room temperature and that of the hot-pressed material was maintained up to 1000°C. Thermal shock resistance was slightly better than that of hot-pressed  $\beta'$ -sialon. Although this is a preliminary report, the results are promising.

$\alpha'$ -sialons have a potential advantage in that the additive, e.g. Ca, Y or rare earth, that is necessary to provide a high-temperature liquid for densification can subsequently be incorporated into the sialon structure. The phase relationships shown in Figure 55 suggest the possibility of producing  $\alpha' + \beta'$  composites and here again it might be feasible to avoid intergranular glass by a post-preparative heat-treatment that incorporates the oxide additive into the  $\alpha'$ .

# VII. THE CHARACTERIZATION OF $\alpha$ - $\beta$ RELATIONSHIPS IN SIALONS AND SILICON NITRIDES

## VII.1 $\alpha$ and $\beta$ silicon nitrides

All preparative work on  $\alpha'$ -sialons suggests a miscibility gap between  $\alpha$ - $\text{Si}_3\text{N}_4$  and the  $\alpha'$ -phase; see Figure 55. The  $\alpha'$  compositions closest to  $\text{Si}_3\text{N}_4$  are



and



To stabilise the structure, the equivalent of not less than half a cationic valency ( $\text{Ca}_{0.25}$  or  $\text{Y}_{0.16}$ ) is required in each of the two interstices.

It is suggested that this is also the requirement for  $\alpha$ -silicon nitride. Depending on whether or not oxygen is available for valency compensation, the corresponding two compositions are



and



$\text{Si}^{4+}$  is not large enough to be accommodated in the structural interstices and so a lower valency  $\text{Si}^{2+}$  is assumed; the observed length of  $2.2\text{\AA}$  for the resultant Si-N bond seems reasonable for  $\text{Si}^{2+}$ . The partial occupation of the interstitial sites accounts for the structural distortion around them in  $\alpha$  as well as in  $\alpha'$ . Further, the calculated density for the composition containing oxygen (12) is in agreement with the density range observed for  $\alpha$  needles (63) produced by reaction of silicon monoxide with nitrogen,  $3171 \text{ kg.m}^{-3}$ , and which cannot be explained by the composition  $\text{Si}_3\text{N}_4$ . Figure 56 summarises the relationship between  $\alpha$  and  $\alpha'$  and the differences between non-oxygen and oxygen-containing  $\alpha$ -silicon nitride compositions.

## VII.2 Unit-cell dimensions

There is no doubt that  $\alpha$ -" $\text{Si}_3\text{N}_4$ " shows a relatively wide variation in unit-cell dimensions that must be due to a variation in composition. Figure 57 shows values for 26 different specimens prepared by (i) reacting Si with  $\text{N}_2$ ; (ii) the reaction of SiO with  $\text{N}_2$ ; and (iii) chemical vapour deposition from silicon halides. The same precise method was used in each case by the same investigator (Dr. D.P. Thompson) and the variation in dimensions ( $a = 7.7491 - 7.7572$ ;  $c = 5.6164 -$

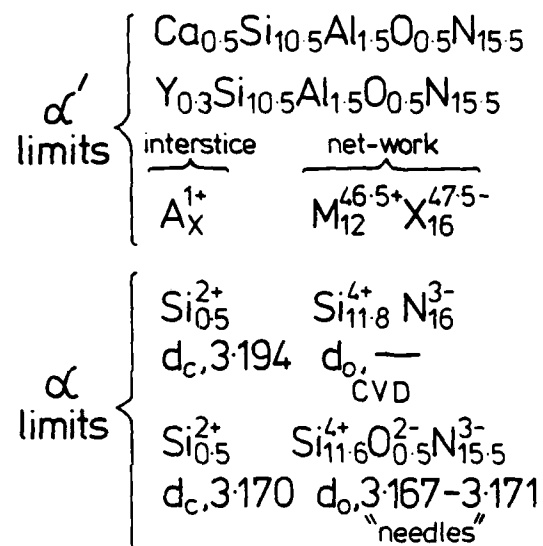


Figure 56. Comparison of  $\alpha$  and  $\alpha'$  phases

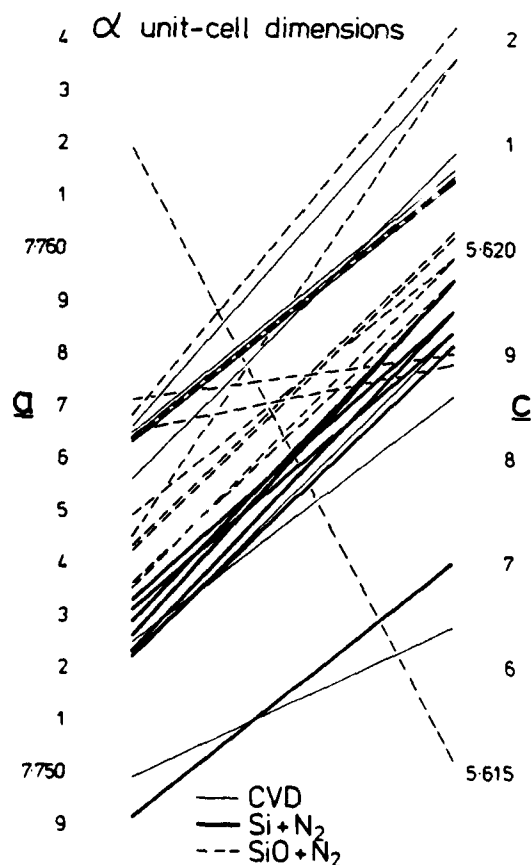


Figure 57. Unit cell dimensions of different  $\alpha$ -silicon nitrides

5.6221Å) is well outside the experimental error ( $\pm 0.0005\text{\AA}$ ). The one anomalous value ( $a = 7.7619$ ;  $c = 5.6151\text{\AA}$ ) is excluded and must be due to dissolved impurity but otherwise the axial ratios  $c/a$  are reasonably constant. In general, reaction (ii) gives higher values than (i) but different specimens of CVD cover the whole range.

### VII.3 Oxygen-containing $\alpha$ - $\text{Si}_3\text{N}_4$

There is also no doubt that  $\alpha$ - $\text{Si}_3\text{N}_4$  can accommodate oxygen even though it now seems not to be essential for the stability of the structure. The precipitation of silicon nitrides by nitriding Fe-Si alloys at low temperatures, 500-720°C, showed not only that  $\alpha$  and  $\beta$  were not, as previously supposed, merely low and high temperature forms (64) but that pure  $\beta$  was formed at very low oxygen potentials and pure  $\alpha$  at higher ones; see Figure 58.

Furthermore, the extensive thermodynamic investigations of the Si-O-N system (65, 66, 67) cannot be ignored. The discrepancy between the work at Newcastle (66) and Trondheim (67) was completely resolved (68) when it was realised that different values for the activity coefficients of silicon in iron had been used in calculating free energies. All results are completely consistent and mutually supporting and can be summarised by the thermochemical diagram of Figure 59. This shows that  $\alpha$  (containing oxygen) becomes unstable with respect to  $\beta$ - $\text{Si}_3\text{N}_4 + \text{Si}_2\text{N}_2\text{O}$  at  $\sim 1400^\circ\text{C}$  and  $P_{\text{O}_2} \sim 10^{-20}$  atm.

It should be noted that  $\alpha$ -silicon nitride formed in absence of oxygen, e.g. CVD silicon nitride of composition (11), is not necessarily unstable with respect to  $\beta$  until temperatures much higher than 1400°C.

### VII.4 The $\alpha/\beta$ silicon nitride question

Morgan (69) has suggested that seeding with pre-formed  $\alpha$  or  $\beta$  is the main determiner of the modification that is produced by nitriding silicon, but this does not indicate whether the two crystalline forms - if they are both  $\text{Si}_3\text{N}_4$  - are monotropic or enantiotropic. Even if equilibrium seldom exists in nitriding systems it is useful to know the directions of driving forces. Morgan also emphasises that  $\alpha$  and  $\beta$  are soluble in liquid silicon - a feature implied by the earlier thermodynamic investigations - but the coexistence of two solid phases with liquid silicon and nitrogen gas makes the two-component Si-N system invariant. Except at one specific temperature and pressure, one phase must disappear unless another component (e.g. oxygen) is introduced.

### VII.5 CVD silicon nitride

Silicon nitride deposited on graphite by reaction of silicon halides with ammonia at 1200 - 1500°C is amorphous or crystalline



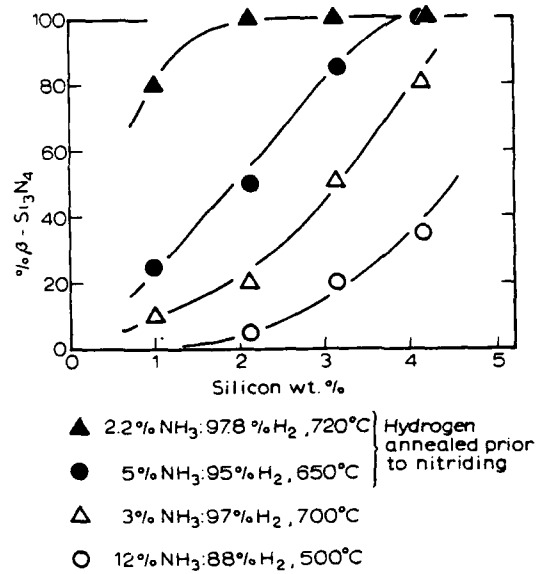


Figure 58. The precipitation of  $\alpha$ - and  $\beta$ -silicon nitrides from Fe-Si alloys

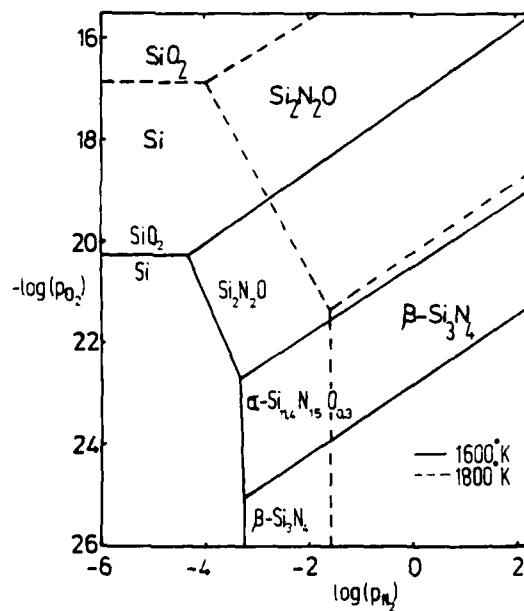


Figure 59. Thermochemical diagram for the Si-O-N system

and varies in colour (white, brown, purple, black); the crystalline deposits are invariably  $\alpha$ . Oxygen contents of CVD $\alpha$  are often lower than required by composition (12) and the dense material is remarkably stable. Thus, although Messier and Riley (70) observed some transformation to  $\beta$  with addition of MgO at 1600°C, Hampshire (7) observed none even at 1800°C.

The transformation  $\alpha \rightleftharpoons \beta$  is a reconstructive one involving the breaking and reforming of Si-N bonds and requiring either an intermediate vapour phase or a solvent. Dense CVD $\alpha$  is regarded as the purest silicon nitride and if it contains no oxygen or other impurities that might provide liquid, it might be expected to be highly resistant to transformation.

Recently, Dr. P. Korgul at Newcastle has examined white and black CVD $\alpha$  supplied by Dr. F. Galasso (United Technologies Research Center) and prepared by deposition on graphite from SiF<sub>4</sub> at 1500°C (71). Even the "white" silicon nitride contains an appreciable density of inclusions when examined by electron microscopy; Figure 60. Black CVD contains a higher concentration which at higher magnifications (see Figure 61) are shown to be thin discs approximately 250Å average diameter parallel with (00.1) planes and about  $2d_{(00.1)} = 11.3\text{Å}$  thick. In addition, black CVD contains needle-shaped bubbles lying in (hk.0) planes and about  $2d_{(10.0)} = 13\text{Å}$  in diameter; see Figure 62.

The disc-shaped precipitates produce large matrix strains. Heat-treatment of white CVD $\alpha$  in nitrogen in a graphite furnace at 1725°C causes coalescence within each disc and it is then possible to show that the precipitates are amorphous. After 1h at 1850°C, about 20% conversion to  $\beta$  takes place and examination of the  $\beta$  crystals shows that they contain no precipitates or other inclusions. It seems likely that the amorphous precipitates in CVD $\alpha$  are silica and that at 1850°C  $\alpha - \beta$  transformation occurs by solution and recrystallisation from a small amount of silica liquid.

#### VII.6 The control of $\alpha:\beta$ phase composition

By analogy with  $\alpha'$ , it is suggested that lower-valency Si occupying interstitial sites is necessary for the existence of the  $\alpha$  structure. At temperatures below 1400°C this is possible by valency compensation with oxygen.

It has further been suggested by Dr. H. Priest, AMMRC, Watertown (72) that control of phase composition to produce a high  $\alpha$  content is based on the presence of divalent Si compounds. H<sub>2</sub>, O<sub>2</sub> or H<sub>2</sub>O vapour in the nitriding gas that are known to promote  $\alpha^2$  formation will product divalent Si in the form of SiO, while in the formation of CVD $\alpha$  at 1500°C the gas contains at least 50% SiF<sub>2</sub> or SiCl<sub>2</sub>.

It seems possible that this suggestion by Dr. Priest can be reconciled with the structural occurrence in  $\alpha$  of Si<sup>2+</sup>.

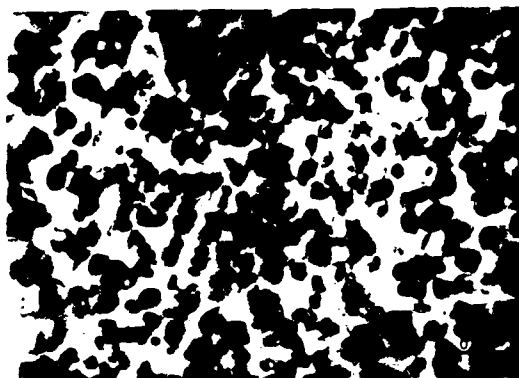


Figure 60. White CVD  $\alpha$ -silicon nitride (x 50,000)

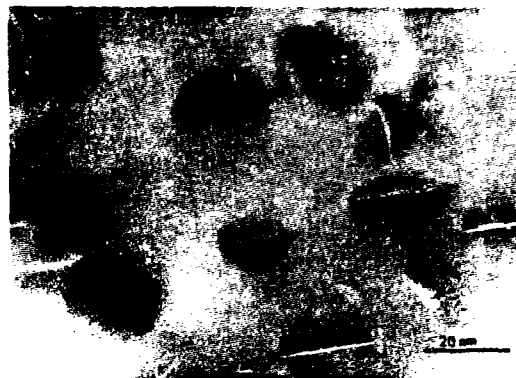


Figure 61. Black CVD  $\alpha$ -silicon nitride showing disc-shaped precipitates on (00.1) (x 400,000)



Figure 62. Black CVD  $\alpha$ -silicon nitride showing needle-bubbles on (hk.0) (x 400,000)

## Appendix I

## X-ray diffraction data for sialon phases

The previous report included a list of X-ray data for fifty metal silicon aluminium oxynitride phases. A number of additional phases have been prepared since the previous compilation and their X-ray patterns are included in the present report. Data have been collected on  $\text{CuK}\alpha$  radiation using a Hagg-Guinier focusing camera and unit cell dimensions obtained by least squares refinement. Six compounds are listed in Table A-1 and their indexed powder patterns with observed and calculated d-spacings, together with observed intensities, follow the table on separate sheets.

Table A-1

Compound

(51)	Cerium nitrogen melilite $\text{Ce}_2\text{Si}_3\text{O}_3\text{N}_4$	Tetragonal	$\underline{a} = 7.771(3)\text{\AA}$ $\underline{c} = 5.079(2)\text{\AA}$	
(52)	Cerium nitrogen apatite $\text{Ce}_{10}(\text{SiO}_4)_6\text{N}_2$	Hexagonal	$\underline{a} = 9.644(4)\text{\AA}$ $\underline{c} = 7.184(2)\text{\AA}$	
(53)	Cerium nitrogen $\alpha$ -wollastonite $\text{Ce}_3\text{Si}_3\text{O}_6\text{N}_3$	Monoclinic	$\underline{a} = 12.525(5)\text{\AA}$ $\underline{b} = 7.269(2)\text{\AA}$ $\underline{c} = 28.40(1)\text{\AA}$	$\underline{\beta} = 90.38(2)^\circ$
(54)	YAM-type cerium silicon oxynitride $\text{Ce}_4\text{Si}_2\text{O}_7\text{N}_2$	Monoclinic	$\underline{a} = 7.949(3)\text{\AA}$ $\underline{b} = 10.877(4)\text{\AA}$ $\underline{c} = 11.119(4)\text{\AA}$	$\underline{\beta} = 111.26(3)^\circ$
(55)	Cerium silicon oxynitride $\text{Ce}_2\text{Si}_6\text{O}_3\text{N}_8$	Monoclinic	$\underline{a} = 17.92(1)\text{\AA}$ $\underline{b} = 4.860(3)\text{\AA}$ $\underline{c} = 7.874(4)\text{\AA}$	$\underline{\beta} = 114.50(5)^\circ$
(56)	Cerium aluminium oxynitride $\text{Ce}_2\text{AlO}_3\text{N}$	Tetragonal	$\underline{a} = 3.736(2)\text{\AA}$ $\underline{c} = 12.72(1)\text{\AA}$	

(51) Cerium nitrogen melilite,  $\text{Ce}_2\text{Si}_3\text{O}_{13}\text{N}_4$ 

Tetragonal  $\frac{a}{c} = 7.771(3)\text{\AA}$   
 $\frac{c}{a} = 5.079(2)\text{\AA}$

hkl	d <sub>calc</sub>	d <sub>obs</sub>	I <sub>obs</sub>
110	5.495	5.496	m
001	5.079	5.079	s
101	4.251	4.258	vw
200	3.886	3.883	m
111	3.730	3.730	m
210	3.475	3.475	s
201	3.086	3.087	s
211	2.868	2.867	s
220	2.747	2.748	mw
002	2.540	2.540	m
310	2.457	2.458	m
221	2.417}	2.415	w
102	2.414}		
301	2.308}	2.306	mw
112	2.305}		
311	2.212	2.212	m
202	2.126	2.126	mw
212	2.050	2.050	s
321	1.984	1.984	m
400	1.943	1.943	mw
410	1.885	1.885	m
222	1.865	1.865	mw
401	1.815	1.815	w
411	1.767}	1.766	s
312	1.766}		
420	1.738	1.738	mw
331	1.723	1.723	m
003	1.693	1.693	w

(52) Cerium nitrogen apatite,  $\text{Ce}_{10}(\text{SiO}_4)_6\text{N}_2$ 

Hexagonal  $\begin{array}{l} a = 9.644(4)\text{\AA} \\ c = 7.184(2)\text{\AA} \end{array}$

hkl	d <sub>calc</sub>	d <sub>obs</sub>	I <sub>obs</sub>
101	5.448	5.458	vw
110	4.822	4.822	mw
200	4.176	4.175	m
111	4.004	4.002	m
002	3.594	3.592	mw
102	3.301	3.300	s
210	3.157	3.158	s
211	2.890	2.890	vs
112	2.881	2.886	vs
300	2.784	2.782	s
202	2.724	2.723	mw
220	2.411	2.412	w
212	2.372	2.377	vw
310	2.316	2.316	mw
221	2.286	2.285	mw
302	2.201	2.201	mw
113	2.145	2.145	m
400	2.088	2.087	mw
203	2.078	2.079	w
222	2.002	2.002	s
312	1.947	1.946	s
320	1.916	1.915	mw
213	1.908	1.908	s
321	1.851	1.851	ms
410	1.823	1.822	ms
303	1.816	1.816	ms
402	1.805	1.805	ms
004	1.797	1.797	m
411	1.767	1.767	w
223	1.699	1.700	vw
322	1.691	1.690	vw
114	1.684	1.683	w
500	1.670	1.669	w
204	1.650	1.650	mw
412	1.625	1.625	mw
420	1.578	1.578	mw
403	1.574	1.573	w
331	1.569	1.568	mw
214	1.562	1.561	m
421	1.542	1.541	w
502	1.515	1.514	m
304	1.510	1.509	m
323	1.496	1.496	mw

(53) Cerium nitrogen  $\alpha$ -wollastonite,  $\text{Ce}_3\text{Si}_3\text{O}_6\text{N}_3$ 

Monoclinic  $\begin{array}{l} a = 12.525(5)\text{\AA} \\ b = 7.269(2)\text{\AA} \\ c = 28.40(1)\text{\AA} \end{array} \quad \beta = 90.38(2)^\circ$

hkl	$d_{\text{calc}}$	$d_{\text{obs}}$	$I_{\text{obs}}$
$11\bar{1}$	6.147}	6.170	vw
$111$	6.134}		
$11\bar{2}$	5.764}	5.767	vw
$112$	5.751}		
$00\bar{6}$	4.733	4.733	s
$11\bar{5}$	4.227}	4.209	w
$115$	4.222}		
$\{200\}$	3.634	3.634	s
$\{130\}$	3.624	3.624	vs
$\{13\bar{3}\}$	3.396}	3.396	mw
$\{203\}$	3.393}		
$\{133\}$	3.374	3.376	w
$\{13\bar{6}\}$	2.891	2.892	vs
$\{206\}$	2.882	2.883	s
$\{136\}$	2.864	2.864	vs
$0012$	2.366	2.366	s
$\{330\}$	2.096	2.097	s
$\{060\}$	2.091	2.091	m
$\{131\bar{2}\}$	1.991	1.991	m
$\{2012\}$	1.983	1.983	m
$\{1312\}$	1.973	1.973	m
$\{06\bar{6}\}$	1.921}	1.921	s
$\{33\bar{6}\}$	1.921}		
$\{336\}$	1.913	1.912	m
$\{066\}$	1.905	1.905	mw
$\{400\}$	1.817	1.816	m
$\{260\}$	1.812	1.812	m
$\{26\bar{6}\}$	1.698}	1.698	m
$\{406\}$	1.696}		
$\{266\}$	1.687	1.687	mw
$\{0612\}$	1.576	1.576	m
$\{3312\}$	1.574	1.574	mw
$\{3312\}$	1.565	1.565	mw
$\{0612\}$	1.558	1.558	w



(54) YAM-type cerium silicon oxynitride,  $\text{Ce}_4\text{Si}_2\text{O}_7\text{N}_2$ 

Monoclinic  $\begin{array}{l} a = 7.949(3)\text{\AA} \\ b = 10.877(4)\text{\AA} \\ c = 11.119(4)\text{\AA} \end{array} \quad \beta = 14.26(3)^\circ$

hkl	d <sub>calc</sub>	d <sub>obs</sub>	I <sub>obs</sub>
011	7.503	7.490	m
110	6.123	6.113	w
020	5.439	5.432	mw
002	5.181	5.192	w
021	4.816	4.814	w
012	4.678	4.677	s
022	3.751	3.744	mw
202	3.718	3.720	w
212	3.518	3.516	w
031	3.422	3.416	mw
013	3.292	3.294	m
221	3.209	3.208	vs
222	3.069	3.069	w
220	3.061	3.063	w
213	3.036	3.035	w
211	3.021	3.022	w
032	2.971	2.971	m
023	2.916	2.915	s
040	2.719	2.720	w
041	2.630	2.630	mw
204	2.614	2.614	mw
202	2.600	2.600	mw
232	2.596}	2.596	w
230	2.591}		
004	2.591}		
214	2.542	2.542	w
212	2.529	2.529	w
014	2.520	2.521	vw
233	2.383}	2.380	w
231	2.376}		
323	2.255	2.254	w
241	2.244	2.245	mw
051	2.129	2.129	vw
234	2.121	2.121	mw
232	2.113	2.114	mw
151	2.088	2.088	w
321	2.061	2.061	mw
015	2.036	2.036	m
402	1.987	1.988	m
315	1.948	1.948	mw
143	1.940}	1.939	w
312	1.938}		

/continued

(54) YAM-type cerium silicon oxynitride (continued)

hkl	d <sub>calc</sub>	d <sub>obs</sub>	I <sub>obs</sub>
134	1.886}	1.885	mw
344	1.885}		
252	1.878	1.877	m
422	1.867	1.868	w
404	1.859}	1.858	w
233	1.859}		
053	1.841	1.841	w
204	1.833	1.833	w
410	1.826	1.824	w
216	1.816	1.816	w
214	1.808}	1.807	m
115	1.806}		
253	1.792}	1.791	w
251	1.789}		
125	1.725	1.724	w
433	1.720	1.720	w
161	1.712}	1.711	w
313	1.712}		
062	1.711}		
153	1.711}		
016	1.706	1.706	mw
245	1.699}	1.699	w
411	1.697}		
054	1.666	1.666	mw
434	1.655	1.654	w
323	1.651}	1.650	w
261	1.650}		
026	1.646}	1.645	w
425	1.646}		
421	1.639}	1.638	m
136	1.638}		
262	1.629	1.629	w
063	1.605	1.605	m
443	1.586	1.587	w
263	1.573	1.573	w
215	1.564}	1.564	w
333	1.564}		
106	1.561	1.562	w
071	1.537}	1.537	mw
514	1.536}		
422	1.511	1.509	vw
126	1.501	1.501	w
500	1.482	1.483	w
327	1.481	1.480	w
046	1.458	1.458	vvw
451	1.452}	1.452	vvw
532	1.452}		

(55) Cerium silicon oxynitride,  $\text{Ce}_2\text{Si}_6\text{O}_3\text{N}_8$ 

Monoclinic  $\begin{array}{l} a = 17.92(1)\text{\AA} \\ b = 4.860(3)\text{\AA} \\ c = 7.874(4)\text{\AA} \end{array}$   $\beta = 114.50(5)$

hkl	d <sub>calc</sub>	d <sub>obs</sub>	I <sub>obs</sub>
200	8.154	8.161	m
001	7.164	7.175	m
110	4.658	4.659	s
201	4.530	4.536	vs
40 $\bar{1}$	4.418	4.417	s
11 $\bar{1}$	4.135	4.136	w
20 $\bar{2}$	3.935	3.938	ms
31 $\bar{1}$	3.667	3.664	mw
002	3.582	3.581	m
401	3.042	3.042	s
11 $\bar{2}$	3.017	3.017	vs
31 $\bar{2}$	2.994	2.993	m
601	2.985	2.980	w
311	2.924	2.923	vs
51 $\bar{1}$	2.883	2.882	vs
60 $\bar{2}$	2.794	2.789	mw
600	2.718	2.717	vw
510	2.708	2.708	mw
112	2.690	2.690	w
51 $\bar{2}$	2.642	2.641	m
20 $\bar{3}$	2.601	2.601	mw
40 $\bar{3}$	2.579	2.579	mw
020	2.430	2.429	s
003	2.388	2.388	w
60 $\bar{3}$	2.338	2.338	ms
021	2.301	2.302	w
511	2.286	2.286	w
40 $\bar{2}$	2.265	2.263	vw
71 $\bar{1}$	2.257	2.256	w
31 $\bar{2}$	2.255		
11 $\bar{3}$	2.235	2.235	vw
80 $\bar{2}$	2.208		
71 $\bar{2}$	2.208	2.207	mw
51 $\bar{3}$	2.207		
221	2.141	2.140	mw
421	2.129	2.128	m
710	2.101	2.100	w
420	2.087	2.089	vvw
203	2.072	2.070	m
22 $\bar{2}$	2.068	2.067	m
800	2.039	2.037	mw
113	2.030	2.029	mw
80 $\bar{3}$	2.018	2.018	w
022	2.011	2.011	w

(56) Cerium aluminium oxynitride,  $\text{Ce}_2\text{AlO}_3\text{N}$ 

Tetragonal  $\begin{array}{l} a = 3.736(2)\text{\AA} \\ c = 12.72(1)\text{\AA} \end{array}$

hkl	d <sub>calc</sub>	d <sub>obs</sub>	I <sub>obs</sub>
002	6.361	6.386	vw
101	3.584	3.586	s
004	3.181	3.181	m
103	2.803	2.803	vs
110	2.641	2.642	s
112	2.439	2.440	mw
006	2.120	2.120	mw
105	2.103	2.104	w
114	2.032	2.032	s
200	1.868	1.868	m
211	1.656	1.655	mw
116	1.654	1.653	mw
107	1.634	1.634	mw
204	1.611	1.611	mw
206	1.402	1.401	mw
215	1.397	1.397	w
118	1.362	1.363	mw

## APPENDIX II

## Attendance at Scientific Meetings

1. Dr. Thompson and Dr. Rae attended the 11th International Congress of Crystallography in Warsaw, Poland in August 1978 and presented papers on "Polytypes in the Si-Al-O-N and related systems" by D.P. Thompson, and "The crystal structures of yttrium and cerium silicon oxynitrides" by K.B. Buang, A.W.J.M. Rae and D.P. Thompson. Dr. Thompson and Dr. Rae also attended a conference on Applied Crystallography at Kozubnik, Poland where they presented papers on "The Hagg-Guinier camera in materials research of new nitrogen ceramics" by D.P. Thompson, "Structure determination of nitrides and oxynitrides using powder methods" by D.P. Thompson, and "X-ray determination of expansion coefficients of sialons" by A.W.J.M. Rae and K. Liddell.
2. Professor Jack and Dr. Hendry attended the 5th Polish Conference on Electron Microscopy of the Solid State in Warsaw in October 1978 and Dr. Hendry presented a paper "The electron microscopy of sialon ceramics" by A. Hendry and K.H. Jack.
3. Dr. G. Singh (S.R.C. Visiting Research Fellow from Banaras Hindu University, India) attended a meeting on Microscopy of Amorphous, Disordered and Partially Ordered Solids in Cambridge in March 1979 and presented a paper on "Lattice imaging in structure investigations of sialon polytypes" by G. Singh and D.P. Thompson.
4. Dr. Hendry and Dr. Thompson attended a meeting on Phase Transformations at York in April 1979 where Dr. Thompson presented a paper on "Layer structures in the Si-Al-O-N and related systems" by D.P. Thompson.
5. Dr. Thompson and Dr. Hampshire were invited to the 4th Journees d'Etude sur les Nitrides in Limoges, France in May 1979 and presented papers on "The characterisation of  $\alpha$ - and  $\beta$ -silicon nitrides" by K.H. Jack and D.P. Thompson, and "The densification of nitrogen ceramics" by S. Hampshire, A.W.J.M. Rae, D.P. Thompson and K.H. Jack.
6. Professor Jack attended the 4th Cimtec meeting at St. Vincent, Italy in June 1979 and presented a paper "The processing and properties of sialons and related nitrogen ceramics" by K.H. Jack.
7. Professor Jack attended the 10th Science of Ceramics conference in Berchtesgaden, West Germany in September 1979 where he presented a paper on " $\alpha$ -Sialon ceramics" by H.K. Park, D.P. Thompson and K.H. Jack.

## APPENDIX III

## Publications

- (i) S. Hampshire, H.K. Park, D.P. Thompson and K.H. Jack, " $\alpha$ '-Sialon ceramics", Nature 274, 880, (1978).
- (ii) A. Hendry and K.H. Jack, "The electron microscopy of sialon ceramics", Proc. 5th Polish Electron Microscopy Conf., Warsaw, 1978, p. 397.
- (iii) I.B. Cutler, P.D. Miller, W. Rafaniello, H.K. Park, D.P. Thompson and K.H. Jack, "New materials in the Si-C-Al-O-N and related systems", Nature 275, 434, (1978).
- (iv) K.H. Jack, "The sialons", Mat. Res. Bull. 13, 1327, (1978).
- (v) P.M. Johnson and A. Hendry, "The microstructure of hot-pressed sialon polytypes", J. Mat. Sci. 14, 2439, (1979).
- (vi) K.H. Jack, "Phase assemblages in nitrogen ceramics and their relationship with properties", Proc. B. Cer. Soc. 28, 295, (1979).
- (vii) K.H. Jack, "The processing and properties of sialons and related nitrogen ceramics", Materials Science Monograph, 6: "Energy and Ceramics" (Ed. P. Vincenzini), 534, Amsterdam: Elsevier (1980).  
(Proc. of the 4th Cimtec Meeting, St. Vincent, Italy (1979)).
- (viii) H.K. Park, D.P. Thompson and K.H. Jack, " $\alpha$ '-sialon ceramics", Proc. of the 10th Int. Conf. "Science of Ceramics", Science of Ceramics 10, 251, Deutsche Keramische Gesellschaft, (1980).

## REFERENCES

1. N.A. Toropov and V.A. Vasil'eva, Soviet Physics (Crystallography) 6, 779, (1962).
2. M.L. Kieth and R. Roy, J. Mineral. Soc. Am. 39, 4, (1954).
3. S.J. Schneider, R.S. Roth and J.L. Waring, J. Res. Matl. Bur. Stand. 65A, 345, (1961).
4. R.L. Drew, Ph.D. Thesis, University of Newcastle upon Tyne, (1980).
5. W.D. Kingery, J. Appl. Phys. 30, 301, (1959).
6. A.L. Prill, H.W. Hayden and J.H. Brophy, Tr. Met. Soc. A.I.M.E. 233, 960, (1965).
7. S. Hampshire, Ph.D. Thesis, University of Newcastle upon Tyne, (1980).
8. F.F. Lange, S.C. Singhal and R.C. Kuznicki, J. Am. Cer. Soc. 60, 249, (1977).
9. M.H. Lewis and P. Barnard, J. Mat. Sci. 15, 443, (1980).
10. S. Wild, P. Grieveson, K.H. Jack and M.J. Latimer, "Special Ceramics 5" 377, Stoke-on-Trent: B. Ceram. R.A. (1972).
11. K. Nuttall and D.P. Thompson, J. Mat. Sci. 9, 850, (1974).
12. T.H. Elmer and M.E. Nordberg, J. Am. Cer. Soc. 50, 275, (1967).
13. F.L. Harding and R.J. Ryder, Glass Techn. 11, 54, (1970).
14. H.O. Mulfinger, J. Am. Cer. Soc. 49, 462, (1966).
15. T. Kelen and H.O. Mulfinger, Glasstechn. Ber. 41, 230, (1968).
16. M.W. Davies and S.G. Meherali, Met. Trans. 2, 2729, (1971).
17. K.H. Jack, J. Mat. Sci. 11, 1135, (1976).
18. K.H. Jack, "Nitrogen Ceramics" (Ed. F.L. Riley), 257, Leyden: Noordhof (1977).
19. K.H. Jack, "The role of additives in the densification of nitrogen ceramics", Technical Report, U.S. E.R.O. Grant No. DAERO-76-G-067 (1977).
20. R.E. Loehman, J. Am. Cer. Soc. 62, 491, (1979).

21. K. Ghyung and R.R. Wusirika, U.S. Patent No. 4070198 (1978).
22. K.H. Jack, "Phase diagrams: Materials Science and Technology, Vol. V", Chapter V (Ed. E.M. Alper), 241, New York: Academic Press (1978).
23. G. Hetherington, K.H. Jack and J.C. Kennedy, Phys. Chem. Glasses 5, 5, (1964).
24. S. Hampshire and K.H. Jack, "Special Ceramics 7", 37, Stoke-on-Trent: B. Ceram. R.A. (1981).
25. J. Lang, P. Verdier, R. Pastuszak and R. Marchand, Ann. Chimie Science des Materiaux 5, 663, (1980).
26. G.K. Layden, "Process development for pressureless sintering of SiAlON ceramic components", Technical Report R75-91072-4, United Technologies Research Centre (1976).
27. P.H.A. Roebuck, Ph.D. Thesis, University of Newcastle upon Tyne (1978).
28. I.K. Naik, L.J. Gauckler and T.Y. Tien, J. Am. Cer. Soc. 61, 332, (1978).
29. A. Mikishima, T. Yoshiaki and T. Sakaino, J. Am. Cer. Soc. 61, 332, (1978).
30. J.S. Thorp and S.V.J. Kenmuir, J. Mat. Sci. 16, 1407, (1981).
31. C.J. Leedenke and R.E. Loehman, J. Am. Cer. Soc. 63, 190, (1980).
32. K.H. Jack, Tr. J. Brit. Ceram. Soc. 72, 376, (1973).
33. L.J. Gauckler, H.L. Lukas and G. Petzow, J. Am. Cer. Soc. 58, 346, (1975).
34. K.H. Jack, J. Mat. Sci. 11, 1135, (1976).
35. A.R. Verma and P. Krishna, "Polymorphism and polytypism in crystals", New York: Wiley (1966).
36. Report of the International Mineralogical Association and the International Union of Crystallography Joint Committee on Nomenclature, Acta Cryst. A33, 681, (1977).
37. R. Collongues, J.C. Gilles, A.M. Lejus, M. Perez y Jorba and D. Michel, Mat. Res. Bull. 2, 837, (1967).
38. L.J. Gauckler, Ph.D. Thesis, University of Stuttgart (1976).



39. T. Sakai, *Yogyo-Kyokai-Shi* 86, 125, (1978).
40. S.F. Bartram and G.A. Slack, *Acta Cryst.* B35, 2281, (1979).
41. K.B. Buang, Ph.D. Thesis, University of Newcastle upon Tyne (1979).
42. J.C. Huseby, H.L. Lukas and G. Petzow, *J. Am. Cer. Soc.* 58, 377, (1975).
43. D.P. Thompson, *J. Mat. Sci.* 11, 1377, (1976).
44. D.P. Thompson and L.J. Gauckler, *J. Am. Cer. Soc.* 60, 470, (1977).
45. D.P. Thompson, "Nitrogen Ceramics" (Ed. F.L. Riley), 131, Leyden: Noordhof (1977).
46. D.R. Clarke, T.M. Shaw and D.P. Thompson, *J. Mat. Sci.* 13, 217, (1978).
47. T.M. Shaw and G. Thomas, *J. Sol. State Chem.* 33, 63, (1980).
48. D.R. Clarke and T.M. Shaw, *Mat. Sci. Res.* 11, 589, (1978).
49. P.M. Johnson and A. Hendry, *J. Mat. Sci.* 14, 2439, (1979).
50. Y. Oyama and K. Kamigaito, *Jap. J. Appl. Phys.* 10, 1637, (1971).
51. K.H. Jack and W.I. Wilson, *Nature* 238, 28, (1972).
52. P. Drew and M.H. Lewis, *J. Mat. Sci.* 9, 1833, (1974).
53. S. Wild, "Special Ceramics 6", 309, Stoke-on-Trent: B. Ceram. R.A. (1975).
54. E. Gugel, I. Petzenhauser and A. Fickel, *Powder Met. Int.* 7, 66, (1975).
55. A. Zangvil, *J. Mat. Sci.* 13, 1370, (1978).
56. F.P. Okamura and Z. Inoue, Private communication.
57. A. Zangvil, L.J. Gauckler and M. Rühle, *J. Mat. Sci.* 15, 788, (1980).
58. S.A.B. Jama, D.P. Thompson and K.H. Jack, "Special Ceramics 6", 299, Stoke-on-Trent: B. Ceram. R.A. (1975).
59. H. Masaki, Y. Oyama and O. Kamigaito, *Jap. J. Appl. Phys.* 14, 301, (1975).

AD-A116 581

NEWCASTLE-UPON-TYNE UNIV (ENGLAND)

F/G 11/2

THE ROLE OF ADDITIVES IN THE DENSIFICATION OF NITROGEN CERAMICS--ETC(U)

OCT 79 K H JACK

DA-ERO-78-6-012

ML

UNCLASSIFIED

2 OF 2  
AD-A  
- 6-82



END  
DATE  
FILMED  
7-82  
DTIC

60. M. Mitomo, *Yogyo-Kyoka-Shi* 85, 50, (1977).
61. D.P. Thompson and M. Patience, Unpublished research, University of Newcastle upon Tyne.
62. M. Mitomo, H. Tanaka, K. Muramatsu, N. Ii and Y. Fujii, Private communication.
63. S. Wild, P. Grieveson and K.H. Jack, "Special Ceramics 5", 385, B. Ceram. R.A. Stoke on Trent: (1972).
64. W. Roberts, P. Grieveson and K.H. Jack, *J.I.S.I.* 210, 931, (1972).
65. S. Wild, P. Grieveson and K.H. Jack, "Special Ceramics 5", 271, Stoke-on-Trent: B. Ceram. R.A., (1972).
66. I. Colquhoun, S. Wild, P. Grieveson and K.H. Jack, *Proc. B. Ceram. Soc.* 22, 207, (1973).
67. K. Blegen, "Special Ceramics 6", 223, Stoke-on-Trent: B. Ceram. R.A., (1975).
68. A. Hendry, "Nitrogen Ceramics" (Ed. F.L. Riley), 183, Leyden: Noordhof, (1977).
69. P.E.D. Morgan, *J. Mat. Sci.* 15, 791, (1980).
70. D.R. Messier and F.L. Riley, "Nitrogen Ceramics", (Ed. F.L. Riley), 141, Leyden: Noordhof, (1977).
71. F. Galasso, U. Kuntz and W.J. Croft, *J. Am. Cer. Soc.* 55, 431, (1972).
72. H. Priest, Private communication.

